



**UNIVERSIDADE FEDERAL DO CEARÁ**  
**CENTRO DE TECNOLOGIA**  
**DEPARTAMENTO DE ENGENHARIA METALÚRGICA E DE MATERIAIS**  
**PROGRAMA DE PÓS-GRADUAÇÃO EM ENGENHARIA E CIÊNCIA DE**  
**MATERIAIS**

**STEFANE NUNES COSTA**

**USE OF CHEMICALLY MODIFIED AZOLES FOR USE IN COPPER**  
**CORROSION INHIBITORS IN ACID MEDIUM: THEORETICAL AND**  
**EXPERIMENTAL ASPECTS**

**FORTALEZA**

**2023**

STEFANE NUNES COSTA

USE OF CHEMICALLY MODIFIED AZOLES FOR USE IN COPPER CORROSION  
INHIBITORS IN ACID MEDIUM: THEORETICAL AND EXPERIMENTAL ASPECTS

Tese apresentada ao Programa de Pós-Graduação em Engenharia e Ciências de Materiais da Universidade Federal do Ceará como requisito para a obtenção do título de Doutor em Engenharia e Ciências de Materiais. Área de concentração: Processos de Transformação e Degradação dos Materiais

Orientador: Prof. Dr. Pedro de Lima Neto

FORTALEZA

2023

Dados Internacionais de Catalogação na Publicação  
Universidade Federal do Ceará  
Sistema de Bibliotecas  
Gerada automaticamente pelo módulo Catalog, mediante os dados fornecidos pelo(a) autor(a)

---

- C875u Costa, Stefane Nunes.  
Use of chemically modified azoles for use in copper corrosion inhibitor in acid medium: theoretical and experimental aspects / Stefane Nunes Costa. – 2023.  
89 f. : il. color.
- Tese (doutorado) – Universidade Federal do Ceará, Centro de Tecnologia, Programa de Pós-Graduação em Engenharia e Ciência de Materiais, Fortaleza, 2023.  
Orientação: Prof. Dr. Pedro de Lima Neto.
1. Inibidor de corrosão. 2. Cobre. 3. Imidazol. 4. Triazol. 5. DFT. I. Título.

CDD 620.11

---

STEFANE NUNES COSTA

USE OF CHEMICALLY MODIFIED AZOLES FOR USE IN COPPER CORROSION  
INHIBITORS IN ACID MEDIUM: THEORETICAL AND EXPERIMENTAL ASPECTS

Tese apresentada ao Programa de Pós-Graduação em Engenharia e Ciências de Materiais da Universidade Federal do Ceará, como requisito para a obtenção do título de Doutor em Engenharia e Ciências de Materiais. Área de concentração: Processos de Transformação e Degradação dos Materiais

Aprovada em

BANCA EXAMINADORA

---

Prof. Dr. Pedro de Lima Neto (Orientador)  
Universidade Federal do Ceará (UFC)

---

Prof. Dr. Othon Souto Campos  
Universidade Federal do Espírito Santo (UFES)

---

Prof. Dr. Emmanuel Silva Marinho  
Universidade Estadual do Ceará (UECE)

---

Prof. Dr. Walney Silva Araújo  
Universidade Federal do Ceará (UFC)

---

Prof. Dr. Marcelo José Gomes da Silva  
Universidade Federal do Ceará (UFC)

## **DEDICATION**

*Dedico este trabalho a todos aqueles que me  
ajudaram na realização do meu sonho”*

## ACKNOWLEDGEMENT

Agradeço a Deus pelos dons que me deu nesta existência que serviram na realização deste projeto.

Aos meus pais, Antônio Arimateia Costa e Teresinha de Jesus Nunes Costa, e aos meus irmãos, Mariane Nunes e Vinícius Nunes, por sempre me incentivarem e acreditarem que eu seria capaz de superar os obstáculos que a vida me apresentou.

A minha filha, Lyana Marly, que é o bem mais precioso, a pessoa mais importante da minha vida.

Deixo um agradecimento especial ao meu orientador, Prof. Pedro de Lima Neto, pelo incentivo e pela dedicação do tempo ao meu projeto de pesquisa.

Este trabalho de pesquisa é dedicado ao amigo Professor Othon Campos que sempre me ajudou com sua experiência e conhecimentos. As incontáveis horas de troca de ideias valeram a pena. Muito obrigado meu amigo.

Ao Professor Dr. Emmanuel Marinho, pelos compartilhamentos de conhecimentos e conselhos dados.

Aos Professores do GELCORR, Adriana Nunes Correia e Paulo Naftali da Silva Casciano pelo acolhimento no laboratório, e o compartilhamento de conhecimentos.

Aos meus colegas do GELCORR Ana Aline Alcanfor, David Alves, Joelson Pires, Juliermes Carvalho, Uilson Alves, Francisco Gilvane Sampaio, Eudásio Batista, Natália Gomes, Raíssa Costa, Luiz Henrique Aragão, Luís Paulo Santos, Delmar Rodrigues, pelas ajudas, apoio, discussões e aprendizagem recíproca.

Aos meus colegas do GQT, Francisco Wagner e Emmanuelle Marinho, também pelas ajudas, apoio, discussões e aprendizagem recíproca.

A Universidade Federal do Ceará, ao Departamento de Engenharia Metalúrgica e de Materiais e ao Programa de Pós-graduação em Engenharia e Ciência de Materiais pela oportunidade e credibilidade depositada no meu trabalho.

A Fundação Cearense de Apoio ao Desenvolvimento (Funcap) e ao Conselho Nacional de Desenvolvimento Científico e Tecnológico (CNPq) pelo apoio financeiro concedido.

A todos que, mesmo não sendo citados, contribuíram de alguma forma para a realização deste trabalho.

*“Porque todo o que é nascido de Deus  
vence o mundo; e esta é a vitória  
que vence o mundo: a nossa fé”  
(1 João 5.4)*

## RESUMO

Este trabalho apresenta a aplicação de moléculas azóles (imidazol e triazol) modificadas para aplicação como inibidor de corrosão para eletrodo de cobre em ácido sulfúrico 0,5 mol L<sup>-1</sup>. Os compostos a serem avaliados são: 4-(1H-imidazol-1-il)benzaldeído (IB), 4-(1H-imidazol-1-il)anilina (IA), [4-(1H-imidazol-1-il)-Fenil]Metanol (MFI), 4-(Imidazol-1-il)-Fenol (IF), 1-fenil-2-(1H-1,2,4-triazol-1-il)etanona (TR-1), 1-(2,4-difluorofenil)-2-(1H-1,2,4-triazol-1-il)etanona (TR-2), 1-(4-clorofenil)-2-(1H-1,2,4-triazol-1-il)etanona (TR-3) e 1-(p-toluil)-2-(1H-1,2,4-triazol-1-il)etanona (TR-4). Várias técnicas eletroquímicas, como Potencial de Circuito Aberto (PCA), Polarização Potenciodinâmica Linear (PPL) e Espectroscopia de Impedância Eletroquímica (EIE), foram realizadas, bem como modelagem química foi aplicada usando técnicas de Monte Carlo e DFT. Todos os derivados do imidazol inibiram a corrosão do cobre, e os valores de inibição situaram-se entre 80 e 94%. Uma boa correlação entre os valores de eficiência de inibição e energia de adsorção de Gibbs foram encontrados, mostrando que quanto mais energia de Gibbs negativa, melhor interação do inibidor de corrosão com a superfície cobre, diminuindo sua corrosão em meio 0,5 mol L<sup>-1</sup> H<sub>2</sub>SO<sub>4</sub>. Os cálculos da DFT mostraram diferenças nas propriedades eletrônicas e de reatividade do imidazol e outras moléculas. Quanto mais alto a inibição da corrosão de derivados imidazólicos pode ser explicada pela característica eletrofílica de essas moléculas, uma vez que existem orbitais moleculares vazios espalhados principalmente em anéis de benzeno que fazem uma transferência de carga metal-ligante, recebendo densidade eletrônica da superfície do cobre por backbonding, de acordo com as funções eletrônicas de Fukui e a distribuição de carga potencial considerando o mapa de potencial eletrostático. Em relação aos triazóis, as análises dos dados eletroquímicos mostraram que TR-2 apresentou a maior eficiência de inibição (95,12% para LPP e 83,55% para EIE). A análise isotérmica mostrou que TR-s apresentaram a maior constante de adsorção, assim como a menor energia de adsorção de Gibbs. Considerando as simulações de Monte Carlo, a molécula de TR-2 é adsorvida na superfície do eletrodo pelo grupo triazol, o que favorece a criação de um filme estável sobre o eletrodo. A análise eletrônica dos cálculos DFT mostra que a polaridade e as energias LUMO das moléculas desempenham um papel importante na criação de um complexo de coordenação entre a superfície do eletrodo e a molécula inibidora de TR-2.

**Palavras-chave:** inibidor de corrosão, cobre; imidazol, triazol, DFT



## ABSTRACT

This work presents the application of modified azole molecules (imidazole and triazole) for application as a corrosion inhibitor for copper electrode in sulfuric acid 0.5 mol L<sup>-1</sup>. The compounds to be evaluated are: 4-(1H-imidazole-1-yl)benzaldehyde (IB), 4-(1H-imidazole-1-yl)aniline (IA), [4-(1H-imidazole-1-yl)-Phenyl]Methanol (IFM), 4-(Imidazole-1-yl)-Phenol (IF), 1-phenyl-2-(1H-1,2,4-triazole-1-yl)ethanone (TR-1), 1-(2,4-difluorophenyl)-2-(1H-1,2,4-triazole-1-yl)ethanone (TR-2), 1-(4-chlorophenyl)-2-(1H-1,2,4-triazole-1-yl)ethanone (TR-3) and 1-(p-toluy)l)-2-(1H-1,2,4-triazole-1-yl)ethanone (TR-4). Electrochemical techniques such as Open Circuit Potential (OCP), Linear Potentiodynamic Polarization (LPP) and Electrochemical Impedance Spectroscopy (EIS) were performed, as well as chemical modeling was applied using Monte Carlo and DFT techniques. All imidazole derivatives inhibited copper corrosion, and the inhibition values were between 80 and 94%. A good correlation between the values of inhibition efficiency and Gibbs adsorption energy were found, showing that the more negative Gibbs energy, the better interaction of the corrosion inhibitor with the copper surface, decreasing its corrosion in 0.5 mol L<sup>-1</sup> medium H<sub>2</sub>SO<sub>4</sub>. DFT calculations showed differences in the electronic and reactivity properties of imidazole and other molecules. The higher corrosion inhibition of imidazole derivatives can be explained by the electrophilic characteristic of these molecules, since there are empty molecular orbitals scattered mainly in benzene rings that transfer metal-to-binder charge, receiving electron density from the copper surface. By backbonding, according to the Fukui electronic functions and the potential charge distribution considering the electrostatic potential map. Regarding the triazoles, the analysis of the electrochemical data showed that TR-2 presented the highest inhibition efficiency (95.12% for LPP and 83.55% for EIE). The isothermal analysis showed that TR-s presented the highest adsorption constant, as well as the lowest Gibbs adsorption energy. Considering the Monte Carlo simulations, the TR-2 molecule is adsorbed on the electrode surface by the triazole group, which favors the creation of a stable film on the electrode. Electronic analysis of the DFT calculations shows that the polarity and LUMO energies of the molecules play an important role in creating a coordination complex between the electrode surface and the TR-2 inhibitor molecule.

**Keywords:** corrosion inhibitors, imidazole, triazole, copper, DFT

## LISTS OF FIGURES

|          |  |    |
|----------|--|----|
| Figure 1 | 2D chemical representations of imidazole_IM (a), 4-(1H-Imidazol-1-yl)aniline_IA (b), 4-(1H-imidazol-1-yl)benzaldehyde_IB (c), 4-(1H-imidazol-1-yl)phenol_IF (d) and (4-(1H-imidazol-1-yl)phenyl)methanol_IFM (e).....  | 26 |
| Figure 2 | Variation of the open circuit potential with the immersion time of Cu in 0.5 mol L <sup>-1</sup> H <sub>2</sub> SO <sub>4</sub> . These measurements were carried out at laboratory room temperature (≈ 25 °C) and in the presence and absence (blank) of triazole-based compounds at 1×10 <sup>-3</sup> mol.....  | 29 |
| Figure 3 | Potentiodynamic polarization curves obtained for Cu <sup>0</sup> in 0.5 mol L <sup>-1</sup> H <sub>2</sub> SO <sub>4</sub> medium in the absence (blank) and presence of imidazole-based compounds at 1×10 <sup>-3</sup> mol L <sup>-1</sup> . All curves were achieved at laboratory room temperature (≈ 25 °C).....  | 30 |
| Figure 4 | Nyquist (a) and Bode (b,c) plots obtained for Cu <sup>0</sup> after 1h of immersion in 0.5 mol L <sup>-1</sup> H <sub>2</sub> SO <sub>4</sub> in the absence and presence of imidazole and its derivatives at 1×10 <sup>-3</sup> mol L <sup>-1</sup> . All diagrams were obtained at room temperature of the laboratory (≈ 25 °C). The solid lines represent the impedance simulation carried out by the equivalent circuit shown in Figure 5..... | 33 |
| Figure 5 | Drawing of the equivalent electrical circuit used to fit the EIS diagrams.....   | 34 |
| Figure 6 | Nyquist diagrams obtained for Cu <sup>0</sup> immersed in 0.5 mol L <sup>-1</sup> H <sub>2</sub> SO <sub>4</sub> at different concentrations of the studied corrosion inhibitors and obtained at room temperature (≈ 25 °C). The solid lines represent the adjust of the experimental data by the equivalent electric circuit shown in Figure 5.....   | 38 |
| Figure 7 | Langmuir's linear relationships obtained for the corrosion inhibition of Cu <sup>0</sup> in 0.5 mol L <sup>-1</sup> H <sub>2</sub> SO <sub>4</sub> solution in presence of imidazole and imidazole-based compounds.....  | 40 |
| Figure 8 | Frumkin adsorption isotherms obtained for imidazole and its derivatives.....   | 41 |
| Figure 9 | Temkin adsorption isotherms obtained for imidazole and its derivatives.....  | 43 |

|           |  |    |
|-----------|--|----|
| Figure 10 | Optimized molecular geometry of the IM (a), IA (b), IB (c), IF (d), and IFM (d) obtained at M06-2X/6-311++G(d,p) level of theory in water as implicit solvent.....   | 45 |
| Figure 11 | Frontier Molecular Orbitals calculated at M06-2X/6-311++G(d,p) level of theory in water for the molecules IM (a), IA (b), IB (c), IF (d), and IFM (e) with isovalue = 0.03.....  | 45 |
| Figure 12 | Isosurfaces for the Electronic Fukui Functions for nucleophilic ( $f^+$ ) and electrophilic ( $f^-$ ) attack for the molecules IM (a), IA (b), IB (c), IF (d), and IFM (e) with isovalue = 0.36.....   | 49 |
| Figure 13 | Molecular Electrostatic Potential computed for the molecules IM (a), IA (b), IB (c), IF (d), and IFM (e) at M06-2X/6-311++G(d,p) level of theory in water with isovalue = 0.01.....  | 51 |
| Figure 14 | Scheme of synthesis of the lateral modification of triazole compounds. For 1a to 1e compounds, R2 = -H and R3 = -Br. For 1f compound, R2 = -F and R3 = -Cl, and R1 = -F. For 1a to 1d compounds, R1 was, respectively, -H, -CH <sub>3</sub> , -F, and -Cl.....   | 56 |
| Figure 15 | 2D representation of the inhibitor molecules that were studied in this paper.....  | 57 |
| Figure 16 | Variation of the open circuit potential with the immersion time of Cu in 0.5 mol L <sup>-1</sup> H <sub>2</sub> SO <sub>4</sub> . These measurements were carried out at laboratory room temperature ( $\cong$ 25 °C) and in the presence and absence (blank) of triazole-based compounds at 1 $\times$ 10 <sup>-3</sup> mol.....                              | 61 |
| Figure 17 | Potentiodynamic polarization curves obtained for Cu in 0.5 mol L <sup>-1</sup> H <sub>2</sub> SO <sub>4</sub> medium in the absence (blank) and presence of triazole-based compounds at 1 $\times$ 10 <sup>-3</sup> mol L <sup>-1</sup> . All curves were achieved at laboratory room temperature ( $\cong$ 25 °C).....  | 61 |
| Figure 18 | Nyquist (a) and Bode (b,c) plots obtained for Cu after 1h of immersion in 0.5 mol L <sup>-1</sup> H <sub>2</sub> SO <sub>4</sub> in the absence and presence of triazole and its derivatives at 1 $\times$ 10 <sup>-3</sup> mol L <sup>-1</sup> . All diagrams were obtained at room temperature of the laboratory ( $\cong$ 25 °C). The solid lines represent |    |

|           |   |    |
|-----------|---|----|
|           | impedance simulation carried out by the equivalent circuit shown in Figure 19.....  | 64 |
| Figure 19 | Drawing of the equivalent electrical circuit used to fit the EIS diagrams..   | 64 |
| Figure 20 | Nyquist diagrams obtained for Cu immersed in 0.5 mol L <sup>-1</sup> H <sub>2</sub> SO <sub>4</sub> at different concentrations of the studied corrosion inhibitors and obtained at room temperature ( $\cong$ 25 °C). The solid lines represent the adjust of the experimental data by the equivalent electric circuit shown in Figure 19... | 67 |
| Figure 21 | Langmuir's linear relationships obtained for the corrosion inhibition of Cu in 0.5 mol L <sup>-1</sup> H <sub>2</sub> SO <sub>4</sub> solution in presence of triazole and triazole-based compounds.....  | 69 |
| Figure 22 | Optimized geometries at 6-311++G(d,p) level of theory for the inhibitors (A) TR (B) TR-1 (C) TR-2 (D) TR-3 and (E) TR-4.....  | 71 |
| Figure 23 | Calculated Frontier Molecular Orbitals (FMO) at 6-311++G(d,p) level of theory for the inhibitors (A) TR (B) TR-1 (C) TR-2 (D) TR-3 and (E) TR-4.....  | 72 |
| Figure 24 | Isosurface for the Electronic Fukui functions for the nucleophilic attack ( $f^+$ ), electrophilic attack ( $f^-$ ), and radical attack ( $f^0$ ) for the (a) TR (b) TR-1 (c) TR-2 (d) TR-3 and (e) TR-4.....   | 76 |
| Figure 25 | Calculated Molecular Electrostatic Potential (MEP) for the (a) TR (b) TR-1 (c) TR-2 (d) TR-3 and (e) TR-4.....  | 77 |
| Figure 26 | Energy probability distribution of adsorption energy of the inhibitor molecules using a copper surface along COMPASS force field in vacuum (a) and explicit water molecules (b).....  | 79 |
| Figure 27 | Correlation between adsorption energies from maximum probabilities in Figure 26 and inhibition efficiency for vacuum (a) and explicit water (b) media using COMPASS force field.....  | 80 |
| Figure 28 | Preferred molecular orientation of the inhibitor molecules over a copper surface in a simulation with explicit water molecules.....   | 82 |
| Figure 29 | Correlation between corrosion efficiency and dipolar moment for all inhibitor molecules.....  | 83 |

## LISTS OF TABLES

|          |  |    |
|----------|--|----|
| Table 1  | Electrochemical parameters obtained for $\text{Cu}^0$ corrosion in $0.5 \text{ mol L}^{-1}$ $\text{H}_2\text{SO}_4$ medium in the absence and presence of imidazole-based compounds at $1 \times 10^{-3} \text{ mol L}^{-1}$ ..... | 32 |
| Table 2  | Fitted values from applied equivalent circuit shown in Figure 4 and inhibition efficiency obtained from fitted data. The constant phase element was converted to pseudocapacitance using the Brug method.....                      | 35 |
| Table 3  | EIS parameters derived from the Nyquist plots shown in Figure 6.....   | 39 |
| Table 4  | Intermolecular factor from linearized Frumkin isotherm model from Figure 8 for lateral groups of the studied molecule inhibitors for copper in $\text{H}_2\text{SO}_4$ $0.5 \text{ mol L}^{-1}$ solution.....                      | 42 |
| Table 5  | $K_{\text{ads}}$ and $\Delta G_{\text{ads}}$ values for imidazole derivatives in $0.5 \text{ mol L}^{-1}$ $\text{H}_2\text{SO}_4$ solution for $\text{Cu}^0$ surface.....  | 43 |
| Table 6  | Global quantum reactivity descriptors computed for the molecules IM, IA, IB, IF, and IFM at M06-2X/6-311++G(d,p) level of theory.....  | 47 |
| Table 7  | Electrochemical parameters obtained for Cu corrosion in $0.5 \text{ mol L}^{-1}$ $\text{H}_2\text{SO}_4$ medium in the absence and presence of triazole-based compounds at $1 \times 10^{-3} \text{ mol L}^{-1}$ .....             | 63 |
| Table 8  | Fitted values from applied equivalent circuit shown in Figure 18 and inhibition efficiency obtained from fitted data. The constant phase element was converted to pseudocapacitance using Brug method.....                         | 65 |
| Table 9  | EIS parameters derived from the Nyquist plots shown in Figure 7.....   | 68 |
| Table 10 | $K_{\text{ads}}$ and $\Delta G_{\text{ads}}$ values for triazole derivatives in $0.5 \text{ mol L}^{-1}$ $\text{H}_2\text{SO}_4$ solution for Cu surface.....  | 70 |
| Table 11 | Calculated global quantum reactivity descriptors at 6-311++G(d,p) level of theory.....   | 73 |
| Table 12 | Interaction energies from studied inhibitor molecules.....   | 81 |

## LIST OF ABBREVIATIONS AND ACRONYMS

|      |  |
|------|--|
| DFT  | Density Functional Theory                                |
| EIS  | Electrochemical Impedance Spectroscopy                   |
| HOMO | Highest occupied molecular orbital                       |
| IM   | Imidazole  |
| IB   | 4-(1H-Imidazol-1-yl)benzaldehyde                         |
| IA   | 4-(1H-Imidazol-1-yl)aniline                              |
| IFM  | [4-(1H-Imidazol-1-yl)-Phenyl]Methanol                    |
| IF   | (Imidazol-1-yl)-Phenol                                   |
| LUMO | Lowest unoccupied molecular orbital                      |
| Q    | Phase constant element                                   |
| OCP  | Open Circuit Potential                                   |
| ORR  | Oxygen reduction reaction                                |
| R    | Resistance   |
| LPP  | Linear Potentiodynamic Polarization                      |
| MC   | Monte Carlo  |
| MEP  | Molecular Electrostatic Potential                        |
| TR-1 | 1-phenyl-2-(1H-1,2,4-triazol-1-yl)ethanone               |
| TR-2 | 1-(2,4-difluorophenyl)-2-(1H-1,2,4-triazol-1-yl)ethanone |
| TR-3 | 1-(4-chlorophenyl)-2-(1H-1,2,4-triazol-1-yl)ethanone     |
| TR-4 | 1-(p-toluy)l)-2-(1H-1,2,4-triazol-1-yl)ethanone          |
| W    | Warburg impedance  |

## SUMMARY

|            |  |           |
|------------|--|-----------|
| <b>1</b>   | <b>INTRODUCTION.....</b>   | <b>17</b> |
| <b>2</b>   | <b>OBJECTIVE.....</b>  | <b>23</b> |
| <b>2.1</b> | <b>General Objective.....</b>  | <b>23</b> |
| <b>2.2</b> | <b>Specific Objectives.....</b>  | <b>23</b> |
| <b>3</b>   | <b>INHIBITION OF COPPER CORROSION IN ACID MEDIUM BY<br/>IMIDAZOLE-BASED COMPOUNDS: ELECTROCHEMICAL AND<br/>MOLECULAR APPROACHES.....</b> | <b>24</b> |
| <b>3.1</b> | <b>Introduction.....</b>   | <b>24</b> |
| <b>3.2</b> | <b>Details Experimental.....</b>   | <b>26</b> |
| 3.2.1      | <i>Electrochemical experiments.....</i>  | <i>26</i> |
| 3.2.2      | <i>Computational calculations.....</i>   | <i>27</i> |
| <b>3.3</b> | <b>Results and discussion.....</b>   | <b>29</b> |
| 3.3.1      | <i>Electrochemical Studies.....</i>  | <i>29</i> |
| 3.3.2      | <i>Adsorption Isotherm.....</i>  | <i>37</i> |
| 3.3.3      | <i>Computational results.....</i>  | <i>44</i> |
| <b>3.4</b> | <b>Conclusions.....</b>  | <b>53</b> |
| <b>4</b>   | <b>INHIBITION OF COPPER CORROSION IN ACID MEDIUM BY<br/>TRIAZOLE-BASED COMPOUNDS: ELECTROCHEMICAL AND<br/>MOLECULAR APPROACHES.....</b>  | <b>54</b> |
| <b>4.1</b> | <b>Introduction.....</b>   | <b>54</b> |
| <b>4.2</b> | <b>Experimental Details.....</b>   | <b>56</b> |
| 4.2.1      | <i>Synthesis of the modified triazole molecules.....</i>   | <i>56</i> |
| 4.2.2      | <i>Electrochemical experiments.....</i>  | <i>57</i> |
| 4.2.3      | <i>Computational calculations.....</i>   | <i>58</i> |
| 4.2.4      | <i>Monte Carlo simulations.....</i>  | <i>59</i> |
| <b>4.3</b> | <b>Results and discussion.....</b>   | <b>60</b> |

|       |                                      |    |
|-------|--------------------------------------|----|
| 4.3.1 | <i>Electrochemical studies</i> ..... | 60 |
| 4.3.2 | <i>Adsorption Isotherm</i> .....     | 67 |
| 4.3.3 | <i>Computational results</i> .....   | 70 |
| 4.4   | <b>Conclusions</b> .....             | 84 |
|       | <b>REFERENCES</b> .....              | 85 |



## 1 INTRODUCTION

Corrosion is a critical problem worldwide that heavily affects both natural and industrial environments. Currently, corrosion and pollution are considered to be interrelated harmful processes, as many pollutants accelerate corrosion and corrosion products, such as rust, also pollute water bodies. Therefore, it is essential to develop and apply corrosion engineering control methods and techniques.

In this context, the practice of acid cleaning in industry originally arose from the desire to develop technology to improve the recovery of fluids from oil wells. Acid cleaning involves using highly reactive acids such as hydrochloric acid, sulfuric acid, citric acid, and sulfamic acid to dissolve surface deposits and scale. However, industrial acid cleaning processes simultaneously cause severe corrosion of the base metal in the absence of a suitable corrosion inhibitor in the cleaning medium. Recently, various types of corrosion inhibitors have been used to effectively prevent corrosion of metallic structures in acidic environments.

A very common example is the degradation of copper pipes used to conduct water in industrial equipment. Despite the protective characteristic of the copper passivation layer, this metal undergoes pitting corrosion in the presence of an acidic environment, which may cause leaks in pipes. This metal is widely used in the manufacture of electronic components, connections, electrical wiring, piping, water supply systems and heat exchangers, among others, because it has several properties such as: high electrical and thermal conductivity, ductility and good resistance to heat. However, copper materials are susceptible to corrosion when exposed to aggressive environments. For this reason, the importance of a method capable of preventing or mitigating this phenomenon is undeniable (SILVA et al., 2021).

According to data from the Brazilian Association of Corrosion, it is estimated that corrosion is responsible for an annual cost of 3% of GDP, approximately R\$ 280 billion, compared to this percentage according to a North American study. According to ABRACO, if corrosion protection measures were correctly applied, after deducting the costs of applying these measures, savings could reach at least R\$ 112 billion.

Therefore, despite the nature of metals to oxidize and corrode, damage caused by corrosion can be delayed over time, greatly reduced, and sometimes even avoided altogether. To achieve these goals, it is necessary to identify reliable and cost-effective

methods of protection and control. In this sense, companies will encourage research into new technological developments and the introduction of anti-corrosion methods.

Corrosion inhibitors play an important role in the engineering and economics of metal protection. According to equipment and other industries, the use of corrosion inhibitors is an effective and cost-effective anti-corrosion method (CHITER et al., 2022). Any process of slowing down corrosion or reducing the rate of metal oxidation by adding a chemical compound to the system is due to corrosion inhibitors (CALDONA et al., 2021). Inhibitors are generally easy to apply and provide the benefit of application without causing significant process disruption. The use of corrosion inhibitors is one of the best methods of combating corrosion.

However, there are several factors to be considered when choosing an inhibitor, such as the cost of the inhibitor, but be very careful in comparing products by price, as price is directly related to quality; inhibitor toxicity can cause adverse effects in humans and other living species; the availability of the inhibitor on the market; The inhibitor must be environment friendly (LIU et al., 2022).


Adsorption inhibitors are indicated for the protection of metallic materials in acidic environments, as they adsorb in the cathodic and/or anodic regions of the metal, which prevents the corrosion process on the metal surface (WAZZAN; OBOT; FAGIEH, 2022). These inhibitors have polar groups that act through adsorption on metallic surfaces. Adsorption of organic molecules occurs because the interaction forces between the inhibitor and the metal surface are greater than the interaction forces between water molecules and the metal surface. General rules the inhibitor acts by adsorption on the metal surface forming a protective film or pellicle that has a high affinity for the same surface, preventing the dissolution of the metal in the electrolyte (VARVARA et al., 2021).

The adsorption process occurs when particles are retained on the surface of solids. The substance that accumulates on the surface of the material and undergoes an increase in concentration is called adsorbate, while the surface on which the process takes place is known as adsorbent. As the adsorbed components are concentrated on the external surface, the larger this surface per solid mass unit, the more favorable the adsorption will be. Adsorbent characteristics include surface area, pore size, density, functional groups present on the surface and hydrophobicity of the material. Based on this, for efficient adsorption of the inhibitor on the metal surface, the interaction forces between the two must be greater

than the interaction forces of the metal with water, as mentioned above (JIANG et al., 2014).

However, traditional inhibitors have shown limitations, such as toxicity. Therefore, research on green and eco-friendly corrosion inhibitors has been directed towards more efficient but less expensive molecules with minimal impact on the environment (QIU et al., 2022). Much research in this regard has focused on a variety of compounds such as Schiff bases, triazepines, thiosemicarbazones, hydroxyquinoline derivatives, amino acids, plant extracts, triazoles, imidazoles, pyrazoline, and oxazole derivatives.

Heterocyclic organic compounds with N, O and S heteroatoms have been shown to be an alternative and effective source of corrosion inhibitors, especially in acidic environments (FOUDA et al., 2020). This can be explained by the electronegativities of the atoms involved. Most studies indicate that the inhibition of the corrosive process is mainly due to the formation of a donor-acceptor complex on the metal surface and the donation of electrons by organic inhibitors (MA et al., 2017). Among the various nitrogenous compounds studied as inhibitors, azole compounds are considered an excellent class of inhibitors to reduce the corrosion rate and hydrogen embrittlement of steel and copper in acid medium (ITUEN et al., 2020).

The azoles and their derivatives have been shown to be potent corrosion inhibitors. This seems to be due to their polar groups and ability to complex with metallic surfaces, making it more likely that these compounds will adsorb to metallic surfaces in aggressive environments. In addition, they exhibit various agronomic, industrial and biological characteristics, such as anticancer, antiviral, antibacterial, antifungal, etc. All these properties have demonstrated their anti-toxic properties. They also have many  electrons and unshared electron pairs on the nitrogen atom, which can interact with the d orbitals of any metal to form a protective film (QIU et al., 2022). Therefore, in recent years, research on azole-derived inhibitors has been an important topic. Many efforts have been made by researchers to test new triazole derivatives in hopes of improving their inhibitory efficacy. A common route to increase the corrosion inhibiting effect of a given heterocyclic is to modify its structure with different radicals or functional groups.

Although experimental electrochemical techniques can provide valuable information about the behavior of anticorrosive compounds and their adsorption process on the metallic surface. Insights at the molecular level through modern computational tools can interpret and explain many experimental observations. Density functional theory can

provide us with reactivity parameters and the site for nucleophilic and electrophilic interactions between organic molecules and the metal surface (PARLAK et al., 2022). On the other hand, Monte Carlo (MC) simulation can provide details about the adsorption configuration, how the inhibitor molecule can orient towards the metal surface. The parameters obtained from the MC simulation can be used to evaluate and interpret which molecule/molecule adsorbs most strongly on the metal surface (MA et al., 2020).

The addition of computational studies, especially Monte Carlo simulation (MC) and density functional theory (DFT) calculations, makes this branch of research more environmentally friendly to investigate corrosion inhibitor performance. The green character of these theoretical tools has to do with the fact that unlike traditional corrosion monitoring techniques, these methods do not require the discharge or use of any environmentally harmful materials (TANTAWY; SOLIMAN; ABD EL-LATEEF, 2020).

According to Ma et al., they found that all azole-derived inhibitors (Benzotriazole (BTZ), 1,2,4-triazole (TRZ) and 2,2'-[[[(5-Methyl-1H-benzotriazol-1-yl) methyl] imino] bisethanol (TT-LYK)) showed corrosion inhibition on the copper surface and this effect was more positive with increasing concentration. To obtain these results they used several techniques such as: density functional calculation and Monte Carlo simulation combined with electrochemical experiments and PMC (chemical mechanical polishing). In particular, the TT-LYK inhibitor has a stronger corrosion inhibition effect, verified by the electrochemical and CMP measurements and for the molecular dynamics results it was verified that there are several adsorption sites between the TT-LYK in relation to the surface of the copper. Concluding that the combination of molecular dynamics methods and experimental approach may be able to study corrosion inhibitors at the micro level and predict better molecular structures that are more suitable for improving copper corrosion inhibition efficiency (MA et al., 2020).

According to Huang et al., the inhibition performances of benzimidazole (BI), 2-mercaptobenzimidazole (MBI) and benzotriazole (BTA) in galvanic corrosion of copper coupled with silver in 3.5% NaCl solution demonstrate that the introduction of an atom of nitrogen and sulfhydryl group in the benzimidazole molecule increased the physisorption and chemisorption of inhibitors on the copper surface which improves the inhibition efficiency of the inhibitors, while the galvanic effect between copper and silver reduces the inhibition efficiency of the inhibitors. In this work, several techniques were also used, such

as: electrochemistry, surface analysis, quantum chemical calculations and molecular dynamics (HUANG; BU, 2020).

Jog and collaborators studied pyrazole and 1,2,4-triazole and their derivatives not only as an inhibitor, but also studied the toxicity of these substances. They verified that the compounds, the azole compounds substituted by dimethyl and diethyl, presented an excellent result in relation to the IC<sub>50</sub> (concentration capable of inhibiting 50% of cell growth) from 30 to 700 times lower in comparison with the original unsubstituted compounds, the best performance went to compound 3,5-diethyltriazole which turned out to be completely non-toxic. With regard to the inhibition efficiency of alkyl-substituted azole compounds under alkaline conditions, it was found that all tested azoles were able to significantly inhibit copper corrosion. For pyrazoles, corrosion inhibition performance improved with the addition of dimethyl and diethyl substituents. The efficiency of inhibition by pyrazole, 3,5-dimethylpyrazole and 3,5-diethylpyrazole was 71.5, 77.6 and 85.0%, respectively. In the case of triazoles, the corrosion inhibition efficiency was slightly lower for alkyl-substituted triazoles (77.7% for 3,5-dimethyl-1,2,4-triazole and 82.9% for 3,5-diethyl -1,2,4-triazole) than for the unsubstituted 1,2,4-triazole (89.6%). These results show that it is possible to substitute conventional azole compounds for their non-toxic equivalents for industrial applications. This would prevent inhibition of microbial nitrification without compromising the effectiveness of azoles as inhibitors of copper corrosion (JOG et al., 2022).

Research by El Asri and collaborators analyzed Methylimidazole and 1H-benzimidazole as corrosion inhibitors for the copper surface, determining that these compounds are mixed inhibitors obtaining, respectively, 66% and 80% of corrosion inhibition efficiency. The Langmuir adsorption isotherm was also obtained, which showed good agreement between the results obtained by the different experimental techniques. These same correlations were observed between the theory-experience results (EL ASRI et al., 2022).

Swathi and co-workers developed a new triazole derivative, (E)-4-(4-(dimethylamino)benzylideneamino)-5-(pyridin-4-yl)-2H-1,2,4-triazol-3(4H)-thiona (DPT) and then performed the inhibition study on the carbon steel surface. Studies revealed that DPT is highly efficient with a value of 90% at very low concentrations (250ppm). Furthermore, the addition of DPT resulted in decreased cathode and anode current densities, which is the indication of mixed-type inhibition. Characterization

techniques such as: SEM, EDX and XPS were used, showing that the inhibitor strongly adsorbs on the metal surface. The excellent result of the inhibition efficiency of the DPT compound was in agreement with the theoretical studies and, therefore, the DPT acts as a good inhibitor of carbon steel (SWATHI et al., 2022).

Tchoumene and collaborators produced a new hybrid kaolinite that was obtained for the first time by intercalating 1,2,4-triazole (TAZ) in the interlamellar space of methoxykaolinite. Subsequently, the material was used as a copper corrosion inhibitor in a concentrated aqueous solution of 0.5 M NaCl. K-TAZ showed characteristics of a mixed inhibitor with an inhibition efficiency reaching 96.9% for an inhibitor concentration of 320 mg L<sup>-1</sup> was used. They found that the inhibition of the cathodic reaction is due to free methoxykaolinite particles, while the deintercalated TAZ molecules provide the anodic protection. Thermodynamic studies of the process revealed that K-TAZ protects copper by reinforcing the protective layer made of copper oxide and chlorides produced when the metal reacts with corrosive sodium chloride solution. This work clearly demonstrated the potential use of kaolinite for use as a copper corrosion inhibitor (TCHOUMENE; KENNE DEDZO; NGAMENI, 2022).

Belghiti et al studied the inhibition performance of 3,5-bis(4-methylphenyl)-4-amino-1,2,4-triazole (MeAT) and 3,5-bis(4-methoxyphenyl)-4-amino-1,2,4-triazole (MxAT) on copper corrosion in acid medium. The results showed that the investigated 1,2,4-triazole derivatives are efficient corrosion inhibitors for copper. the adsorption of MxAT molecules fits the Langmuir isotherm model and the corresponding value of the Gibbs free energy adsorption pattern is associated with a chemisorption mechanism. Computational studies by DFT and Monte Carlo Simulations (MCs) were also performed to correlate the inhibition properties and the quantum chemical parameters of the investigated inhibitors that showed good correlations (BELGHITI et al., 2020).

In this work, the chemical substances derived from azole were studied, as it has already been shown that compounds of this class inhibit copper corrosion in acidic media, and this property is associated with the good solubility of these compounds in water, the high stability and the pairs of unshared electrons on the nitrogen atoms, which can interact with the empty orbitals of the metal. Finally, correlations between experimental results and theoretical results were also made.

## 2 OBJECTIVE

### 2.1 General Objective

This work aims to associate electrochemical techniques and molecular modeling studies, in order to establish molecular parameters that act in the inhibition of copper corrosion in  $\text{H}_2\text{SO}_4$   $0.5 \text{ mol L}^{-1}$  medium, using, as possible inhibitors, derivatives of imidazole and triazole.

### 2.2 Specific Objectives

- Investigate the inhibitory action of imidazole and triazole derivatives on copper corrosion in  $0.5 \text{ mol L}^{-1} \text{H}_2\text{SO}_4$  medium, using electrochemical methods. The compounds to be evaluated are: 4-(1H-Imidazol-1-yl)benzaldehyde (IB), 4-(1H-Imidazol-1-yl)aniline (IA), [4-(1H-Imidazol-1-yl)-Phenyl]Methanol (IFM), 4-(Imidazol-1-yl)-Phenol (IF), 1-phenyl-2-(1H-1,2,4-triazol-1-yl)ethanone (TR-1), 1-(2,4-difluorophenyl)-2-(1H-1,2,4-triazol-1-yl)ethanone (TR-2), 1-(4-chlorophenyl)-2-(1H-1,2,4-triazol-1-yl)ethanone (TR-3) and 1-(p-toluy)l)-2-(1H-1,2,4-triazol-1-yl)ethanone (TR-4).

- Evaluate the behavior of inhibitors with concentration variation of  $0.1 \cdot 10^{-3} \text{ mol L}^{-1}$ ,  $0.25 \cdot 10^{-3} \text{ mol L}^{-1}$ ,  $0.5 \cdot 10^{-3} \text{ mol L}^{-1}$  and  $1 \cdot 10^{-3} \text{ mol L}^{-1}$ , as well how to determine adsorption free energy values ( $\Delta G_{\text{ads}}$ ) and adsorption isotherms.

- Use quantum molecular modeling calculations, in order to relate the corrosion inhibition efficiency with the main molecular descriptors, such as: energy of the border orbitals, absolute molecular hardness, total charge of the molecule, etc.

- Determine, by Monte Carlo simulation, the interaction energies of the molecules with the copper surface, verifying which of the substituents has a greater influence on the inhibition.

- Propose a calculation protocol, using molecular modeling methods, that allows classifying organic molecules in relation to their corrosion inhibition efficiencies for copper in an acid medium.

### 3 INHIBITION OF COPPER CORROSION IN ACID MEDIUM BY IMIDAZOLE-BASED COMPOUNDS: ELECTROCHEMICAL AND MOLECULAR APPROACHES

#### 3.1 Introduction

The corrosion of materials, specifically the metallic ones, is one of the major problems faced by humankind, which leads to huge economic losses that also contribute to environmental pollution (ABDULAZEEZ et al., 2019). Copper ( $\text{Cu}^0$ ) is one of those metallic materials that has been widely used in industries, having many technological applications due to its high electrical and thermal conductivity, good malleability, and excellent corrosion resistance (EL-KATORI; ABOUSALEM, 2019). However, when  $\text{Cu}^0$  is attacked by hydrochloric and sulfuric acids, which are frequently used in pickling industrial processes, can suffer dissolution in those aggressive media (DAGDAG et al., 2020a).

For preventing metallic corrosion, one of the most applied methods is the use of organic or inorganic compounds as corrosion inhibitors (CHAOUIKI et al., 2019). Regarding organic substances, the corrosion inhibition usually happens based on the adsorption of the molecule over the surface of the metallic materials through heteroatoms, such as nitrogen (N), oxygen (O), sulfur (S), and phosphorus (P), in addition to multiple bonds or aromatic rings (ARKHIPUSHKIN et al., 2019).

Several types of substances are being investigated as potential corrosion inhibitors for  $\text{Cu}^0$ , such as azoles (HUANG; BU, 2020), amines (BURKE; PERDEW; WANG, 1998), amino acids (HAMADI et al., 2018), thiazoles (FARAHATI et al., 2019a), pyrimidine (XU et al., 2018), and Schiff's base (ZHANG et al., 2016). In addition to having interesting chemical and pharmacological properties, imidazole-based compounds have aromatic heterocyclic containing heteroatoms (N), which contribute to the adsorption of these species on the metal surface (IBRAHIMI et al., 2016; KOVAČEVIĆ; MILOŠEV; KOKALJ, 2015). Although imidazole (IM) itself is not a promising corrosion inhibitor (KOVAČEVIĆ; MILOŠEV; KOKALJ, 2015; QIANG et al., 2017a), the corrosion inhibition efficiency ( $\epsilon_{\text{inh}}$ ) increases when polar chemical groups are added to the IM, such as phenyl, methoxy, amino, sulfhydryl, etc (DAGDAG et al., 2020b).



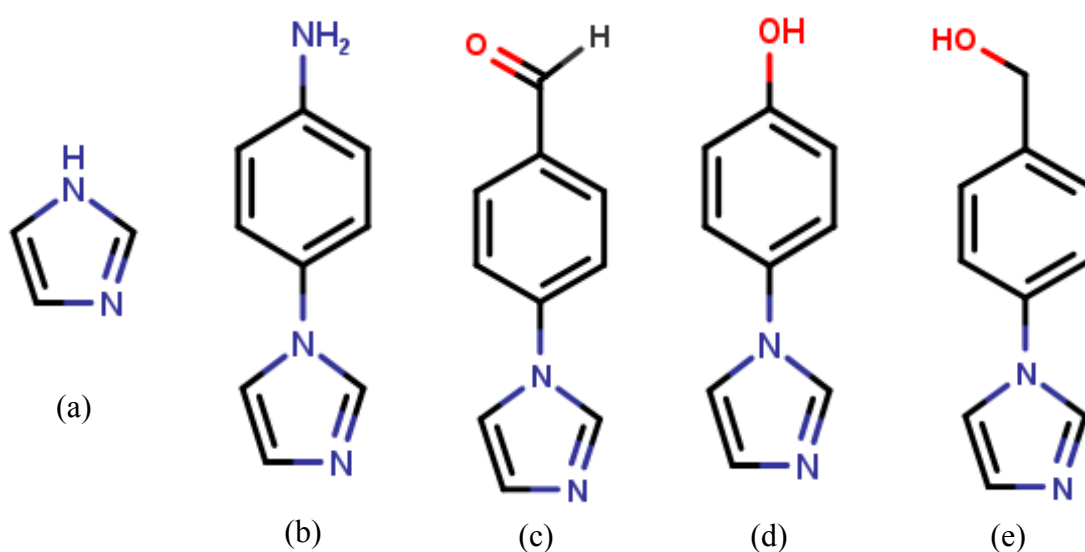
This is attributed to the heteroatoms of these substituents which tend to create a coordination compound between the corrosion inhibitor and the metallic surface, improving to the adsorption of molecules on the metal surface (MARINESCU; CHEMISTRY, 2019). In this context, the understanding of the interactions between the corrosion inhibitor and the metallic surface at a microscopic level has great importance for corrosion inhibition researchers since one knows which molecular or electronic properties could be related to corrosion inhibition, making it possible to correlate the calculated molecular properties with experimental data, such as  $\epsilon_{inh}$ , for proposing chemical modifications of the molecule to synthesise new molecules with better corrosion inhibition performance (MARINESCU; CHEMISTRY, 2019). In recent years, the so-called computational chemistry has been present in research not only on the subject of corrosion inhibitors but also in the chemistry of materials such as the use of machine learning tools to study failures in metallic structures (LOURENÇO et al., 2020) or even using the *ab initio* method based on density functional theory (DFT) methodology, which uses quantum mechanics to determine molecular properties to evaluate macroscopic phenomena such as adsorption of inhibitor at the electrode/solution interface (NJOKU; OGUZIE; LI, 2017). Thus, the correlation between experimental results and theoretical calculations allows deepening the physical and chemical understandings of the phenomenon of corrosion inhibition (CHAOUIKI et al., 2018).

Therefore, the aim of this investigation is the application of imidazole-based compounds towards  $Cu^0$  corrosion inhibition in an acidic medium and correlating these experimental data with *in silico* analysis of the inhibitor molecules by using DFT methods.

### 3.2 Details Experimental

All chemicals were purchased from Sigma-Aldrich and used as received, without any further purification or separation. The 2D representations of investigated molecules are shown in Figure 1.

Figure 1 - 2D chemical representations of imidazole\_IM (a), 4-(1H-Imidazol-1-yl)aniline\_IA (b), 4-(1H-imidazol-1-yl)benzaldehyde\_IB (c), 4-(1H-imidazol-1-yl)phenol\_IF (d) and (4-(1H-imidazol-1-yl)phenyl)methanol\_IFM (e).



Source: Author

#### 3.2.1 Electrochemical experiments

Electrochemical techniques, such as open circuit potential monitoring ( $E_{oc}$ ), Linear Potentiodynamic Polarization (LPP) and Electrochemical Impedance Spectroscopy (EIS), were used to assess the performance of the imidazole and its derivatives as inhibitors of the  $\text{Cu}^0$  corrosion  $0.5 \text{ mol L}^{-1} \text{ H}_2\text{SO}_4$ . All electrochemical experiments were carried out in a conventional three-electrode connected to Autolab PGSTAT 302N potentiostat/galvanostat from Metrohm<sup>®</sup> (Utrecht, The Netherlands) and controlled by Metrohm<sup>®</sup> NOVA<sup>®</sup> 2.1.4 software (Utrecht, The Netherlands), which allows the acquisition of experimental data and further treatment and analysis. The working electrode was a  $\text{Cu}^0$  disk embedded in glass tubes with epoxy resin and with a disk exposed area of approximately  $0.18 \text{ cm}^2$ . The

counter electrode was a platinum plate with an area of  $1.13 \text{ cm}^2$  and the reference electrode was  $\text{Ag}_{(\text{s})}/\text{AgCl}_{(\text{s})}/\text{Cl}^-$  (aq., saturated KCl). All solutions used in this investigation were prepared with water purified by the Milli-Q system (Darmstadt, Germany).

Prior to the electrochemical corrosion tests, the  $\text{Cu}^0$  surface was submitted to a sanding process with silicon carbide (SiC) sandpapers with 100, 220, 400, and 600 mesh granulations. After, the  $\text{Cu}^0$  surface was washed with water. Finally, the samples were immersed in a  $0.5 \text{ mol L}^{-1} \text{ H}_2\text{SO}_4$  aerated solution and in the absence (blank solution) and presence of the imidazole-based compounds in the following concentrations:  $0.1 \times 10^{-3} \text{ mol L}^{-1}$ ,  $0.25 \times 10^{-3} \text{ mol L}^{-1}$ ,  $0.5 \times 10^{-3} \text{ mol L}^{-1}$  and  $1 \times 10^{-3} \text{ mol L}^{-1}$ . The impedance data were obtained at  $E_{oc}$  and after 1 hour of immersion of the  $\text{Cu}^0$  in the testing solution. The frequency ranged between 20 kHz to 6 mHz and a potential amplitude of 10 mV was applied. The PP curves were obtained at the concentration of  $1 \times 10^{-3} \text{ mol L}^{-1}$ , after 1 hour of immersion time, and the potential was swept between  $\pm 300 \text{ mV}$  around the  $E_{oc}$  value, and the scan rate used was  $1 \text{ mV s}^{-1}$ . All electrochemical experiments were carried out at the laboratory room temperature ( $\approx 25^\circ \text{C}$ ) in triplicate.

### 3.2.2 Computational calculations

The input files were prepared using the GaussView 5.0 (DENNINGTON; KEITH; MILLAM, 2009) software and all the calculations were done using the Gaussian 09 software. Since the acidic medium was used in the experimental tests, the DFT calculations were carried out considering that all molecules were protonated.

To make a proper theoretical-experimental model, the inhibitor molecules were optimized using the Minnesota 06 hybrid meta exchange-correlation functional (M06-2X) with the 6-311++G(d,p) basis set (DITCHFIELD; HEHRE; POPL, 1971; ZHAO; TRUHLAR, 2008). All molecules were submitted for calculation with water as implicit solvent by the solvation method IEF-PCM (CANCÈS; MENNUCCI; TOMASI, 1997; MENNUCCI; CANCÈS; TOMASI, 1997). The isosurfaces of the frontier molecular orbitals (FMO) were rendered using the trial version of the ChemCraft software (ZHURKO, 2014).

Then, the global quantum reactivity descriptors were calculated from the energy values of the highest occupied molecular orbital (HOMO) and lowest unoccupied molecular orbital (LUMO): the energy gap ( $\Delta G_{\text{ads}}$ , Eq.1) (PEARSON, 1963b), the

ionization potential (IP, Eq.2) (Koopmans, 1934), the electron affinity (A, Eq.3) (Koopmans, 1934), the electronegativity ( $\chi$ , Eq.4) (Chermette, 1999; Iczkowski; Margrave, 1961), the global hardness ( $\eta$ , Eq.5) (Janak, 1978; Pearson, 1987b; Von Szentpály, 1991a), the global softness (S, Eq.6) (Yang; Parr, 1985b), the global electrophilicity index ( $\omega$ , Eq.7) (Parr; Szentpály; Liu, 1999a), the global nucleophilicity index ( $\varepsilon$ , Eq.8) (Chattaraj; Giri; Duley, 2011), and fraction of transferred electrons ( $\Delta N$ , Eq.9) (Obot; MacDonald; Gaseem, 2015a). For the  $\text{Cu}^0$  metallic bulk, it can be classified as soft ( $\eta_M=0$ ) (Dewar et al., 1985b) and its electronegativity has the value of 4.68 eV (Michaelson, 1977a). Finally, to create a local reactivity characterization map, the electronic Fukui functions for the nucleophilic ( $f^+$ ) and the electrophilic ( $f^-$ ) attack obtained from the Multiwfn software (Lu; Chen, 2012) and the Molecular Electrostatic Potential (MEP) were calculated using the M06-2X/6-311++G(d,p) computational level and the isosurfaces were rendered by the VESTA (Momma; Izumi, 2011) and Gabedit (Allouche, 2011) software respectively.

$$\Delta E_{GAP} = E_{LUMO} - E_{HOMO} \quad (\text{Eq.1})$$

$$IP = - E_{HOMO} \quad (\text{Eq.2})$$

$$A = - E_{LUMO} \quad (\text{Eq.3})$$

$$\chi = \frac{I+A}{2} \quad (\text{Eq.4})$$

$$\eta = \frac{I-A}{2} \quad (\text{Eq.5})$$

$$S = \frac{1}{\eta} \quad (\text{Eq.6})$$

$$\omega = \frac{\chi^2}{2\eta} \quad (\text{Eq.7})$$

$$\varepsilon = \frac{1}{\omega} \quad (\text{Eq.8})$$

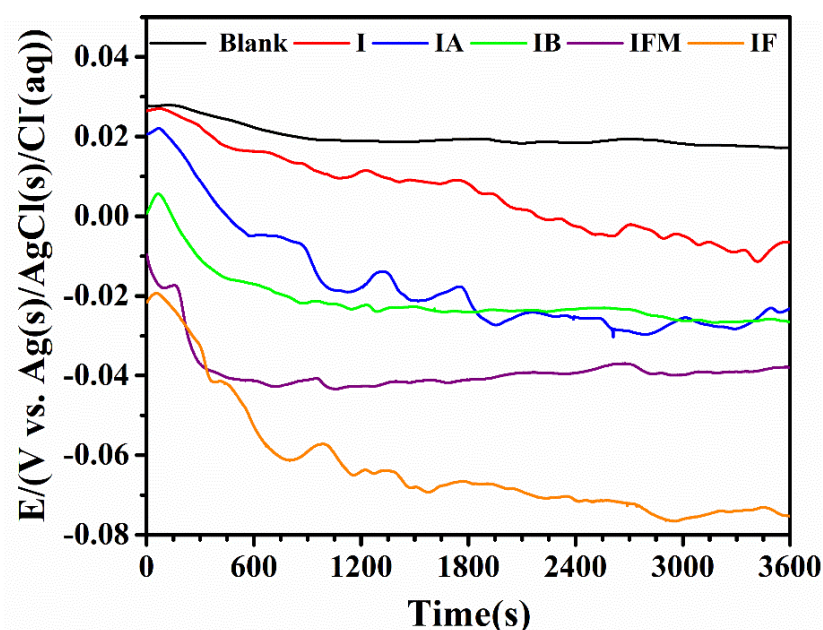
$$\Delta N = \frac{\chi_M - \chi_{inh}}{2(\eta_M + \eta_{inh})} \quad (\text{Eq.9})$$

### 3.3 Results and discussion

#### 3.3.1 Electrochemical Studies

Figure 2 shows the evolution of the  $E_{oc}$  values with the immersion time of the  $\text{Cu}^0$  electrode in  $0.5 \text{ mol L}^{-1} \text{ H}_2\text{SO}_4$  solution. Considering the blank solution, the  $E_{oc}$  values showed a slight shift towards more negative potential (from 27 mV to 19 mV), followed by the formation of a potential plateau after 900 s. Other solutions containing imidazole-based compounds had their  $E_{oc}$  values more negative if compared with blank solution. Furthermore, it can be noted that for all investigated corrosion inhibitors, the  $E_{oc}$  values shift towards more negative, and the stabilization period of 1 h was enough to reach a steady state (MIHAJLOVIĆ et al., 2017). This shows that imidazole and its derivatives probably have a greater inhibitory effect on the cathodic reaction than the anodic reaction of the  $\text{Cu}^0$  corrosion (DHOUIBI et al., 2021). This phenomenon is explained by the adsorption of the imidazole-based molecules on the active sites on the  $\text{Cu}^0$  surface, changing the oxygen concentration at the electrode/solution interface (DHOUIBI et al., 2021; JMIAI et al., 2018; TAN et al., 2019a).

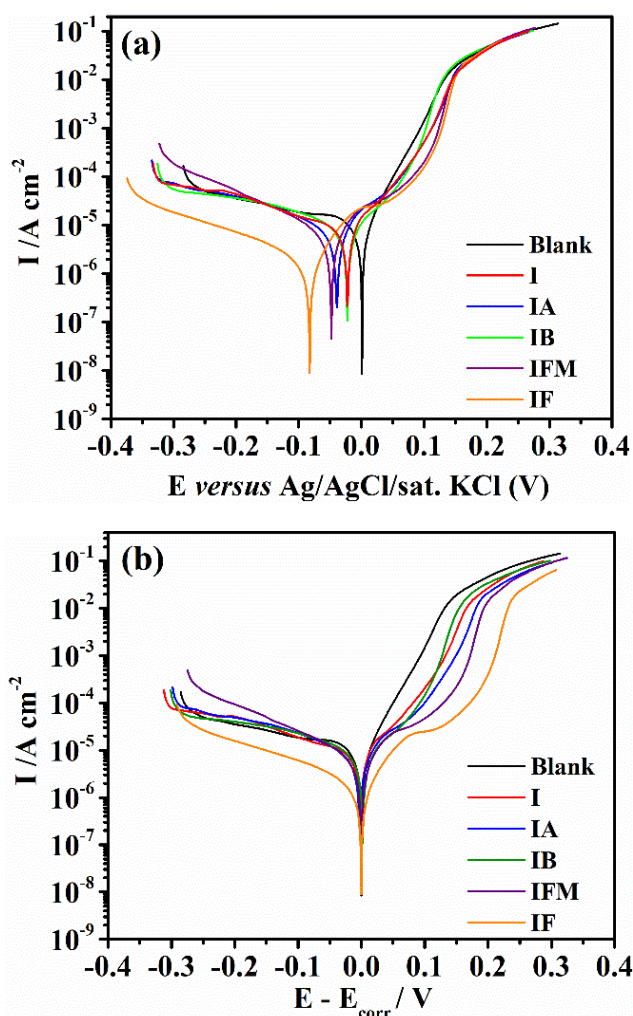
Figure 2 - Variation of the open circuit potential with the immersion time of Cu in  $0.5 \text{ mol L}^{-1} \text{ H}_2\text{SO}_4$ . These measurements were carried out at laboratory room temperature ( $\approx 25^\circ\text{C}$ ) and in the presence and absence (blank) of triazole-based compounds at  $1 \times 10^{-3} \text{ mol}$ .



Source: Author

Potentiodynamic polarization curves obtained for  $\text{Cu}^0$  in aerated  $0.5 \text{ mol L}^{-1} \text{H}_2\text{SO}_4$  solution in the presence and absence of the imidazole-based compounds are shown in Figure 3. Figure 3a shows that the corrosion potentials ( $E_{\text{corr}}$ ) for imidazole-based compounds are shifted towards more negative values in comparison to the blank curve, as seen in Figure 2. In addition, the cathodic branches of all curves showed a tendency to reach a current density plateau, indicating that the predominant cathodic reaction on  $\text{Cu}^0$  surface in  $\text{H}_2\text{SO}_4$  medium is the oxygen reduction reaction (ORR) (ZHOU et al., 2020). Thus, the shifting of the  $E_{\text{corr}}$  towards more negative values in the presence of the imidazole based compounds was attributed to the inhibition of the ORR related to the adsorption of the investigated molecules blocking the cathodic sites of  $\text{Cu}^0$  electrode.

Figure 3 - Potentiodynamic polarization curves obtained for  $\text{Cu}^0$  in  $0.5 \text{ mol L}^{-1} \text{H}_2\text{SO}_4$  medium in the absence (blank) and presence of imidazole-based compounds at  $1 \times 10^{-3} \text{ mol L}^{-1}$ . All curves were achieved at laboratory room temperature ( $\approx 25^\circ \text{C}$ ).



Source: Author

Two distinct regions (from 0.0 to 0.15 V and from 0.15 to 0.30V) can be seen in the anodic branch from blank solution (Figure 3) which suggest that Cu<sup>0</sup> corrodes in aerated 0.5 mol L<sup>-1</sup> H<sub>2</sub>SO<sub>4</sub> by two different dissolution pathways through two intermediates, Cu<sup>I</sup><sub>ads</sub> and Cu<sup>II</sup><sub>ads</sub>, as described by Cordeiro *et al* (CORDEIRO; BARCIA; MATTOS, 1993). The mechanism proposed by Cordeiro *et al* (CORDEIRO; BARCIA; MATTOS, 1993) was described by the electrochemical reactions Eq. 10 to 13. According to this mechanism, near the corrosion potential only Cu<sup>I</sup><sub>ads</sub> species are present and the copper electrodisolution occurs via k<sub>2</sub>. For higher anodic overpotentials the second electrodisolution path (k<sub>4</sub>) becomes important and Cu<sup>II</sup><sub>ads</sub> species predominates on the copper surface. Finally, since the electrochemical impedance measurements were obtained at open circuit potential, we will consider the dissolution to Cu<sup>II</sup><sub>sol</sub> only through Cu<sup>I</sup><sub>ads</sub> (k<sub>2</sub>), followed by its diffusion to the solution.

The addition of all corrosion inhibitors decreased the anodic density current. Initially, there is the formation of the cuprous ion on the Cu<sup>0</sup> surface (Cu<sup>I</sup><sub>ads</sub>, Eq.10), which is adsorbed on the surface of the electrode as described by Mattos and coworkers (CORDEIRO; BARCIA; MATTOS, 1993). In the absence of the imidazole-based compounds, Cu<sup>I</sup><sub>ads</sub> ion is oxidized to a cupric ion (Cu<sup>II</sup><sub>ads</sub>, Eq.11), observed for the Cu<sup>0</sup> dissolution in the blank solution. In presence of the imidazole-based molecules, the Cu<sup>I</sup><sub>ads</sub> ion reacts with the inhibitor (I<sub>nh</sub>) to form a complex film adsorbed on the Cu<sup>0</sup> surface (Eq.14), which acts as a physical barrier that alters the Cu<sup>0</sup> dissolution kinetics, causing the non-occurrence of the Tafel's relationship in the anodic curves. Finally, the Figure 3b shows that both values of the cathodic and anodic current densities obtained in the presence of the corrosion inhibitors are smaller compared to those obtained in the absence of the imidazole derivatives, showing that the both ORR and Cu<sup>0</sup> dissolution are inhibited by the studied imidazole-based compounds.



Since the Tafel extrapolation method cannot be applied to determine the corrosion current, the  $\varepsilon_{inh}$  values were calculated from the polarization resistance ( $R_p$ ) values derived from the potentiodynamic polarization curves using the Eq.15 (ZHANG et al., 2020). In this equation,  $R_p^0$  is the polarization resistance obtained from blank solution and  $R_p$  is the corresponding value obtained from the solutions containing the imidazole-based molecules.

$$\varepsilon_{inh} = \left(1 - \frac{R_p}{R_p^0}\right) \times 100 \quad (\text{Eq.15})$$

The corrosion parameters calculated from mathematical analyses of the potentiodynamic polarization curves are displayed in Table 1. Regarding  $E_{corr}$  values, all potential shifts were lower than 85 mV, which can classify imidazole and its derivatives as mixed inhibitors with cathodic efficiency predominantly (MESSALI et al., 2018). According to the  $R_p$  values, it is possible to verify that imidazole and its derivatives favored the inhibition of  $\text{Cu}^0$  dissolution and that the  $\varepsilon_{inh}$  followed the following sequence: IF > IFM > IB > IA > IM. Therefore, all imidazole-based molecules are more efficient in the inhibition of the  $\text{Cu}^0$  dissolution compared to the imidazole molecule.

Table 1 - Electrochemical parameters obtained for  $\text{Cu}^0$  corrosion in  $0.5 \text{ mol L}^{-1} \text{H}_2\text{SO}_4$  medium in the absence and presence of imidazole-based compounds at  $1 \times 10^{-3} \text{ mol L}^{-1}$ .

|              | $E_{corr} \text{ (mV)}^a$ | $R_p \text{ (k}\Omega \text{ cm}^2)^b$ | $\varepsilon_{inh} \text{ (\%)}^c$ |
|--------------|---------------------------|--|------------------------------------|
| <b>Blank</b> | $0.08 \pm 0.01$           | $10.91 \pm 0.19$                       | -                                  |
| <b>IM</b>    | $-22 \pm 0.01$            | $16.58 \pm 0.12$                       | $52.04 \pm 0.09$                   |
| <b>IA</b>    | $-39 \pm 0.02$            | $19.47 \pm 0.09$                       | $78.57 \pm 0.02$                   |
| <b>IB</b>    | $-22 \pm 0.03$            | $19.54 \pm 0.11$                       | $79.21 \pm 0.05$                   |
| <b>IFM</b>   | $-50 \pm 0.01$            | $19.85 \pm 0.04$                       | $82.05 \pm 0.03$                   |
| <b>IF</b>    | $-86 \pm 0.02$            | $21.17 \pm 0.07$                       | $94.07 \pm 0.10$                   |

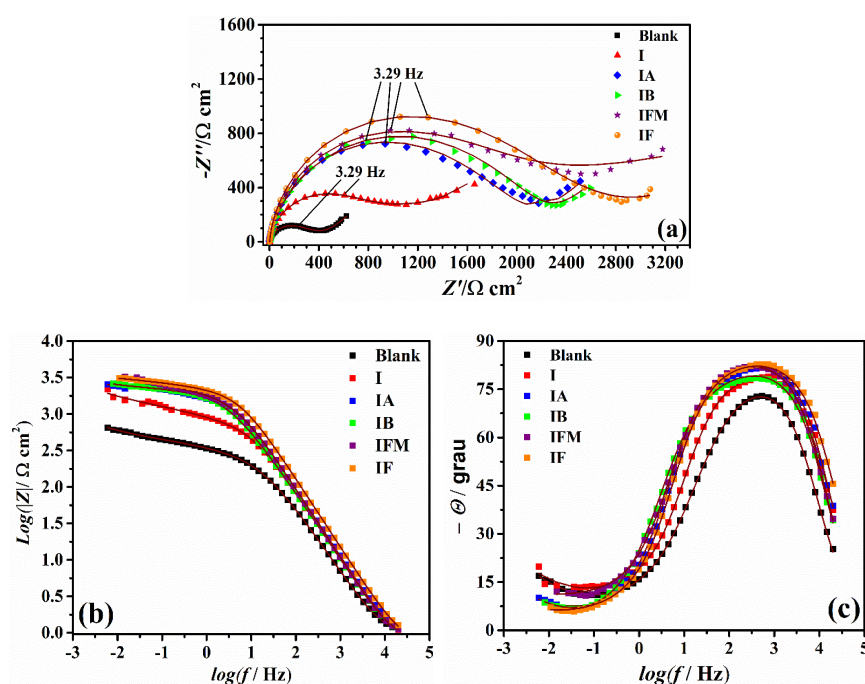
<sup>a</sup>Corrosion potential; <sup>b</sup>Polarization resistance; <sup>c</sup>Inhibition efficiency  
Source: Author

To obtain more information regarding the behavior of inhibitors on the surface of the  $\text{Cu}^0$  electrode, EIE measurements were performed in  $0.5 \text{ mol L}^{-1} \text{H}_2\text{SO}_4$  medium, in the



absence and presence of imidazole derivatives at  $1 \times 10^{-3} \text{ mol L}^{-1}$ , as shown in Figure 4. In Figure 4a, it is possible to observe that all Nyquist curves show one capacitive semicircle in the high-frequency region, followed by a straight line in the low-frequency region (FENG et al., 2018). This straight line is known as Warburg impedance, and it could be associated with the ORR due to the diffusion of the dissolved gas from the solution to the  $\text{Cu}^0$  surface (GAO et al., 2020) and to the diffusion of the  $\text{Cu}^{\text{II}}$  species towards the solution. Since the oxygen dissolved in the electrolyte interacts with  $\text{Cu}^0$  surface, there is an adsorption of the molecule of oxygen gas in the active sites of the electrode, promoting their corrosion. In this context, there is a competition between oxygen gas and inhibitor on the surface of the electrode, and the capacitive arcs achieved for the imidazole and all imidazole derivatives are larger compared to that obtained in the absence of these molecules, indicating that all tested molecules promote an increase in the charge transfer resistance of the  $\text{Cu}^0$  dissolution. The adsorption of the corrosion inhibitors on the  $\text{Cu}^0$  surface becomes a barrier that leads to the inhibition of its kinetics by the blockage of the anodic active sites (FENG et al., 2020).

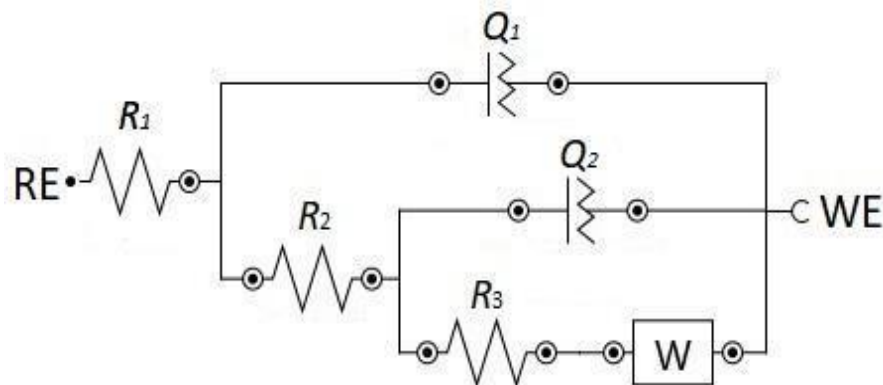
Figure 4 - Nyquist (a) and Bode (b,c) plots obtained for  $\text{Cu}^0$  after 1h of immersion in  $0.5 \text{ mol L}^{-1} \text{ H}_2\text{SO}_4$  in the absence and presence of imidazole and its derivatives at  $1 \times 10^{-3} \text{ mol L}^{-1}$ . All diagrams were obtained at room temperature of the laboratory ( $\approx 25^\circ\text{C}$ ). The solid lines represent the impedance simulation carried out by the equivalent circuit shown in Figure 5.



Source: Author

Figure 4b and 4c show the typical Bode plots obtained for the studied systems. In Figure 4b, it can be noted that the impedance module increased by one order of magnitude in the low-frequency region compared to the blank solution, confirming that the derivatives are efficient against  $\text{Cu}^0$  corrosion in the  $\text{H}_2\text{SO}_4$  medium (TAN et al., 2019b). In addition, in Figure 4c, all phase angle plots display a maximum extension of approximately  $80^\circ$  in the high-frequency region, suggesting the formation of a layer on the  $\text{Cu}^0$  surface (TAN et al., 2018; ZHOU et al., 2020).

Since the capacitive arcs observed in the Nyquist diagrams (Figure 4a) are related to two coupled processes, the equivalent electric circuit shown in Figure 5 was used to fit all impedance data (GAO et al., 2020; GONG et al., 2018; GUO et al., 2020; XU et al., 2015). In this circuit,  $R_1$  is the resistance of the solution,  $R_2$  is the resistance of the chemical species adsorbed on the  $\text{Cu}^0$  surface,  $R_3$  is the charge transfer resistance;  $W$  is the Warburg impedance;  $Q_1$  is the element film phase constant, and  $Q_2$  is the double layer phase constant elemento (LI et al., 2020). The phase constant element ( $Q$ ) is used to replace the capacitance in the equivalent electrical circuits since the surface presents irregularities or roughness due to the adsorption of the imidazole derivatives (MENDONÇA et al., 2017). All impedance parameters derived from equivalent electric circuit analyses are listed in Table 2 and the  $\varepsilon_{\text{inh}}$  values were calculated according to Eq.15, where  $R_p^0$  ( $R_p^0 = R_2^0 + R_3^0$ ) is the polarization resistance obtained from the blank solution, while  $R_p$  ( $R_p = R_2 + R_3$ ) is the polarization resistance in the presence of the inhibitor. For instance, Table 2 shows the electrochemical data retrieved from the following equivalent circuits in Figure 5.



Source: Author

Figure 5 - Drawing of the equivalent electrical circuit used to fit the EIS diagrams.

Table 2 - Fitted values from applied equivalent circuit shown in Figure 4 and inhibition efficiency obtained from fitted data. The constant phase element was converted to pseudocapacitance using the Brug method.

| Inhibitor    | $R_2 / \Omega \text{ cm}^2$ <sup>a</sup> | $C_1 \times 10^7 / \text{F cm}^{-2}$ <sup>b</sup> | $R_3 / \Omega \text{ cm}^2$ <sup>c</sup> | $C_2 \times 10^7 / \text{F cm}^{-2}$ <sup>d</sup> | $W_{\text{diff}} / \Omega \text{ cm}^2$ <sup>e</sup> | $\epsilon_{\text{inh}} (\%)$ <sup>f</sup> |
|--------------|--|---|--|---|--|---|
| <b>Blank</b> | $367.72 \pm 1.86$                        | $2.04 \pm 0.97$                                   | $132.24 \pm 7.90$                        | $1.99 \pm 0.23$                                   | $3.20 \pm 0.02$                                      | ---                                       |
| <b>IM</b>    | $936.44 \pm 7.20$                        | $8.90 \pm 2.47$                                   | $64.10 \pm 4.27$                         | $8.92 \pm 5.54$                                   | $2.54 \pm 0.04$                                      | 50.03                                     |
| <b>IA</b>    | $1868.22 \pm 4.79$                       | $4.59 \pm 0.17$                                   | $363.60 \pm 24.18$                       | $4.44 \pm 0.28$                                   | $1.58 \pm 0.01$                                      | 77.60                                     |
| <b>IB</b>    | $2127.63 \pm 4.23$                       | $3.32 \pm 0.89$                                   | $289.38 \pm 23.30$                       | $3.28 \pm 0.26$                                   | $1.57 \pm 0.03$                                      | 79.32                                     |
| <b>IFM</b>   | $2175.60 \pm 9.41$                       | $4.61 \pm 0.41$                                   | $277.47 \pm 7.01$                        | $4.54 \pm 0.49$                                   | $1.13 \pm 0.09$                                      | 79.62                                     |
| <b>IF</b>    | $2281.86 \pm 7.64$                       | $4.30 \pm 0.04$                                   | $353.02 \pm 9.71$                        | $4.22 \pm 0.36$                                   | $1.02 \pm 0.01$                                      | 81.03                                     |

<sup>a</sup>Charge transfer element for  $R_2$ ; <sup>b</sup>Pseudocapacitance from double layer; <sup>c</sup>Charge transfer element for  $R_3$ ; <sup>d</sup>Pseudocapacitance for electrode surface; <sup>e</sup>Diffusion impedance; <sup>f</sup>Inhibition efficiency.

Source: Author

Table 2 shows a significant increase in  $R_2$  values for all imidazole derivatives, confirming that the adsorption of compounds on the  $\text{Cu}^0$  surface prevents the charge transfer process (BRUG et al., 1984; HSU; MANSFELD, 2001; MENDONÇA et al., 2017). Since  $R_2$  represents the double layer resistance from electrode/solution interface,  $Q_1$  also represents the charge distribution in this region. Aiming a better representation for constant phase data, the Hsu and Mansfeld (HSU; MANSFELD, 2001) and Brug et al. (BRUG et al., 1984) models for pseudocapacitance conversion were applied for  $Q_1$  and  $Q_2$  values to, respectively,  $C_1$  and  $C_2$  values, as shown in equations 16-17 (BRUG et al., 1984; HSU; MANSFELD, 2001). In these equations, the resistance of the electrolyte ( $R_1$ ), the charge transfer resistance of the  $\text{Cu}^0$  electrode ( $R_2$ ), the admittance values ( $Y_o$ ) of  $Q_1$  and  $n$  correspond to the values derived from the electrochemical fit.

$$C_1 = Y_o^n R_1^{\frac{1-n}{n}} \quad (\text{Eq.16})$$

$$C_2 = Y_o^n \left( \frac{R_1 \times R_2}{R_1 + R_2} \right)^{\frac{1-n}{n}} \quad (\text{Eq.17})$$

In addition, Table 2 also shows that the  $R_2$  values increased in the following order:  $IM < IA < IB < IFM < IF$ , while  $R_3$  values do not followed any trend. Moreover,  $C_1$  and  $C_2$  followed an inverse trend of charge density. This behavior can be attributed to the replacement of  $H_2O$  molecules on the electrode surface by molecules of imidazole derivatives (LUO et al., 2020). In addition, the diffusion impedance fitted from Warburg element circuit decreased in the same trend from  $R_2$ . This effect suggests a blockage of the active surface area of  $Cu^0$  electrode, and the modified imidazole molecules diminishes the  $Cu^{II}$  diffusion towards solution and that also hinders the oxygen adsorption on  $Cu^0$  surface. The classical Warburg semi-infinite diffusion depends upon the surface coverage, as shown in equations 18 and 19 (ORAZEM; TRIBOLLET, 2008).

$$Z_{diff} = \sigma \omega^{-\frac{1}{2}} (1 - j) \quad (\text{Eq.18})$$

In Eq.18,  $Z_{diff}$  is the impedance of the Warburg element,  $\sigma$  is the Warburg coefficient  $\tau$  is the applied frequency and  $j$  is equal to  $-1^{1/2}$ . The Warburg coefficient for a particular situation which the diffusion of reduced and oxidized species is the same is shown in Eq.19.

$$\sigma = \frac{RT}{AF^2 \sqrt{2DC}} \frac{1}{\theta} \quad (\text{Eq.19})$$

In Eq.19,  $R$  is the universal gas constant,  $T$  the absolute temperature,  $A_s$  the active electrode area,  $F$  the Faraday's constant,  $C$  the concentration of the electrochemical species,  $D$  the diffusion coefficient and  $\theta$  the surface coverage of the electrode. Since the Warburg coefficient is inversely proportional to the surface coverage, this means that the increase of the surface coverage by the inhibitors molecules leads to a decreased the corresponding  $\sigma$  values and, consequently, the diminishing of  $Z_{diff}$  occurs due to  $\sigma$  decrease. For instance, the equivalent impedance equation for this electrochemical system is shown in Eq.20, which represents the equivalent impedance equation for the electric circuit shown in Figure 5.

When  $Z_{diff} \rightarrow 0$ ,  $\frac{1}{R_3 + Z_{diff}} \rightarrow \frac{1}{R_3}$ , and  $Z_{eq}$  equation tends to be like a double RC equivalent circuit equation, given by Eq.21:

$$Z_{eq} = R_1 + \frac{1}{j\omega C_1 + \frac{1}{R_2}} + \frac{1}{j\omega C_2 + \frac{1}{R_3 + Z_{diff}}} \quad (\text{Eq.20})$$

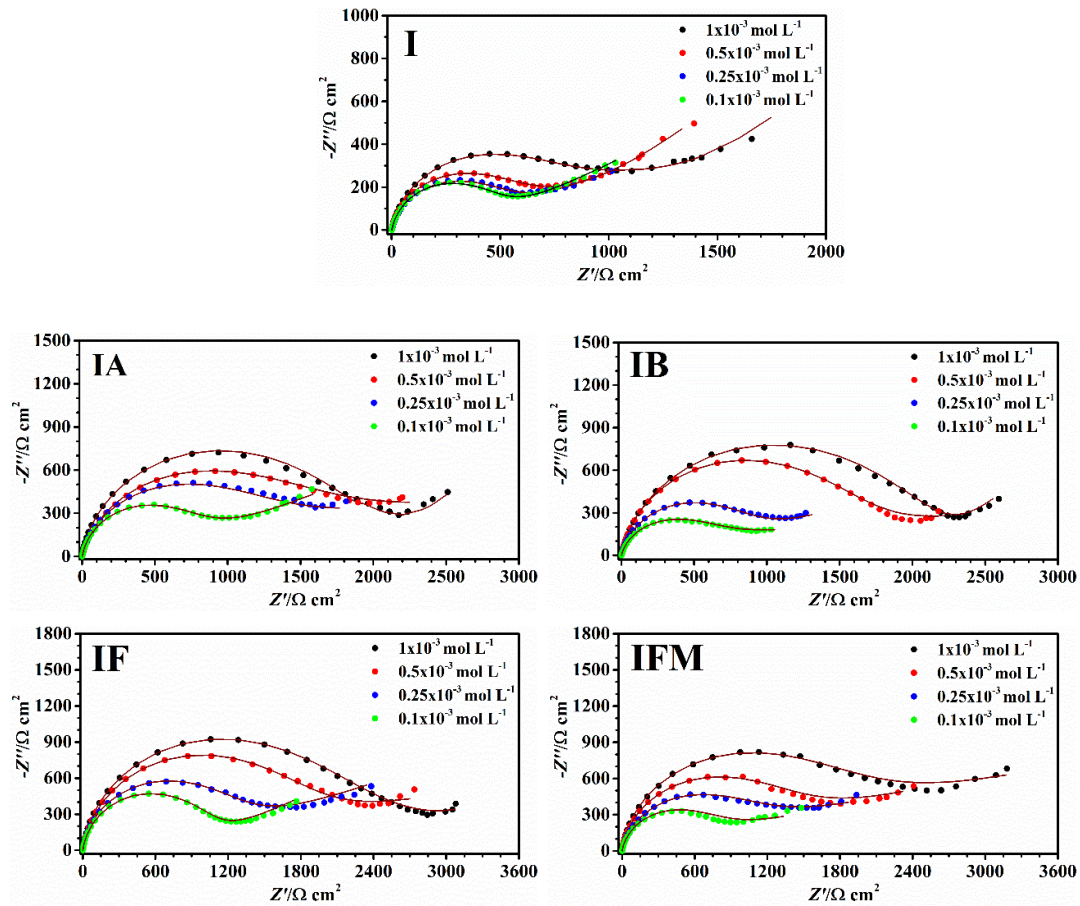
$$Z_{eq} = R_1 + \frac{1}{j\omega C_1 + \frac{1}{R_2}} + \frac{1}{j\omega C_2 + \frac{1}{R_3}} \quad (\text{Eq.21})$$

In an electrochemical application of equation  $Z_{eq}$  in the presented electrochemical cell, the corrosion of  $\text{Cu}^0$  in  $\text{H}_2\text{SO}_4$  0.5 mol  $\text{L}^{-1}$  solution is inhibited by the imidazole-modified molecules and, consequently, the diffusion of  $\text{Cu}^{\text{II}}$  ions does not occur, unlike in blank and IM Bode plots in Figure 4b. In this context, the Bode plots for modified imidazole molecules tend to behave like a pure resistor, in contrast with a blank solution. This behavior agrees with literature showing the effect of inhibitor adsorption over the electrode surface, which hinders the diffusion of  $\text{Cu}^{\text{II}}$  ions to the bulk solution (TAN et al., 2018). The  $\varepsilon_{inh}$  was calculated from Eq. 15, with values greater than 75%, with 81.03% being the highest value obtained for the IF. Thus, as well as the inhibition efficiency determined by the PP technique, the EIS technique presented the same sequence as before: IF > IFM > IB > IA > IM.

### 3.3.2 Adsorption Isotherm

To understand the nature of adsorption process of the inhibitors, EIS measurements were performed with the variation of the concentration for imidazole and its derivatives and the obtained Nyquist plots are shown in Figure 6. In addition, EIS parameters derived from these Nyquist diagrams using the equivalent electric circuit, shown in Figure 5, are displayed in Table 3.

Figure 6 - Nyquist diagrams obtained for  $\text{Cu}^0$  immersed in  $0.5 \text{ mol L}^{-1} \text{H}_2\text{SO}_4$  at different concentrations of the studied corrosion inhibitors and obtained at room temperature ( $\approx 25^\circ\text{C}$ ). The solid lines represent the adjust of the experimental data by the equivalent electric circuit shown in Figure 5.



Source: Author

It can be seen in Table 3 that the polarization resistance presents a gradual increase as the concentration of inhibitors increases in the solution. The surface coverage ( $\theta$ ), calculated from Eq. 22, increases as the inhibitor concentration increased. Thus, the Langmuir isotherm model (CHEN et al., 2019) was applied according to the Eq. 23. In Eq. 22,  $C_{\text{inh}}$  is the inhibitor concentration and  $K_{\text{ads}}$  is the equilibrium constant for the adsorption/desorption process. The isotherm plots of the studied inhibitors are shown in Figure 7.

Table 3 – EIS parameters derived from the Nyquist plots shown in Figure 6.

|                    | $C_{inh} / 10^{-3} \text{ mol L}^{-1}$ | $R_p / \Omega \text{ cm}^2$ <sup>b</sup> | $\theta$ <sup>c</sup> |
|--------------------|--|--|-----------------------|
| <b>Blank soln.</b> | -                                      | $499.95 \pm 0.19$                        | -                     |
| <b>IM</b>          | 0.10                                   | $537.10 \pm 0.11$                        | $0.07 \pm 0.0$        |
|                    | 0.25                                   | $599.30 \pm 0.09$                        | $0.17 \pm 0.0$        |
|                    | 0.50                                   | $713.56 \pm 0.12$                        | $0.30 \pm 0.0$        |
|                    | 1.00                                   | $1000.56 \pm 0.13$                       | $0.50 \pm 0.0$        |
| <b>IA</b>          | 0.10                                   | $935.98 \pm 0.05$                        | $0.47 \pm 0.0$        |
|                    | 0.25                                   | $1380.96 \pm 0.12$                       | $0.64 \pm 0.1$        |
|                    | 0.5                                    | $1774.65 \pm 0.10$                       | $0.72 \pm 0.1$        |
|                    | 1.0                                    | $2231.82 \pm 0.13$                       | $0.78 \pm 0.1$        |
| <b>IB</b>          | 0.10                                   | $771.82 \pm 0.01$                        | $0.35 \pm 0.2$        |
|                    | 0.25                                   | $1073.75 \pm 0.23$                       | $0.53 \pm 0.1$        |
|                    | 0.5                                    | $1837.04 \pm 0.15$                       | $0.73 \pm 0.0$        |
|                    | 1.0                                    | $2416.98 \pm 0.17$                       | $0.79 \pm 0.1$        |
| <b>IFM</b>         | 0.10                                   | $948.46 \pm 0.15$                        | $0.47 \pm 0.1$        |
|                    | 0.25                                   | $1425.85 \pm 0.21$                       | $0.65 \pm 0.1$        |
|                    | 0.50                                   | $1852.39 \pm 0.12$                       | $0.73 \pm 0.1$        |
|                    | 1.0                                    | $2453.07 \pm 0.09$                       | $0.80 \pm 0.1$        |
| <b>IF</b>          | 0.10                                   | $1198.87 \pm 0.03$                       | $0.58 \pm 0.1$        |
|                    | 0.25                                   | $1567.30 \pm 0.02$                       | $0.68 \pm 0.1$        |
|                    | 0.50                                   | $2237.46 \pm 0.09$                       | $0.78 \pm 0.0$        |
|                    | 1.0                                    | $2634.88 \pm 0.09$                       | $0.81 \pm 0.1$        |

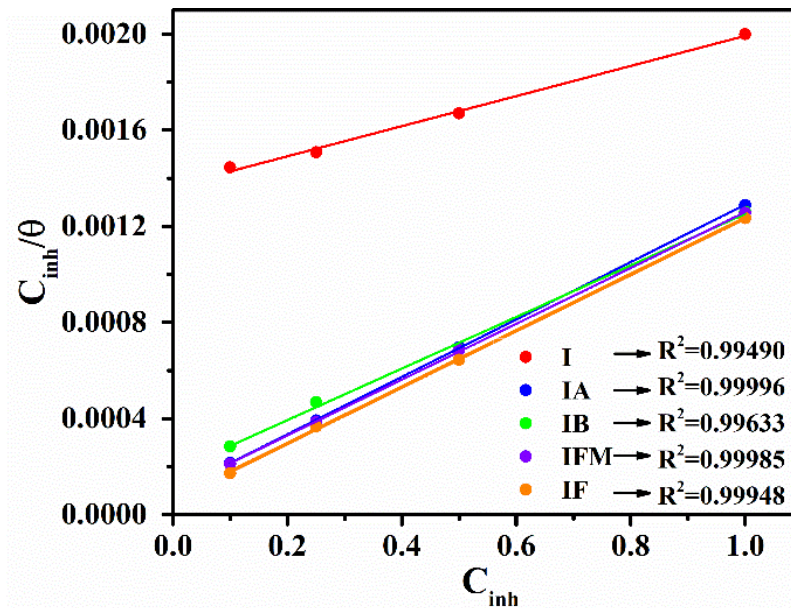
<sup>a</sup>Inhibition concentration; <sup>b</sup>Polarization resistance; <sup>c</sup>Surface coverage.

Source: Author

$$\theta = \left( \frac{R_p - R_p^0}{R_p} \right) \quad (\text{Eq.22})$$

$$\frac{C_{inh}}{\theta} = C_{inh} + \left( \frac{1}{K_{ads}} \right) \quad (\text{Eq.23})$$

Figure 7 - Langmuir's linear relationships obtained for the corrosion inhibition of  $\text{Cu}^0$  in  $0.5 \text{ mol L}^{-1} \text{H}_2\text{SO}_4$  solution in presence of imidazole and imidazole-based compounds.



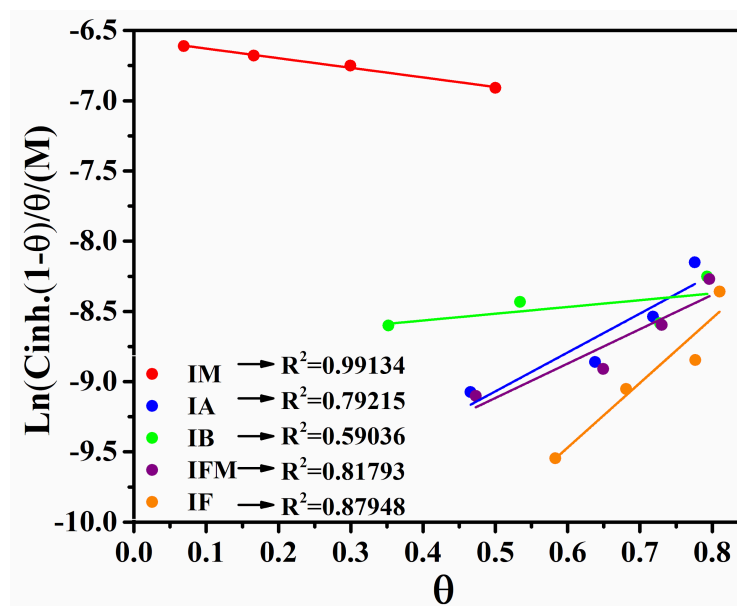
Source: Author

As can be seen in Figure 7, all isotherms are linear, which indicates that the inhibitors formed a monolayer on the substrate surface, effectively reducing the corrosion rate (MESSALI et al., 2018). This gives us the information that each active site is occupied by only one molecule of the derivatives that do not interact with each other (FARAHATI et al., 2019b). Except for the imidazole molecule, the adsorption isotherms obtained for the modified imidazole compounds have similar angular coefficient and intercept. From Langmuir boundary conditions, the adsorption sites are unique and individual for each molecule, and the adsorbate will not interact laterally with other adsorbent sites. Therefore, the Langmuir model indicates that modified imidazole molecules had the same adsorption behavior. Furthermore, the modified imidazole molecules have different lateral groups, therefore, it is expected the existence of lateral interactions between the adsorbed molecules that is not considered in the Langmuir model. Thus, the Frumkin isotherm model (QUIROZ et al., 1995) was applied using Eq.24 to evaluate the lateral interaction between the corrosion inhibitors molecules adsorbed on  $\text{Cu}^0$  surface, and the isotherm plots for each investigated corrosion inhibitor molecule are shown in Figure 8.

$$K_{ads} C_{inh} = \frac{\theta}{1-\theta} \exp \exp (-2b\theta) \quad (\text{Eq.24})$$



Figure 8 - Frumkin adsorption isotherms obtained for imidazole and its derivatives.

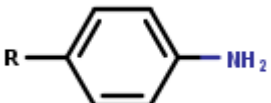
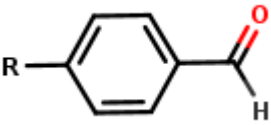
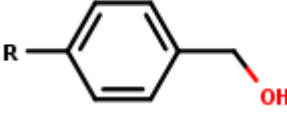
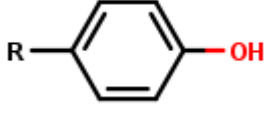


Source: Author

From Figure 8, it can be observed that for the Frumkin model, all isotherms are linear, and, except for the IM molecule, all the other molecules presented a positive slope, which is characteristic of lateral attractions during the adsorption process, while a negative slope stands for lateral repulsion between the adsorbed molecules (BASTIDAS; GÓMEZ; CANO, 2005; KOLEV et al., 2002), and Table 4 shows the fitted intermolecular factor changes regarding the molecular modification of imidazole molecule.

The molecular modification of the imidazole molecule brought the capacity of lateral interactions due to both polar and non-polar groups, which increased the capacity of those molecules to create a protective layer in the copper electrode in acidic medium and the decrescent order of the intermolecular factor is: IF > IA > IFM > IB > IM. Since lateral attractive interactions helps creating a protective layer of corrosion inhibitor molecule, the Frumkin isotherm suggest that the IM molecule is not an efficient corrosion inhibitor for Cu<sup>0</sup> in acidic medium due to the repulsion forces between the IM molecules adsorbed on Cu<sup>0</sup> surface.

Table 4 - Intermolecular factor from linearized Frumkin isotherm model from Figure 8 for lateral groups of the studied molecule inhibitors for copper in  $\text{H}_2\text{SO}_4$   $0.5 \text{ mol L}^{-1}$  solution.

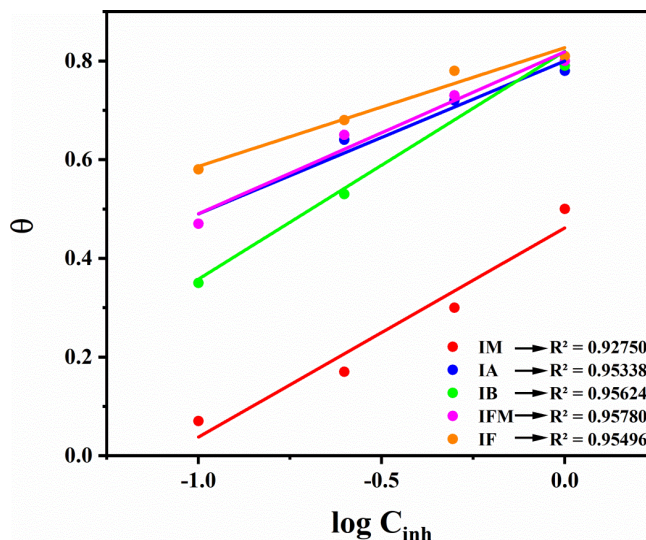
| Molecule | Intermolecular factor (b) | Lateral group  |
|----------|---------------------------|--|
| IM       | -0.68                     | $\text{R}-\text{H}$  |
| IA       | 2.77                      |    |
| IB       | 0.48                      |    |
| IFM      | 2.45                      |   |
| IF       | 4.60                      |  |

Source: Author

For comparison with other isotherms, a Temkin isotherm model was applied by using Eq.25, and the results are presented in Figure 9. In Eq.25,  $b$  is related to the heat of adsorption, while  $A$  is the Temkin adsorption constant. In Figure 9, the Temkin adsorption isotherm, in a qualitative way, showed to be like the Frumkin isotherms in Figure 8: the IFM and IA isotherms were close one to another, but except IB isotherm the other isotherms were parallel. Also, the  $R^2$  values were all greater than 0.9, which means that a strong linear correlation was achieved. Since there is a consideration of the adsorbent-adsorbent interactions, the adsorption enthalpy decreases when the surface coverage increases. In this context, the IF isotherm had the most surface coverage than other molecules, confirming its better corrosion protection towards the copper electrode.

$$\theta = b \ln A + b \ln C_{inh} \quad (\text{Eq.25})$$

Figure 9 - Temkin adsorption isotherms obtained for imidazole and its derivatives.



Source: Author

From the data obtained from the Langmuir and Frumkin isotherms, it was possible to obtain  $K_{ads}$  and, consequently, the free adsorption energy ( $\Delta G_{ads}$ ) of the compounds under study, by Eq.26, where  $\Delta G_{ads}$  is the adsorption energy,  $R$  is the real gas constant and  $T$  is the temperature in kelvin (CORRALES-LUNA et al., 2019). Finally, the computed data for both isotherm models are displayed in Table 5.

$$\Delta G_{ads} = - RT \ln (55.5 \times K_{ads}) \quad (\text{Eq.26})$$

Table 5 -  $K_{ads}$  and  $\Delta G_{ads}$  values for imidazole derivatives in 0.5 mol L<sup>-1</sup> H<sub>2</sub>SO<sub>4</sub> solution for Cu<sup>0</sup> surface.

| Molecules  | $K_{ads}$               | $\Delta G_{ads}$ (kJ mol <sup>-1</sup> ) | $K_{ads}$              | $\Delta G_{ads}$ (kJ mol <sup>-1</sup> ) |
|------------|-------------------------|--|------------------------|--|
|            | (Langmuir) <sup>a</sup> | (Langmuir) <sup>b</sup>                  | (Frumkin) <sup>c</sup> | (Frumkin) <sup>d</sup>                   |
| <b>IM</b>  | $7.30 \times 10^2$      | -26.29                                   | $7.06 \times 10^2$     | -26.21                                   |
| <b>IA</b>  | $3.94 \times 10^3$      | -30.47                                   | $3.45 \times 10^4$     | -35.85                                   |
| <b>IB</b>  | $5.60 \times 10^3$      | -31.34                                   | $6.37 \times 10^3$     | -31.66                                   |
| <b>IFM</b> | $1.03 \times 10^3$      | -32.85                                   | $3.10 \times 10^4$     | -35.57                                   |
| <b>IF</b>  | $1.61 \times 10^4$      | -33.96                                   | $2.05 \times 10^5$     | -40.26                                   |

<sup>a</sup>Adsorption constant from Langmuir isotherm model; <sup>b</sup>Gibbs energy from Langmuir isotherm model; <sup>c</sup>Adsorption constant from Frumkin isotherm model; <sup>d</sup>Gibbs energy from Frumkin isotherm model.

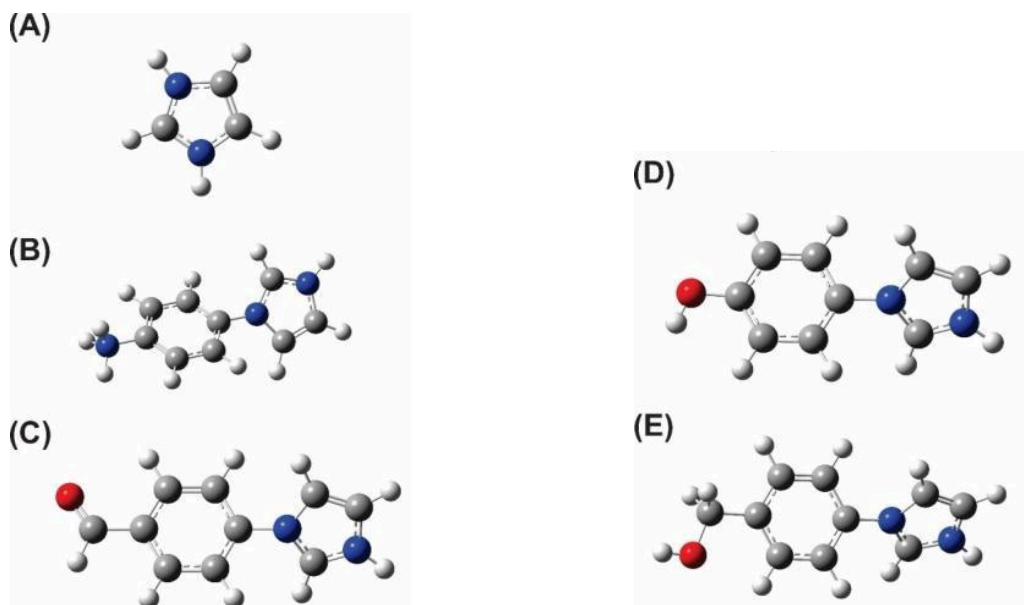
Source: Author

The data displayed in Table 5 show that the Langmuir model fits better the experimental results of the acid  $\text{Cu}^0$  corrosion inhibition in the acid medium by the tested imidazole-based compounds, since the  $K_{\text{ads}}$  value increases and the  $\Delta G_{\text{ads}}$  value shifts to more negative values in the same order of the  $\varepsilon_{\text{inh}}$  (Tables 1 and 2), while for the Frumkin model the order was not followed. In addition, the negative  $\Delta G_{\text{ads}}$  values ensure that the adsorption of inhibitors is a spontaneous process forming a stable layer. Moreover, it is known that  $\Delta G_{\text{ads}}$  values above  $-20 \text{ kJ mol}^{-1}$  are generally attributed to physisorption, that is, to electrostatic interactions between molecules and the electrode surface, while values more negative than  $-30 \text{ kJ mol}^{-1}$ , are attributed to adsorption by chemisorption, that is, to the electronic transfer between the molecules and the surface and, consequently, creating a chemical bond (QIANG et al., 2017b). Therefore, correlating  $\Delta G_{\text{ads}}$  (Table 5) with the  $\varepsilon_{\text{inh}}$  (Tables 1 and 2), it is possible to note that the  $\varepsilon_{\text{inh}}$  increase with the increase of the chemical character of the interaction between the corrosion inhibitor molecule with the  $\text{Cu}^0$  surface.

### 3.3.3 Computational results

The quantum chemical calculations were used to understand the charge transfer process between the candidate molecules for corrosion inhibitors in this work and the  $\text{Cu}^0$  metallic surface. In Figure 10, the optimized structures in water (implicit solvent) are shown using the M06-2X/6-311++G(d,p) computational level for molecules that are candidates for corrosion inhibitors. The simulated molecular structures are not entirely planar, as the aromatic ring is not in the same plane as the imidazole ring. The functional M06-2X predicted similar values for the dihedral angle between the aromatic ring and the imidazole ring:  $47.47^\circ$  (IA),  $45.16^\circ$  (IB),  $49.79^\circ$  (IF), and  $46.69^\circ$  (IFM). Structurally, the only difference between these molecules remains is the functional group bonded in the aromatic ring and the charge value, since the acidic medium was used in the experimental tests, these molecules are in a protonated state according to the methodology used in previous work of the research group (COSTA et al., 2021).

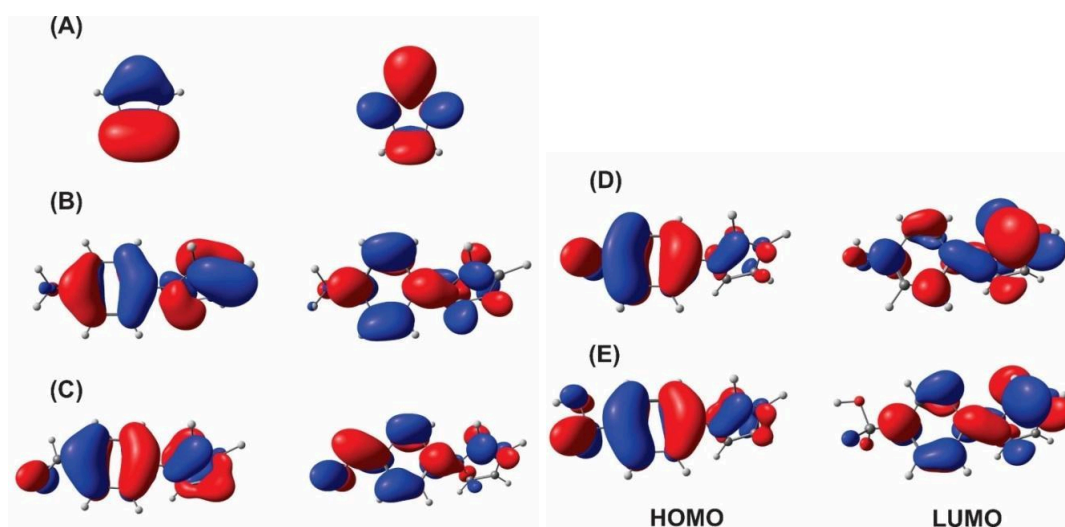
Figure 10 - Optimized molecular geometry of the IM (a), IA (b), IB (c), IF (d), and IFM (d) obtained at M06-2X/6-311++G(d,p) level of theory in water as implicit solvent.



Source: Author

Then, from the optimized structure of these molecules, the frontier molecular orbitals (HOMO and LUMO) were computed at the same level of theory, as well as the energy values of these molecular orbitals. Figure 11 shows the isosurfaces rendered for the HOMO and LUMO of the title molecules of this work.

Figure 11 - Frontier Molecular Orbitals calculated at M06-2X/6-311++G(d,p) level of theory in water for the molecules IM (a), IA (b), IB (c), IF (d), and IFM (e) with isovalue = 0.03.



Source: Author

For the IA molecule, HOMO is mainly spread over the aromatic and imidazole rings, while LUMO is spread over the  $\pi^*$  anti-ligand positions in the aromatic and imidazole rings. There is only a small contribution to the HOMO of the amine (protonated) group. For the IB molecule, HOMO is spread similarly to the IA molecule, however, there is a lower probability density spread over the imidazole ring in the IB molecule compared to the IA. It is possible to see an increase in the contribution of the functional group of the molecule IB (carbonyl group) compared to the amine group present in molecule IA. This fact shows that there is a change in the reactivity site between the IB and IA molecules. For the IF and IFM molecules, the distribution of HOMO is like the isosurfaces spread mainly over the aromatic ring and in the functional groups, phenol, and methoxy, respectively. LUMO also shows to have a similar probability distribution for these two molecules, the electronic density is mainly spread over the  $\pi^*$  antibonding positions in the aromatic and imidazole rings, however, there is an increase in the probability density in the imidazole ring of these two molecules when compared to the IA and IB molecules that have a higher electronic density in the aromatic ring for LUMO.

From the analysis of the frontier molecular orbitals, it is already possible to notice the differences in the reactive sites of the title molecules of this work, while IA and IB show a greater probability of interaction with the metallic  $\text{Cu}^0$  surface using the imidazole ring to donate electronic density and the aromatic ring to receive via retro-donation from the metallic surface. In the case of the IF and IFM molecules, the donation of electronic density is more probable using the aromatic ring, since the acceptance of charge coming from  $\text{Cu}^0$ , is more propensity to occur in the imidazole ring.

As the differences occur in the electronic properties, from the energy values of HOMO and LUMO, the quantum reactivity descriptors for the molecules of interest in this work were calculated and the results are shown in Table 6. The HOMO is related to the power nucleophilic of the molecule, since the higher the energy of this molecular orbital, the higher the propensity to donate electronic density. The LUMO is related to electrophilic power since the lower the energy value, the higher the propensity of the molecule to receive extra electronic density. Analyzing the data obtained in Table 6, it is possible to see that the HOMO energy values for the IA and IB molecules are close when compared to the imidazole molecule, with IB showing a greater difference of approximately 0.3 eV and IA of only 0.017 eV. As stated earlier, the probability density in the imidazole ring is greater than that of the aromatic ring for IA and IB, so when these molecules interact with metallic

$\text{Cu}^0$ , it is to be expected that the spatial arrangement of these molecules is with the imidazole ring preferably facing the metallic surface. The IF and IFM molecules have higher HOMO energy values, which show greater reactivity when the interaction site is the aromatic ring compared to the imidazole ring. This trend is confirmed by the ionization potential (IP), which is related to the energy of HOMO and the nucleophilicity index ( $\omega$ ), hence the IF and IFM molecules, when compared to IA, IB, and the imidazole, have a greater tendency to donate electronic density.

The results for the LUMO energy values show that the IA and IB molecules are more likely to receive electronic density since they have the lowest energy values within the set of the five molecules. For these two molecules, the electronic density is more likely to spread over the empty molecular orbitals in the aromatic ring, which again shows a greater reactivity when compared to the imidazole ring. The IF and IFM molecules also have lower LUMO values than imidazole since they can accommodate the extra negative charge density better than imidazole. This trend is also in agreement with the quantum descriptors such as the electronic affinity (A) and the electrophilicity index ( $\epsilon$ ). Therefore, according to the frontier molecular orbitals, it is noted that the IA and IB molecules have higher electrophilic character, whereas the IF and IFM molecules have higher nucleophilic character. Therefore, these molecules should interact differently with metallic  $\text{Cu}^0$ .

Table 6 - Global quantum reactivity descriptors computed for the molecules IM, IA, IB, IF, and IFM at M06-2X/6-311++G(d,p) level of theory.

|  | IM <sup>a</sup> | IA <sup>b</sup> | IB <sup>c</sup> | IF <sup>d</sup> | IFM <sup>e</sup> |
|--|-----------------|-----------------|-----------------|-----------------|------------------|
| HOMO energy ( $E_{HOMO}$ /eV)                        | -9.519          | -9.502          | -9.182          | -8.273          | -8.623           |
| LUMO energy ( $E_{LUMO}$ /eV)                        | -0.103          | -1.185          | -1.660          | -0.540          | -0.683           |
| Energy gap ( $\Delta E_{Gap}$ / eV)                  | 9.417           | 8.317           | 7.521           | 7.734           | 7.940            |
| Ionization Potential (IP / eV)                       | 9.519           | 9.502           | 9.182           | 8.273           | 8.623            |
| Electron Affinity (A / eV)                           | 0.103           | 1.185           | 1.660           | 0.540           | 0.683            |
| Electronegativity ( $\chi$ / eV)                     | 4.811           | 5.343           | 5.421           | 4.406           | 4.653            |
| Global Hardness ( $\eta$ / eV)                       | 4.708           | 4.159           | 3.761           | 3.867           | 3.970            |
| Global Softness ( $\sigma$ /eV <sup>-1</sup> )       | 0.212           | 0.240           | 0.266           | 0.259           | 0.252            |
| Electrophilicity index ( $\epsilon$ /eV)             | 2.458           | 3.433           | 3.907           | 2.511           | 2.727            |
| Nucleophilicity index ( $\omega$ /eV <sup>-1</sup> ) | 0.407           | 0.291           | 0.256           | 0.398           | 0.367            |
| Fraction of electrons transfered ( $\Delta N$ )      | 0.018           | -0.044          | -0.059          | 0.074           | 0.041            |

<sup>a</sup>Imidazole; <sup>b</sup>4-(1H-Imidazol-1-yl)aniline; <sup>c</sup>4-(1H-imidazol-1-yl)benzaldehyde;

<sup>d</sup>4-(1H-imidazol-1-yl)phenol; <sup>e</sup>(4-(1H-imidazol-1-yl)phenyl)methanol.

Source: Author

Another way to evaluate reactivity is through the energy gap between HOMO and LUMO. When this quantum descriptor is used, both nucleophilic and electrophilic characters are considered, since a smaller value of the energy gap implies a greater propensity to donate and accept electronic density, which confirms greater reactivity. According to the calculated results, the increasing order of the energy gap is  $IB < IF < IFM < IA < IM$ . This trend is the same as that obtained for the descriptors of global hardness and softness. Since a metallic bulk is classified as soft, as the IB molecule has the lowest hardness (greatest softness), it is expected to be the most reactive when considering only the energy gap. However, the order of corrosion inhibition found by the theoretical energy gap was practically the opposite of the experimentally predicted order. The data suggest that as the energy gap considers both the nucleophilic and electrophilic character of the molecules, it was seen that the availability of the LUMO cannot predict a correct order, but only the HOMO, so the energy gap is not a suitable quantum descriptor of reactivity for ranking these molecules as corrosion inhibitors of  $Cu^0$  in acidic media.

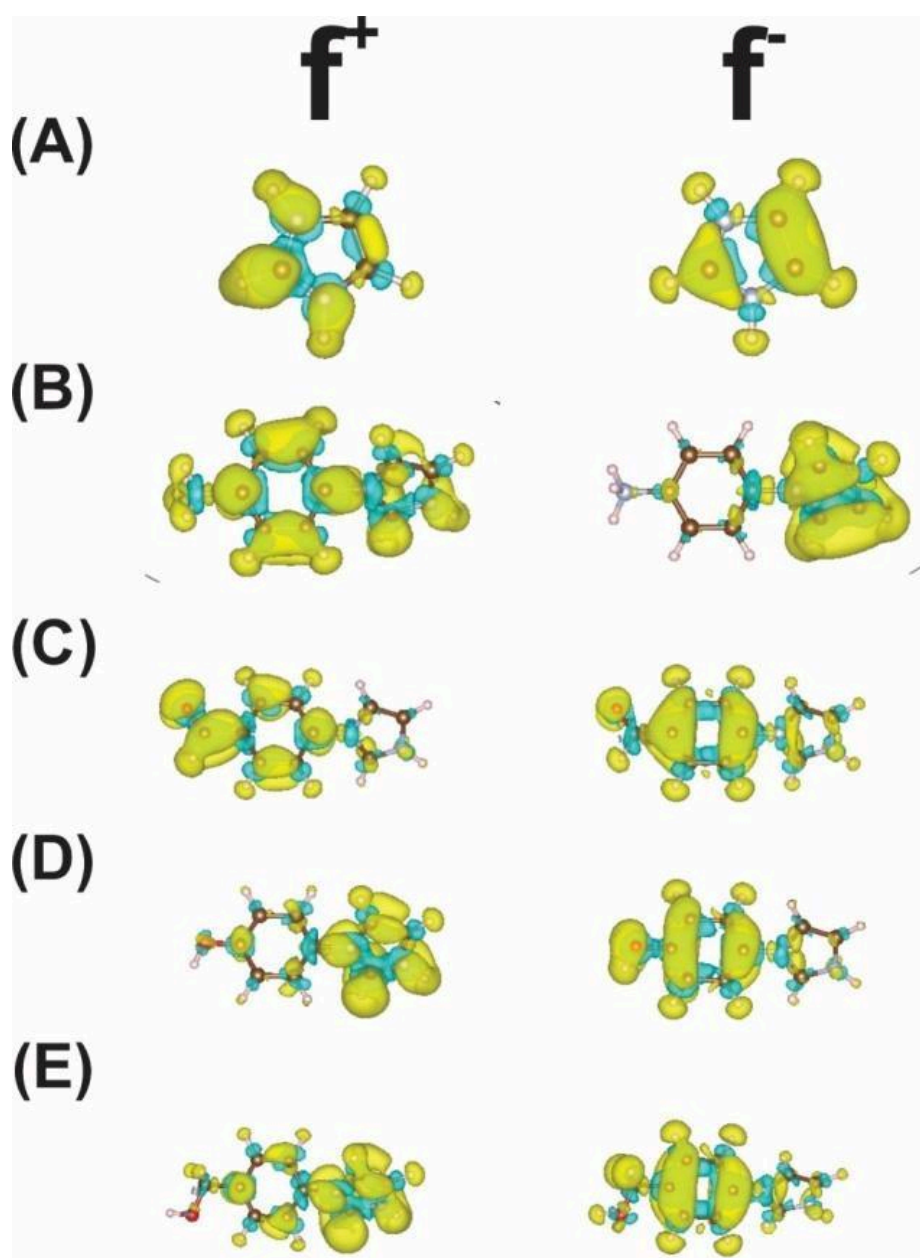
Finally, using the quantum descriptors of electronegativity ( $\chi$ ) and the fraction of electrons transferred ( $\Delta N$ ), it is possible to evaluate how the charge transfer process occurs between the organic molecule and the  $Cu^0$  metallic surface. Molecules IA and IB have greater electronegativity than the metallic surface, so the natural direction of the charge flow will be from  $Cu^0$  to the molecule ( $\Delta N < 0$ ), as previously discussed showing the greater electrophilic character of these two molecules. The IF and IFM molecules, on the other hand, have less electronegativity than metallic Cu, so the charge flow will be from the molecule to the metal ( $\Delta N > 0$ ), thus showing the greater nucleophilic character discussed in the HOMO analysis. Therefore, it can be concluded that the action of these organic molecules as corrosion inhibitors is mainly due to the acceptance of electronic density (IA and IB) and the donation of electronic density (IF and IFM). All of these imidazole derivatives have great potential to act as corrosion inhibitors, with the IB, IF and IFM molecules having greater corrosion efficiencies than the IA molecule since, within the four derivatives, it is the molecule that is least likely to interact with  $Cu^0$ .

It is possible to see in Figure 12 that the calculated isosurfaces for the title molecules show both the probability of donation (HOMO) and acceptance (LUMO) of electronic density. However, a greater understanding of the local reactivity of these molecules is necessary so that it is possible to recognize the trends presented in the global quantum reactivity descriptors. In this context, Electronic Fukui functions were calculated



based on the electronic density calculated for these molecules and the isosurfaces are shown in Figure 12. The green-colored isosurfaces mean positive values of the Fukui functions and those with blue color represent negative values. The greater the value of the Fukui function, the greater the probability that the molecule will suffer a nucleophilic ( $f^+$ ) or electrophilic ( $f^-$ ).

Figure 12 - Isosurfaces for the Electronic Fukui Functions for nucleophilic ( $f^+$ ) and electrophilic ( $f^-$ ) attack for the molecules IM (a), IA (b), IB (c), IF (d), and IFM (e) with isovalue = 0.36.



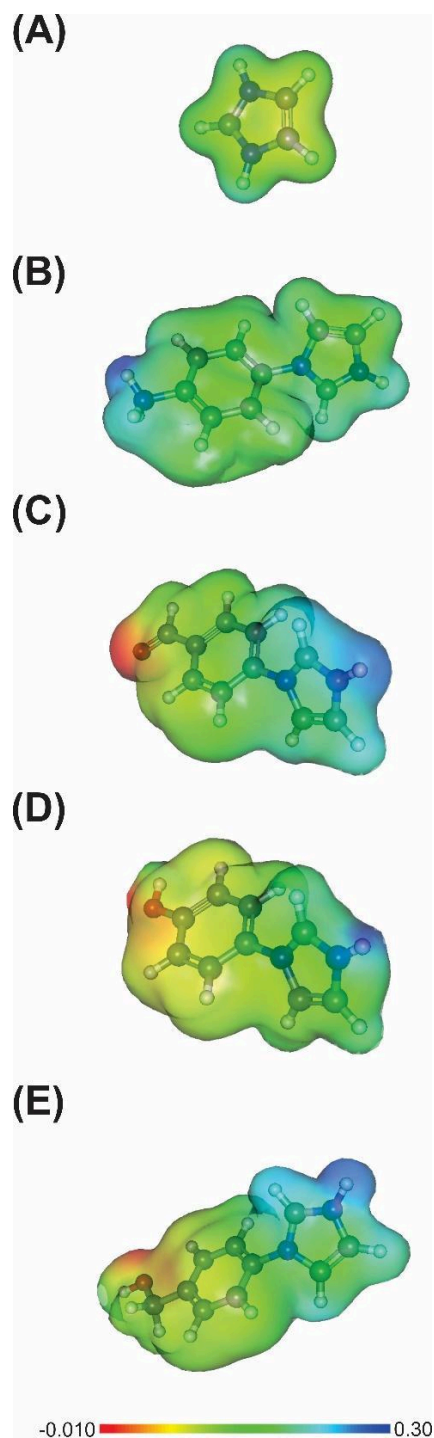
Source: Author

For a nucleophilic attack (the molecule acts as an electrophilic site), the IA molecule has positive values of  $f^+$  function in atoms in the aromatic ring and in the imidazole ring. The IB molecule has positive values predominantly in the aromatic ring and the carbonyl group. The IF and IFM molecules have the distribution of the  $f^+$  function similar with the positive values mostly distributed in the imidazole ring. These values are by the analysis of the frontier molecular orbitals. The IA and IB molecules have a greater electrophilic character because they are more likely to accept electronic density, with the IB molecule being more propensity to stabilize this extra negative charge because of the oxygen atom. The IF and IFM molecules could also have a high electrophilic character, however, it is in the imidazole ring that the electrophilic interaction site resides, so the negative charge cannot be spread efficiently.

For the electrophilic attack (the molecule acts as a nucleophilic site), the IA molecule presents positive values of the Fukui function in the imidazole ring, whereas the IB, IF and IFM molecules have positive values mainly in the aromatic ring and the oxygenated functional group. This result shows that these three molecules have a similar way of donating electronic density, but with greater effectiveness in the stabilization by the resonance effect in the IB molecule, IF and IFM have a greater nucleophilic character as previously predicted.

To finalize the local analysis of reactivity, the Molecular Electrostatic Potential was calculated for molecules at the same level of theory as the frontier molecular orbitals and the results are shown in Figure 13. The region colored in red represents negative charges, the region-colored orange to yellow represents partially negative charges, the region in green represents charges tending to neutrality, the region in light blue, partially positive charges, and the dark blue region positive charges. It is possible to note that the IA molecule has a partial positive charge on the hydrogen atoms attached to the nitrogen atoms, and in the aromatic and imidazole rings the charge density is well distributed, showing that among the four molecules derived from imidazole, it must be the least reactive. The IB, IF and IFM molecules have a similar charge distribution. The three have a partially positive charge on the imidazole ring, a partially negative charge distributed on the aromatic ring, showing that it is in fact a site for the donation of electronic density and a negative charge on the oxygen atoms of the functional groups. This result shows agreement between what has been said about the frontier molecular orbitals and the Electronic Fukui functions.

Figure 13 - Molecular Electrostatic Potential computed for the molecules IM (a), IA (b), IB (c), IF (d), and IFM (e) at M06-2X/6-311++G(d,p) level of theory in water with isovalue = 0.01.



Source: Author

From the results of the adsorption Gibbs energy ( $\Delta G_{\text{ads}}$ ) using the Langmuir isotherm, the increase of adsorption energy follows the same tendency as the electronic

density donation power using the HOMO energy value ( $IM < IA < IB < IFM < IF$ ). According to the HOMO energy value (Table 6), the IF, IFM, and IB molecules have a higher value for the energy for this molecular orbital, which implies a higher tendency to donate the electronic density to the  $Cu^0$  surface. Even though the FMO distribution (Figure 11) showed that the IA molecule has an electronic density in the benzene ring that can be donated, however, the Electronic Fukui function (Figure 12) for the electrophilicity attack ( $f^-$ ) demonstrated that the probability of the electronic density donation using the benzene ring for the IA molecule is almost nonexistent. Hence, for the IA molecule, the interaction with the  $Cu^0$  surface should occur using the imidazole ring and this fact can be seen in the adsorption isotherms since  $\Delta G_{ads}$  is higher considering all the derivatives.

For the IF, IFM, and IB molecules, the donation of the electronic density should occur using the benzene ring as showed the isosurfaces of the Electronic Fukui functions. The IF molecule can interact using both the  $\pi$  electronic density spread over the benzene ring and the electronic density in the hydroxyl group. The IFM molecule can use the electronic density spread over in the aromatic ring and in the methoxy group to donate electrons to the  $Cu^0$ . However, it has a lower probability compared with the hydroxyl group of the IF molecule. The IB molecule can use besides the aromatic ring, the electronic density in the carbonyl group, however, the delocalization effect decreases the probability of electronic donation to the  $Cu^0$  surface, and this molecule should have the higher  $\Delta G_{ads}$  from these three sets of derivatives (IF, IFM, and IB). The MEP distribution (Figure 13) also corroborates with the previous results due to the increase of the yellow-colored region over the aromatic ring for the IB, IFM, and IF molecules. Hence the charge available to be donated to the  $Cu^0$  surface is higher for the IF molecule, which explains the lowest value for the  $\Delta G_{ads}$  for this molecule.

### 3.4 Conclusions

The electrochemical corrosion tests demonstrated that the investigated imidazole derivative molecules inhibit the  $\text{Cu}^0$  corrosion in acidic medium in the following sequence:  $\text{IF} > \text{IFM} > \text{IB} > \text{IA} > \text{IM}$ . The adsorption data demonstrated that the Langmuir model fitted better the experimental inhibition efficiency than the Frumkin model isotherms. Furthermore, the correlation between the  $\Delta G_{\text{ads}}$  values and  $\epsilon_{\text{inh}}$  values showed that the last increased with the chemical character of the interaction between the corrosion inhibitor molecules with the  $\text{Cu}^0$  surface. The different DFT functions did not significantly change the molecular data, but the global hardness of the modified molecules was different in comparison with the imidazole molecule since the chemical groups bring more chemical information and better corrosion inhibition efficiency. Since then, the Fukui analysis showed that modified imidazole modified molecules presented a higher electrophilic behavior, which could be accepted as a good capacity of receiving the electron density from  $\text{Cu}^0$  electrode. In this context, the harmonic correlation of computational and experimental data successfully showed the chemical modification of imidazole molecules for better anticorrosion efficiency in acidic media toward the protection of  $\text{Cu}^0$  surfaces.

## **4 INHIBITION OF COPPER CORROSION IN ACID MEDIUM BY TRIAZOLE-BASED COMPOUNDS: ELECTROCHEMICAL AND MOLECULAR APPROACHES**

### **4.2 Introduction**

Corrosion is a multi-secular humanity problem. This is evident when in ancient world sites, such as Delhi, India, have a 6-ton iron pillar with 7.21 meters high, 41 centimetres wide that was erected between fourth and fifth centuries, and the pillar is still in the same place (BALASUBRAMANIAM, 2000). If corrosion played a crucial role in antiquity, it is evident that the same role in twenty-first century, but the priorities had changed. Today, it is understood that the corrosion process produces harmful compounds that can be environmentally harmful and deadly to human health. In this context, the corrosion process can be link crossed with other important issues, such as climate change, global warming and greenhouse gas emissions (RAJESH KUMAR SINGH VIKAS KUMAR, 2021; ROBERGE, 2010). The production of a non-harmful, green, and non-toxic corrosion inhibitor is one of the worldwide challenges among corrosion researchers.

The corrosion inhibitor is an anticorrosive class of chemical compounds that can be organic or inorganic in nature but can adsorb over the metallic surface and donate charge density towards them to diminish the corrosion rate, and increase the life span of the metallic material, which can be pure metal (like iron, copper, etc) or an alloy (like steel). The use of old corrosion inhibitors, such as zinc chromate and red lead (VERNON, 1996), or even pyridine (POLLOCK, 1943), an organic compound that can cause liver, heart and kidney damage due to prolonged exposure (RAJESH KUMAR SINGH VIKAS KUMAR, 2021). Since corrosion cannot be completely prevented but minimized, a viable approach to minimizing corrosion damage is the use of corrosion inhibitors that can be non-toxic and un harmful to human health and to the environment at the same time.

Considering the protection of pure metals, copper and its alloys are used in many environments and applications due to their desirable properties, such as high ductility, low hardness and higher electrical and thermal conductivity (ATKINS et al., 2009). Although copper is relatively nobler than other metals link iron, the corrosion resistance of copper-based materials is highly dependent upon the environment that is immersed in, like

humidity, sea air, microorganisms and so on (OBOT; MACDONALD; GASEM, 2015b). One of the most effective ways to provide corrosion protection to metals is to add the corrosion inhibitors into the system, and in most cases, adsorption inhibitors appear to affect both anodic and cathodic processes. Compared with inorganic corrosion inhibitors, organic corrosion inhibitors have lower toxicity and can be used in small concentrations, and the lateral intermolecular interactions that arise from those compounds tend to have better film-forming performance. Since lone electron pairs of heteroatoms and electrons in aromatic rings, such as sulphur, nitrogen, and oxygen, can act as active adsorption sites over the metallic surfaces, which can result in a coordinated bonding between the metal and the ligand (MENDONÇA et al., 2017).

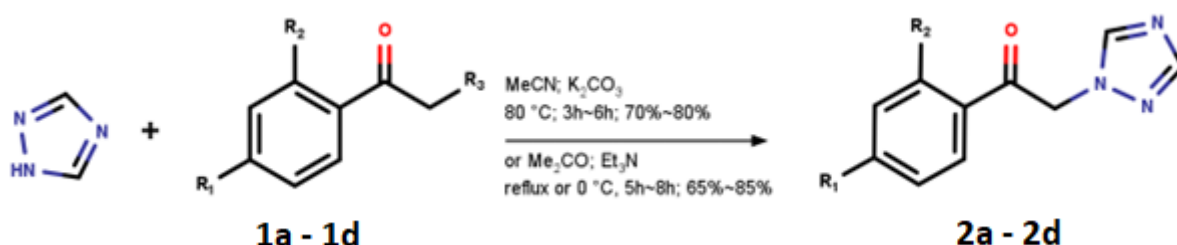
Since corrosion research deals with microscopic aspects of the matter, such as the charge electron reactions and the (electro) chemical species that can arise, there are limitations in the experimental data brought by the traditional electrochemical techniques. In this context, molecular modelling plays a major role in a better understanding of the corrosion process in a microscopic view. Two of those molecular models computes quantum (such as density functional theory) and classical (such as molecular dynamics), and both are complementary techniques. The density functional theory (DFT) brings information regarding the electron density of the molecule, and some quantum chemical models are applied to the corrosion investigation, such as the number of transferred electron, a calculated value that shows the tendency of the electron density is from the inhibitor to the electrode (which favours corrosion inhibitor) or the contrary (which favours the corrosion itself) (OBOT; MACDONALD; GASEM, 2015b). The molecular dynamics, for instance, can use the Monte Carlo algorithm for simulating the adsorptive chemical environment (COSTA et al., 2021). In other words, the presence of the inhibitor towards the metallic electrode surface can be simulated with or without water molecules and solving the Newton equation for this system can bring information the adsorption, such as the molecular picture towards a simulated metallic surface. Therefore, this paper brings the use of triazole and triazole-based molecules for corrosion inhibition of copper electrodes in  $0.5 \text{ mol L}^{-1} \text{ H}_2\text{SO}_4$  solutions.

## 4.2 Experimental Details

### 4.2.1 Synthesis of the modified triazole molecules

The triazole compounds were synthesized as presented by Aquino in their doctorate thesis (BEZERRA, 2020), and the synthesis scheme is shown in Figure 14.

Figure 14 - Scheme of synthesis of the lateral modification of triazole compounds. For 1a to 1e compounds, R<sub>2</sub> = -H and R<sub>3</sub> = -Br. For 1f compound, R<sub>2</sub> = -F and R<sub>3</sub> = -Cl, and R<sub>1</sub> = -F. For 1a to 1d compounds, R<sub>1</sub> was, respectively, -H, -CH<sub>3</sub>, -F, and -Cl.

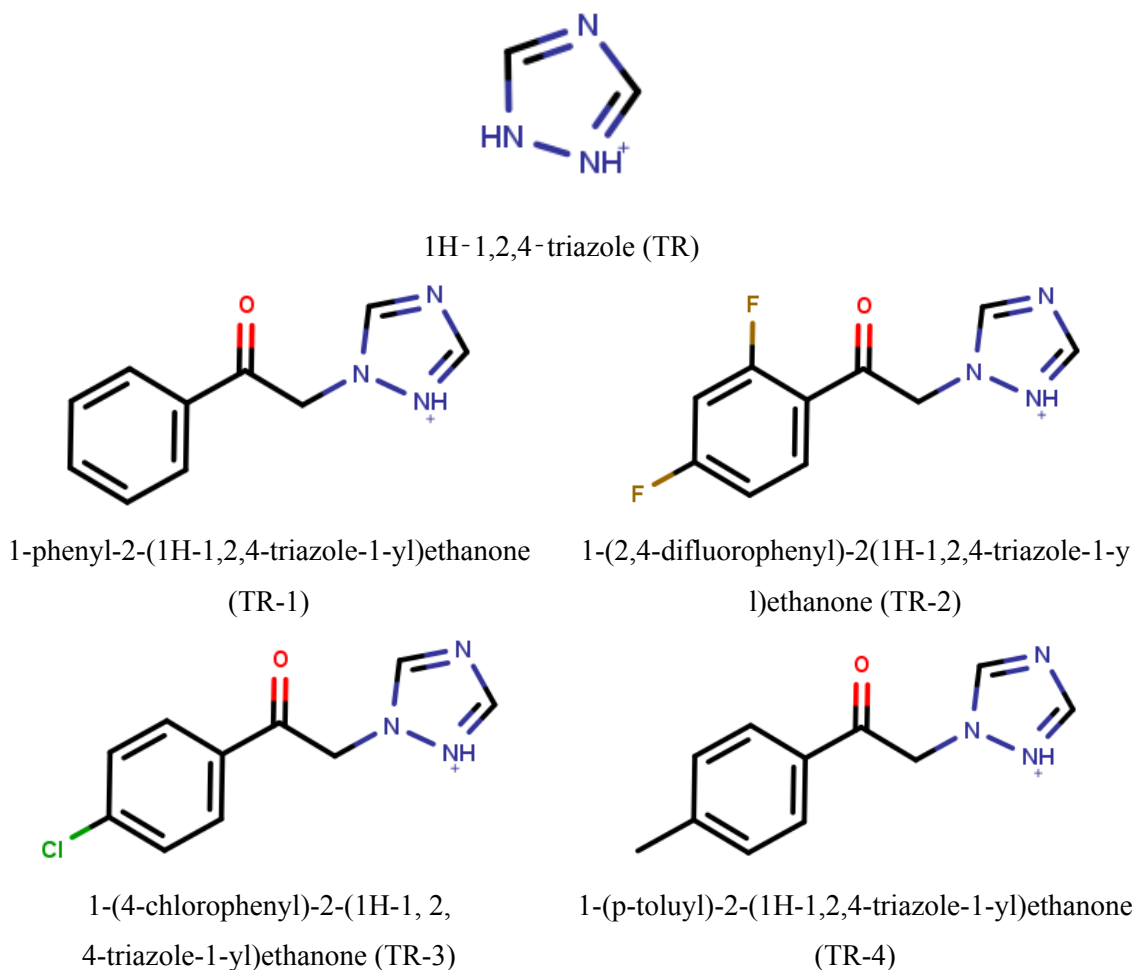


Source: Author

The synthesis of the modified triazole molecules followed these steps: initially, a nucleophilic substitution reaction was carried out between the haloacetophenones (1a-1f) and triazole molecule, as shown in Figure 14, in an alkaline medium, using potassium carbonate in acetonitrile for reactions involving haloacetophenones, as well as triethylamine in acetone for 2a 1-phenyl-2-(1H-1,2,4-triazole-1-yl)ethanone, 2d The reaction time was 5h to obtain substance 2a in 85% yield; for substances 2c 1-(2,4-difluorophenyl)-2-(1H-1,2,4-triazole-1-yl)ethanone and 2d 1-(4-chlorophenyl)-2-(1H-1, 2, 4-triazole-1-yl)ethanone, the reaction time was 6 hours, with substances 2c in 70% yield and for 2d, the yield was 75%; for substance 2b 1-(p-toluy)l)-2-(1H-1,2,4-triazole-1-yl)ethanone the reaction time was 3 h and the yield was 80%. All of them were purified by recrystallization to obtain a colourless crystal for further solution preparation for electrochemical essays. The triazole molecules that were cited in this section are shown in Figure 15.



Figure 15 - 2D representation of the inhibitor molecules that were studied in this paper.



Source: Author

#### 4.2.2 Electrochemical experiments

Electrochemical techniques, such as  $E_{oc}$ , PP and EIS were used to assess the performance of the imidazole and its derivatives as inhibitors of the Cu corrosion 0.5 mol L<sup>-1</sup> H<sub>2</sub>SO<sub>4</sub>. All electrochemical experiments were carried out in a conventional three-electrode connected to Autolab PGSTAT 302N potentiostat/galvanostat from Metrohm® and controlled by NOVA® 2.1.4 software, which allows the acquisition and analyses of the experimental data. The working electrode was a Cu disk embedded in glass tubes with epoxy resin and with a disk exposed area of approximately 0.18 cm<sup>2</sup>. The counter electrode was a platinum plate with an area of 1.13 cm<sup>2</sup> and the reference electrode was Ag<sub>(s)</sub>/AgCl<sub>(s)</sub>/Cl<sup>-</sup> (aq., saturated KCl). All solutions used in this investigation were prepared by water purified by the Milli-Q system.

Prior the electrochemical corrosion tests, the Cu surface was submitted to a sanding process with silicon carbide (SiC) sandpapers with 100, 220, 400 and 600 mesh granulations. After, the Cu surface was washed with water. Finally, the samples were immersed in a 0.5 mol L<sup>-1</sup> H<sub>2</sub>SO<sub>4</sub> aerated solution and in the absence (blank solution) and presence of the imidazole -based compounds in the following concentrations: 0.1×10<sup>-3</sup> mol L<sup>-1</sup>, 0.25×10<sup>-3</sup> mol L<sup>-1</sup>, 0.5×10<sup>-3</sup> mol L<sup>-1</sup> and 1×10<sup>-3</sup> mol L<sup>-1</sup>.

The impedance diagrams were obtained at  $E_{oc}$  and after 1 hour of immersion of the Cu in the testing solution. The frequency ranged between 20 kHz to 6 mHz and a potential amplitude of 10 mV was applied. The polarization curves were obtained at the concentration of 1×10<sup>-3</sup> mol L<sup>-1</sup>, after 1 hour of immersion time, and the potential was sweep between ± 300 mV around the  $E_{oc}$  value, and the scan rate used was 1 mV s<sup>-1</sup>. All electrochemical experiments were carried out at the laboratory room temperature (≅ 25° C). Finally, these experiments were done in triplicate.

#### 4.2.3 Computational calculations

To understand the experimental results of corrosion inhibition efficiency and how the title molecules can act as corrosion inhibitors, the quantum chemical calculations were done using the DFT method. The input files were prepared using the GaussView 5.0 (DENNINGTON; KEITH; MILLAM, 2009) software and all the calculations were done using the Gaussian 09 software (FRISCH et al., 2009). Since the acidic medium was used in the experimental tests, the DFT calculations were carried out considering that all molecules were protonated.

To make a proper theoretical-experimental model, the inhibitors molecules were optimized using the Minnesota 06 hybrid meta exchange-correlation functional (M06-2X) with the 6-311++G(d,p) basis set (DITCHFIELD; HEHRE; POPLER, 1971; ZHAO; TRUHLAR, 2008) and with water as implicit solvent by the solvation method IEF-PCM (CANCÈS; MENNUCCI; TOMASI, 1997; MENNUCCI; CANCEÈS; TOMASI, 1997). The isosurfaces of the FMO were rendered using the trial version of the ChemCraft software ("Chemcraft - graphical software for visualization of quantum chemistry computations", 2004). Then, the global quantum reactivity descriptors were calculated from the energy values of the HOMO and LUMO: the energy gap ( $\Delta E_{gap}$ , Eq.1) (PEARSON, 1963a), the

ionization potential (IP, Eq.2) (KOOPMANS, 1934), the electron affinity (A, Eq.3) (KOOPMANS, 1934), the electronegativity ( $\chi$ , Eq.4) (CHERMETTE, 1999; ICZKOWSKI; MARGRAVE, 1961), the global hardness ( $\eta$ , Eq.5) (JANAK, 1978; PEARSON, 1987a; VON SZENTPÁLY, 1991b), the global softness (S, Eq.6) (YANG; PARR, 1985a), the global electrophilicity index ( $\omega$ , Eq.7) (PARR; SZENTPÁLY; LIU, 1999b), the global nucleophilicity index ( $\epsilon$ , Eq.8) (CHATTARAJ; GIRI; DULEY, 2011), and the fraction of electrons transferred ( $\Delta N$ , Eq.9) (OBOT; MACDONALD; GASEM, 2015b). For the Cu metallic bulk, it can be classified as soft ( $\eta_M = 0$ ) (DEWAR et al., 1985a) and its electronegativity has the value of 4.68 eV (MICHAELSON, 1977b). Finally, to make a local reactivity characterization, the Electronic Fukui functions for the nucleophilic ( $f^+$ ) and the electrophilic ( $f^-$ ) attack obtained from the Multiwfn software (LU; CHEN, 2012) and the Molecular Electrostatic Potential (MEP) were calculated using the M06-2X/6-311++G(d,p) computational level and the isosurfaces were rendered by the VESTA (MOMMA; IZUMI, 2011) and Gabedit (ALLOUCHE, 2011) softwares, respectively.

#### 4.2.4 Monte Carlo simulations

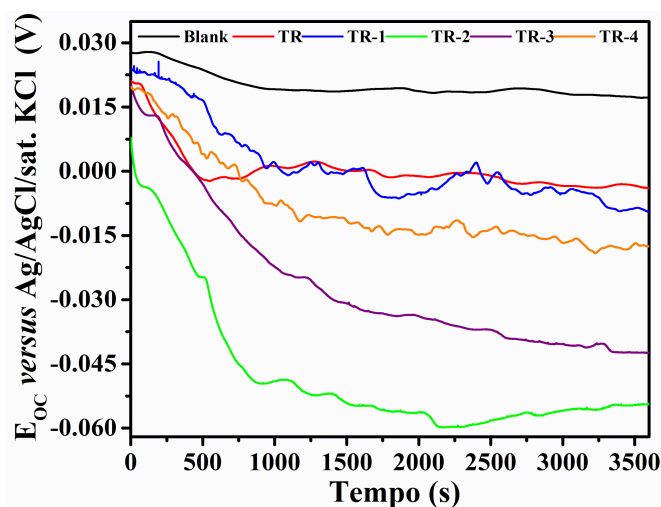
The iron surface was modeled using a unit cell from *Mineralogy Database*, which Miller index were (1 1 1). The unit cell was multiplied to obtain a solid having 8 x 8 x 2 unit cells, having a vacuum box of 30 Å over their surface. The simulations were conducted in vacuum and explicit water solvent situations. The adsorption locator is a tool that uses the Monte Carlo method to confirm the position and orientation of a molecule on a stable substrate and determine its interaction energy. Monte Carlo calculations were made considering the presence and absence of water molecules. To model the presence of water, the space above the surface was filled with prominent water molecules. The force field used was COMPAS as it has parameters for several atoms including Cu. The temperature was varied between 298 and 300 K. Ultrafine grade was used in the calculations, which implies that the parameters used were:  $8.372 \times 10^{-5}$  kJ mol<sup>-1</sup> of energy variation,  $4.186 \times 10^{-3}$  kJ mol<sup>-1</sup>Å<sup>-1</sup> variation of the maximum force and  $10^{-5}$  Å of maximum displacement in the Cartesian coordinates.

### 4.3 Results and discussion

#### 4.3.1 Electrochemical studies

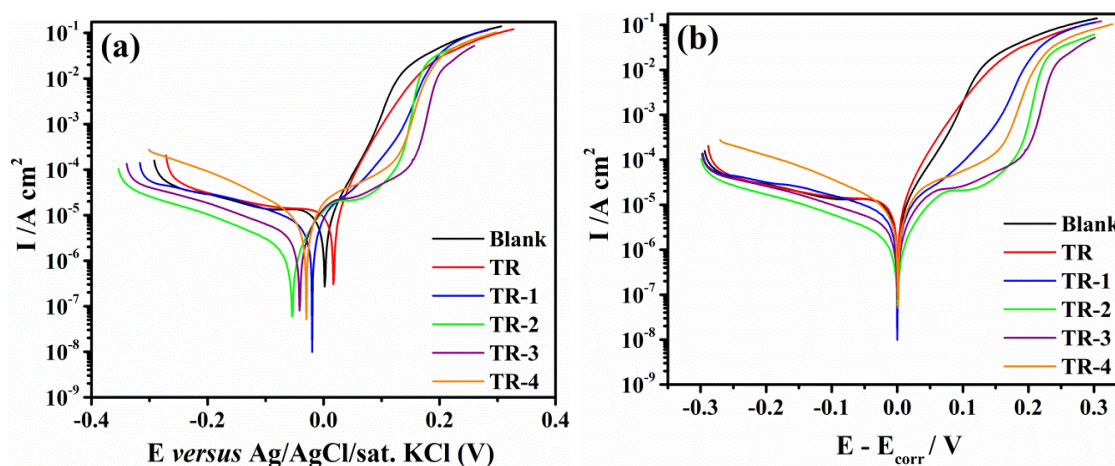
In Figure 16, all molecules had their potentials shifted towards more negative values if compared with blank solutions, which shows a cathodic corrosion inhibition over the Cu electrode. At  $t = 1000$  s, all molecules had their potentials decreased sharply, but after 1000 s the potential went to more stable values. The TR, TR-1 and TR-4 presented a potential difference of circa 40 mV, but TR-2 and TR-3 presented a larger potential difference, around 80 mV. TR-2 and TR-3 are molecules which contains fluoride and chloride atoms, respectively, whereas TR-1, TR-4 had a hydrogen and methyl group, respectively. Since TR is the control triazole molecule, the increase of polarity of the modified molecules had also increased the cathodic effect over the Cu electrode in acidic medium. Since the oxygen gas molecule is apolar, the molecule will directly interact with the electrode surface and the inhibitor molecule itself. Having TR, TR-1 and TR-4 apolar groups in their structure, it is likely the oxygen gas molecule will interact with them, and the Cu electrode will interact with the oxygen gas molecule. On the other hand, TR-2 and TR-3 having polar groups, such as fluorine and chlorine atoms, will increase the polarity of the inhibitor molecules. Since TR-2 and TR-3 molecules are polar, they will repel the apolar oxygen gas molecule, and the OCP difference between those molecules can be correlated with this fact. In this context, in terms of OCP values, the decrescent cathodic effect over Cu electrode is  $TR-2 > TR-3 > TR-4 > TR-1 > TR$ . Since the OCP analysis alone is incomplete in terms of discussion of the electrochemical efficiency of the inhibitors, Figure 17 shows the obtained polarization curves of Cu electrode in acidic medium in absence and presence of the studied corrosion inhibitors.

Figure 16 - Variation of the open circuit potential with the immersion time of Cu in 0.5 mol L<sup>-1</sup> H<sub>2</sub>SO<sub>4</sub>. These measurements were carried out at laboratory room temperature ( $\approx 25\text{ }^{\circ}\text{C}$ ) and in the presence and absence (blank) of triazole-based compounds at  $1 \times 10^{-3}$  mol.



Source: Author

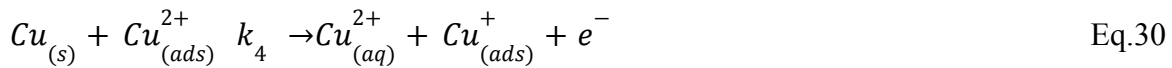
Figure 17 - Potentiodynamic polarization curves obtained for Cu in 0.5 mol L<sup>-1</sup> H<sub>2</sub>SO<sub>4</sub> medium in the absence (blank) and presence of triazole-based compounds at  $1 \times 10^{-3}$  mol L<sup>-1</sup>. All curves were achieved at laboratory room temperature ( $\approx 25\text{ }^{\circ}\text{C}$ ).



Source: Author

In Figure 17a, except for TR, all other molecules presented their polarization curves before blank solution, which characterize those molecules as cathodic inhibitors, since their corrosion potentials were shifted towards negative potential values in comparison with blank curve. Also, it is clear to see the oxygen reduction reaction in the cathodic branch in Figure 17b. Except for TR-4, which presented the highest current density among

all systems including blank solution, the cathodic density current changed little. On the other hand, the anodic branch had changed in comparison with blank solution. In the  $E - E_{\text{corr}}$  range between 0.0 and -0.3 V, the TR-2 inhibitor had lower density current if compared with other inhibitors, which confirms the polarity over corrosion inhibitor hypothesis discussed in the later session. When the anodic branch is considered, except for TR molecule, which was very similar to the blank curve, all other molecules had diminished the anodic current of the Cu electrode. Still in Figure 17b, between 0.0 and 0.2 V, the anodic current density from TR-2, TR-3 and TR-4 changed up to two orders of magnitude towards Cu electrode. After 0.2 V, the current increases but in a slower rate than blank solution and TR. The classical copper corrosion mechanism proposed by Mattos and coworkers, the formation of  $\text{Cu}^+$  ion sparks a sequence of an autocatalytic corrosion of copper in acidic medium (CORDEIRO; BARCIA; MATTOS, 1993):



The mechanism shows that the adsorbed  $\text{Cu}^+$  ion starts the oxidation cascade over the copper electrode. In this context, since the sulfuric acid is not completely ionized in solution, an intermediate is formed in the electrode/solution interface (SHINGAYA; ITO, 1999):



The intermediate shown in Eq.31 adsorbs strongly over the electrode surface. Considering that there is a competition between the  $\text{HSO}_4^-$  ion and the inhibitor molecule, the better adsorption will promote, the better inhibition corrosion will cause in the surface of the electrode. Therefore, the chemical equation that will inhibit the corrosion of copper in acidic medium is:



When inhibitor interacts with  $Cu^+$  ion in the surface of copper electrode, a coordination compound is formed there, and the molecule will deliver a density charge to retard the oxidation of copper electrode, as shown by Eqns. 27 to 30 and, therefore, inhibiting the copper corrosion. For a quantitative discussion, Table 7 shows the electrochemical parameters obtained from polarization curves in presence and absence of the inhibitor molecules.

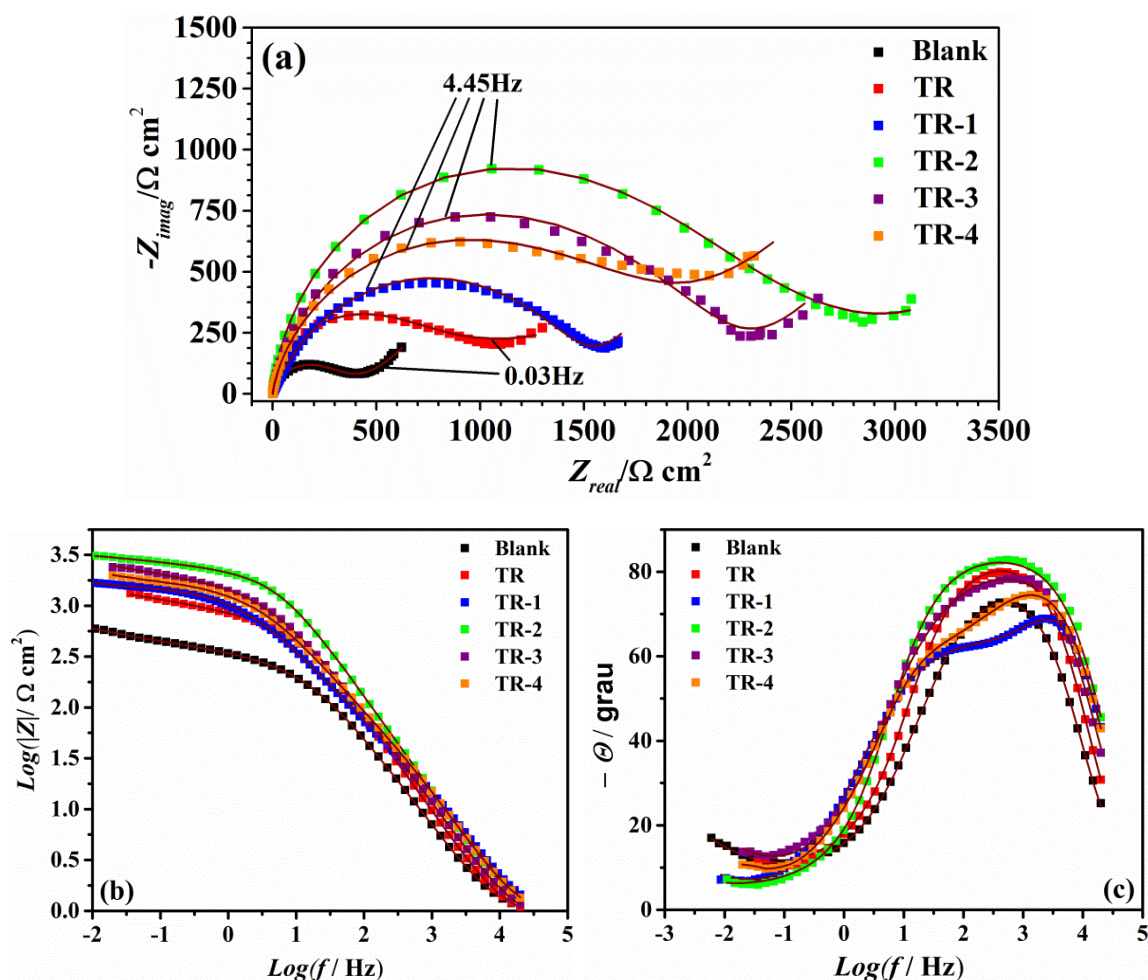
Table 7 - Electrochemical parameters obtained for Cu corrosion in  $0.5 \text{ mol L}^{-1} \text{ H}_2\text{SO}_4$  medium in the absence and presence of triazole-based compounds at  $1 \times 10^{-3} \text{ mol L}^{-1}$ .

|              | $E_{\text{corr}}$ (mV) | $R_p$ ( $k\Omega \text{ cm}^2$ ) | $\epsilon$ (%) |
|--------------|------------------------|----------------------------------|----------------|
| <b>Blank</b> | 14                     | 10.91                            | -              |
| <b>TR</b>    | -4                     | 16.09                            | 47.53          |
| <b>TR-1</b>  | -10                    | 18.75                            | 71.92          |
| <b>TR-2</b>  | -54                    | 21.28                            | 95.12          |
| <b>TR-3</b>  | -42                    | 20.54                            | 88.34          |
| <b>TR-4</b>  | -18                    | 19.71                            | 80.73          |

Source: Author\

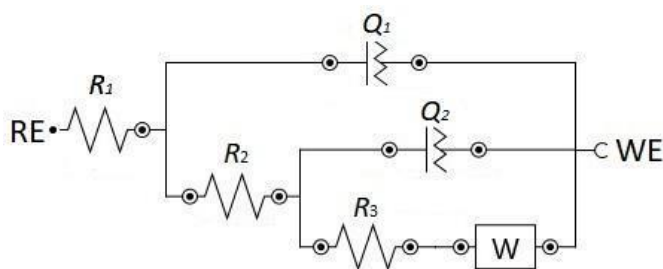
Table 7 shows the inhibition efficiency from polarization curves in Figure 17. As discussed earlier, except for TR molecule, all other inhibitors had performed better than TR. The highest polarization resistance came from TR-2 inhibitor, and the inhibition efficiency reached 95.12%. In this context, the decreasing inhibition trend is: TR-2 > TR-3 > TR-4 > TR-1 > TR. To obtain more information regarding the electrode/solution, electrochemical impedance spectroscopy (EIS) experiments were performed, and Figure 18, shows the achieved results.

Figure 18 - Nyquist (a) and Bode (b,c) plots obtained for Cu after 1h of immersion in  $0.5 \text{ mol L}^{-1} \text{ H}_2\text{SO}_4$  in the absence and presence of triazole and its derivatives at  $1 \times 10^{-3} \text{ mol L}^{-1}$ . All diagrams were obtained at room temperature of the laboratory ( $\approx 25^\circ \text{C}$ ). The solid lines represent impedance simulation carried out by the equivalent circuit shown in Figure 19.



Source: Author

Figure 19 - Drawing of the equivalent electrical circuit used to fit the EIS diagrams



Source: Author



In Figure 18a, the Nyquist plot shows a classical Warburg-like diffusional pattern in the plot (ORAZEM; TRIBOLLET, 2008), since the  $\text{Cu}^+$  ion diffuses towards the bulk solution. Compared with blank solution, all other Nyquist plots presented a higher semicircle and a limited diffusion region. This behaviour can be explained by the complexation of the corrosion inhibitor over the electrode surface, as shown in Eq.32: the diffusion is limited to the  $\text{Cu}^+$  concentration gradient, as shown by Nernst diffusion layer. If there is a small concentration of  $\text{Cu}^+$  ion to diffuse towards the bulk of the solution, the Warburg element will decrease its impedance, and the diffusion decreases. Considering the Bode plot from Figures 18b and 18c, TR-2 molecule, if compared with blank solutions and other molecules, had the highest polarization resistance in impedance modulus plot and lower diffusion rates in phase angle plot. In this case, the lower frequency domain (between  $10^{-1}$  Hz and  $10^{-2}$  Hz), there are some diffusions going on in the electrochemical cell from other systems; TR-1 and TR-2 had almost no diffusion in this frequency range. Therefore, the complexation hypothesis can be sustained here. To quantify some electrochemical data from experimental impedance plots, Figure 19 was used as the equivalent electrical circuit for fitting the EIS diagrams, and Table 8 shows those fitted values.

Table 8 – Fitted values from applied equivalent circuit shown in Figure 19 and inhibition efficiency obtained from fitted data. The constant phase element was converted to pseudocapacitance using Brug method.

| Inhibitor    | $R_2 / \Omega \text{ cm}^2$ | $C_1 / \mu\text{F cm}^{-2}$ | $R_3 / \Omega \text{ cm}^2$ | $C_2 / \mu\text{F cm}^{-2}$ | $\epsilon_{\text{inh}} (\%)$ |
|--------------|-----------------------------|-----------------------------|-----------------------------|-----------------------------|------------------------------|
| <b>Blank</b> | $367.72 \pm 1.86$           | $21.68 \pm 0.11$            | $23.05 \pm 0.44$            | $78.42 \pm 1.50$            | -                            |
| <b>TR</b>    | $935.96 \pm 6.48$           | $6.21 \pm 0.04$             | $53.36 \pm 2.11$            | $11.39 \pm 0.45$            | 60.71                        |
| <b>TR-1</b>  | $1664.90 \pm 8.08$          | $2.58 \pm 0.01$             | $57.83 \pm 1.92$            | $3.23 \pm 0.11$             | 77.91                        |
| <b>TR-2</b>  | $2235.33 \pm 2.63$          | $2.41 \pm 0.01$             | $47.70 \pm 1.89$            | $2.96 \pm 0.12$             | 83.55                        |
| <b>TR-3</b>  | $2007.63 \pm 2.94$          | $3.28 \pm 0.01$             | $29.29 \pm 6.19$            | $4.20 \pm 0.89$             | 81.68                        |
| <b>TR-4</b>  | $1456.70 \pm 7.55$          | $2.05 \pm 0.01$             | $23.05 \pm 0.44$            | $2.21 \pm 0.04$             | 74.76                        |

Source: Author

Table 8 shows the electrical data from impedance diagrams using the equivalent circuit from Figure 19. Also, the capacitances could be calculated using Brug method for calculating the double layer capacitance using  $R_2$  (BRUG et al., 1984), Eq.33, and the calculated capacitance for the inhibitor film over the electrode surface was calculated using Hsu-Mansfeld method. Eq.34 (BRUG et al., 1984):

$$C_{dl} = Y_o^{\frac{1}{n}} (R_2)^{\frac{1-n}{n}} \quad \text{Eq.33}$$

$$C_{film} = Y_o^{\frac{1}{n}} \left( \frac{R_2 \times R_3}{R_2 + R_3} \right)^{\frac{1-n}{n}} \quad \text{Eq.34}$$

In general, all triazole molecules had performed a corrosion inhibition towards the copper electrode. When the polarization resistance ( $R_2 + R_3$ ) along  $C_1$  and  $C_2$  capacitances, TR-2 is the best choice by its higher polarization resistance and lower capacitance. Since the impedance of a capacitor is inversely proportional to the capacitance itself, as shown by Eq.35 (ORAZEM; TRIBOLLET, 2008):

$$Z_c = \frac{1}{j\omega C} \quad \text{Eq.35}$$

In this case, the capacitance being in parallel, the equivalent capacitance is the sum of the individual capacitances, as shown by Eq.36 (ORAZEM; TRIBOLLET, 2008):

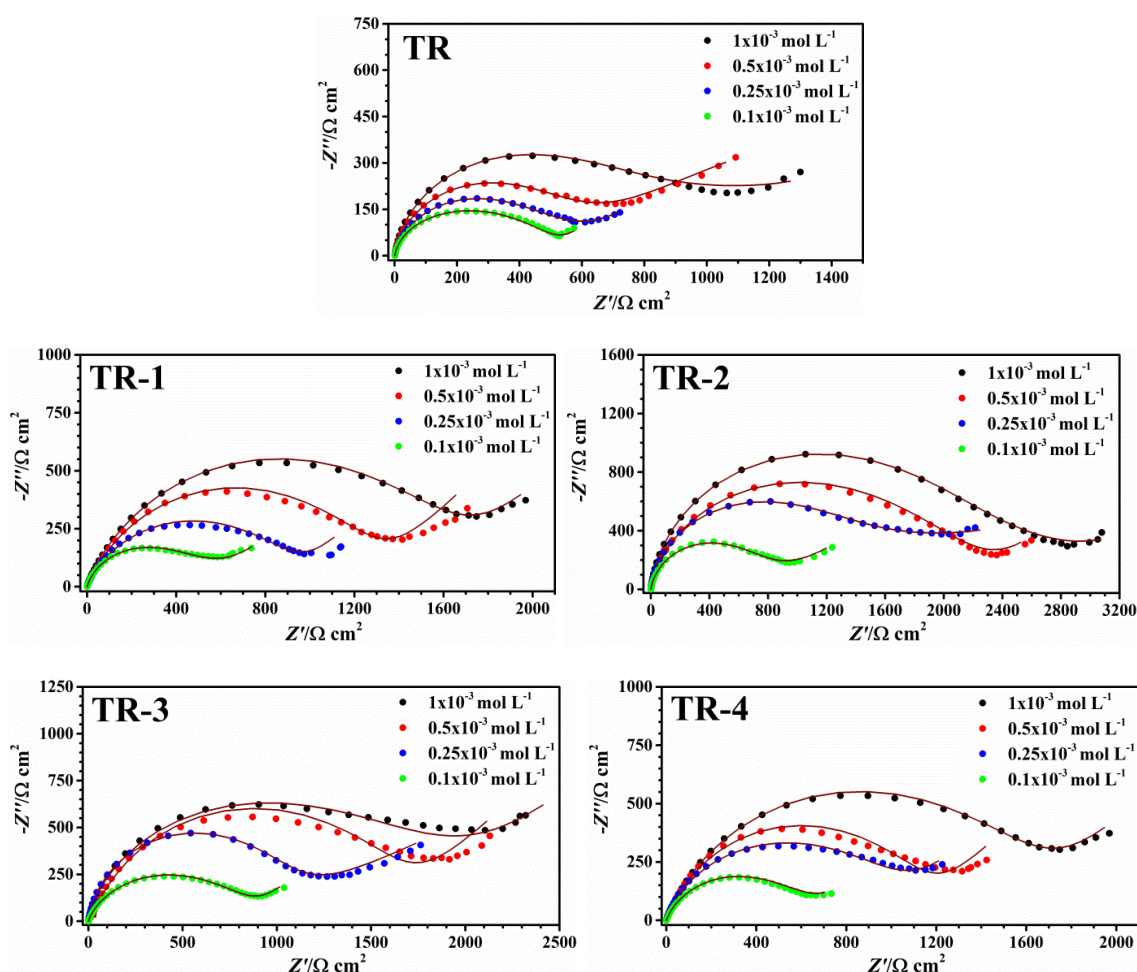
$$C_{eq} = C_1 + C_2 \quad \text{Eq.36}$$

Therefore, the equivalent capacitance is higher than  $C_1$  and  $C_2$  capacitances, and naturally the impedance of the equivalent capacitor will increase, also increasing the copper corrosion inhibition efficiency in acidic medium. The observed trend for corrosion inhibition is  $TR < TR-4 < TR-1 < TR-3 < TR-2$

### 4.3.2 Adsorption Isotherm

To understand how the inhibitor molecules behave in the surface of the copper electrode, Figure 20 shows the isotherm curves using EIS at room temperature.

Figure 20 - Nyquist diagrams obtained for Cu immersed in 0.5 mol L<sup>-1</sup> H<sub>2</sub>SO<sub>4</sub> at different concentrations of the studied corrosion inhibitors and obtained at room temperature ( $\approx 25$  °C). The solid lines represent the adjust of the experimental data by the equivalent electric circuit shown in Figure 19.



Source: Author

Figure 20 shows the Nyquist plots for different inhibitor concentrations for isotherm construction. As expected, the capacitive semicircle of all Nyquist diagrams increases as the concentration also increase. Using the same equivalent circuit shown in Figure 19, the  $R_p$  values were calculated, and the surface coverage was calculated using Eq.37 (VERMA; QURAISHI; SINGH, 2015):

$$\theta = \left( \frac{R_p - R_p^o}{R_p} \right) \quad \text{Eq.37}$$

Since the polarization resistance reflects the inhibitor molecule over the electrode surface, Eq.36 can normalize up to 1.0 (or 100%) the surface coverage that those molecules can bring to the electrode. Table 9 shows the polarization resistance and surface coverage for the copper electrode. In this context, the Langmuir model (SUN; YU, 2018) was applied accordingly to the Eq.38, and the values from Table 9 brought the Langmuir isotherms that are shown in Figure 21.

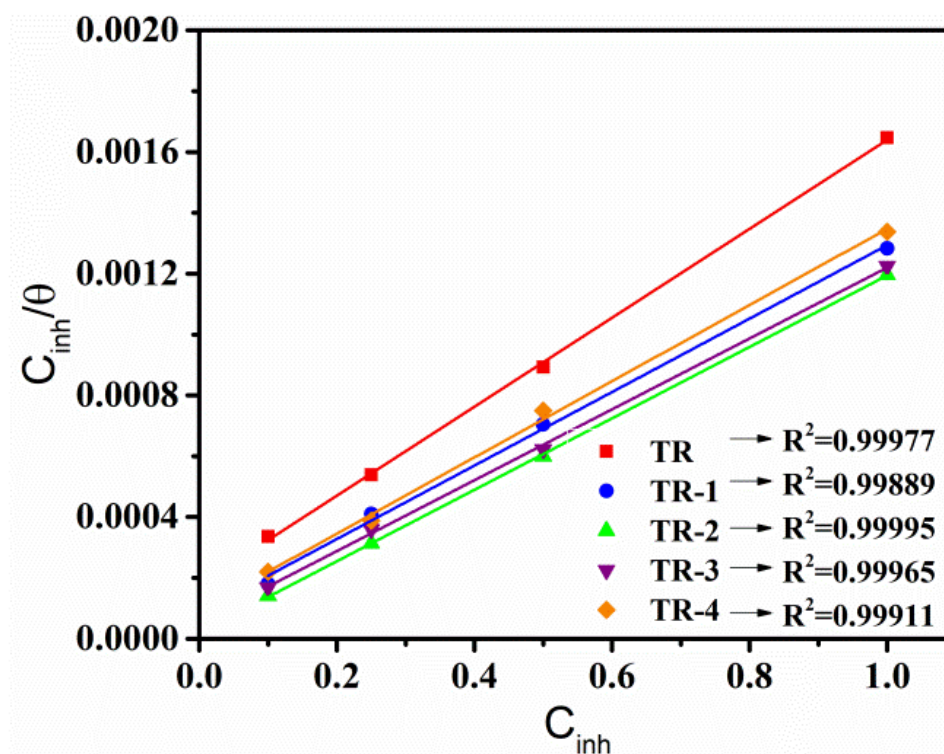
$$\frac{C_{inh}}{\theta} = C_{inh} + \frac{1}{K_{ads}} \quad \text{Eq.38}$$

Table 9 – EIS parameters derived from the Nyquist plots shown in Figure 4.7.

|        | $C_{inh} / 10^{-3} \text{ mol L}^{-1}$ | $R_p / \Omega \text{ cm}^2$ | $\theta$ |
|--------|--|-----------------------------|----------|
| Branco | -                                      | 499.95                      | -        |
| TR     | 0.1                                    | 523.59                      | 0.30     |
|        | 0.25                                   | 686.17                      | 0.46     |
|        | 0.5                                    | 835.13                      | 0.56     |
|        | 1                                      | 935.96                      | 0.61     |
| TR-1   | 0.1                                    | 825.44                      | 0.55     |
|        | 0.25                                   | 941.42                      | 0.61     |
|        | 0.5                                    | 1267.25                     | 0.71     |
|        | 1                                      | 1664.90                     | 0.78     |
| TR-2   | 0.1                                    | 1269.79                     | 0.71     |
|        | 0.25                                   | 1819.80                     | 0.80     |
|        | 0.5                                    | 2208.42                     | 0.83     |
|        | 1                                      | 2235.33                     | 0.84     |
| TR-3   | 0.1                                    | 907.06                      | 0.59     |
|        | 0.25                                   | 1203.30                     | 0.69     |
|        | 0.5                                    | 1871.10                     | 0.80     |
|        | 1                                      | 2007.63                     | 0.82     |
| TR-4   | 0.1                                    | 673.61                      | 0.45     |
|        | 0.25                                   | 1031.58                     | 0.64     |
|        | 0.5                                    | 1103.02                     | 0.67     |
|        | 1                                      | 1456.70                     | 0.75     |

Source: **Author**

Figure 21 - Langmuir's linear relationships obtained for the corrosion inhibition of Cu in 0.5 mol L<sup>-1</sup> H<sub>2</sub>SO<sub>4</sub> solution in presence of triazole and triazole-based compounds.



Source: Author

Figure 21 shows the Langmuir isotherm for all studied inhibitor molecules. It is evident in the plots that the bare TR molecule, without any modification, is separated from other modified triazole molecules, in whose isotherms are closer and parallel to each one. From the linear coefficient from isotherm lines, the adsorption Gibbs energy was calculated by Eq.39 (CHEN et al., 2019)

$$\Delta G_{ads} = - RT \ln \ln (55.6 \times K_{ads}) \quad \text{Eq.39}$$

Where  $\Delta G_{ads}$  stands for the variation of the Gibbs energy, R is the universal gas constant (8.314 J mol<sup>-1</sup> K<sup>-1</sup>), T is the room temperature in kelvin (298 K) and  $K_{ads}$  is the adsorption constant brought by the inverse of the linear coefficient of the isotherm lines in Figure 21. The result of the calculation is shown in Table 10.

Table 10 -  $K_{\text{ads}}$  and  $\Delta G_{\text{ads}}$  values for triazole derivatives in 0.5 mol L<sup>-1</sup> H<sub>2</sub>SO<sub>4</sub> solution for Cu surface.

| <b>Molecules</b> | <b><math>K_{\text{ads}}</math></b> | <b><math>\Delta G_{\text{ads}}</math> (kJ mol<sup>-1</sup>)</b> |
|------------------|------------------------------------|---|
| <b>TR</b>        | 5.631E <sup>+3</sup>               | -31.35  |
| <b>TR-1</b>      | 1.161E <sup>+4</sup>               | -33.14  |
| <b>TR-2</b>      | 5.094E <sup>+4</sup>               | -36.81  |
| <b>TR-3</b>      | 1.822E <sup>+4</sup>               | -34.26  |
| <b>TR-4</b>      | 1.054E <sup>+4</sup>               | -32.91  |

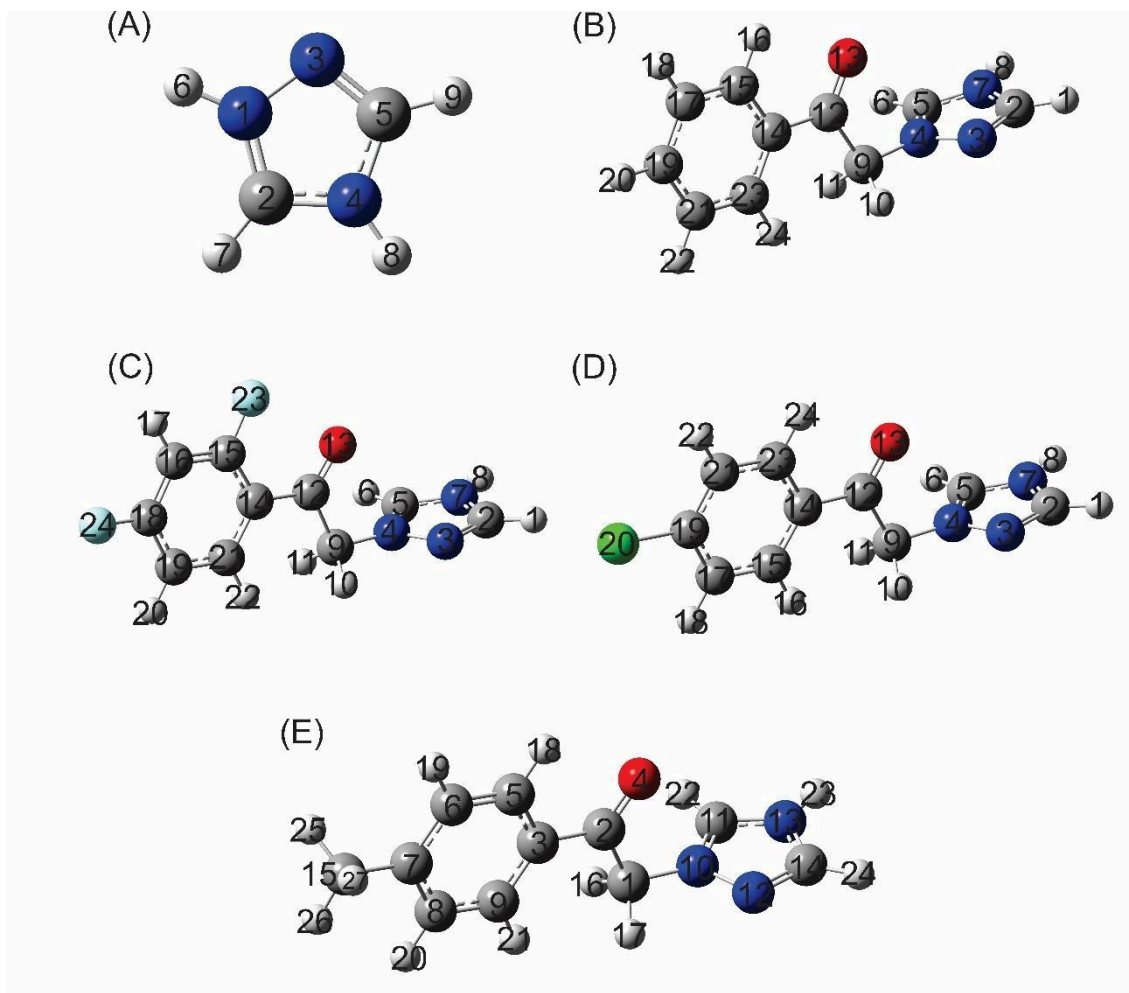
Source: Author

Table 10 shows that the TR-2 inhibitor had the highest adsorption constant and, therefore, the lowest Gibbs adsorption energy. Since this thermodynamical data brings the spontaneity of the processes, TR-2 had more affinity to the adsorption over the copper electrode surface than other molecules. Therefore, the observed trend from isotherm data for Gibbs energy is TR-2 > TR-3 > TR-1 > TR-4 > TR.

#### 4.3.3 Computational results

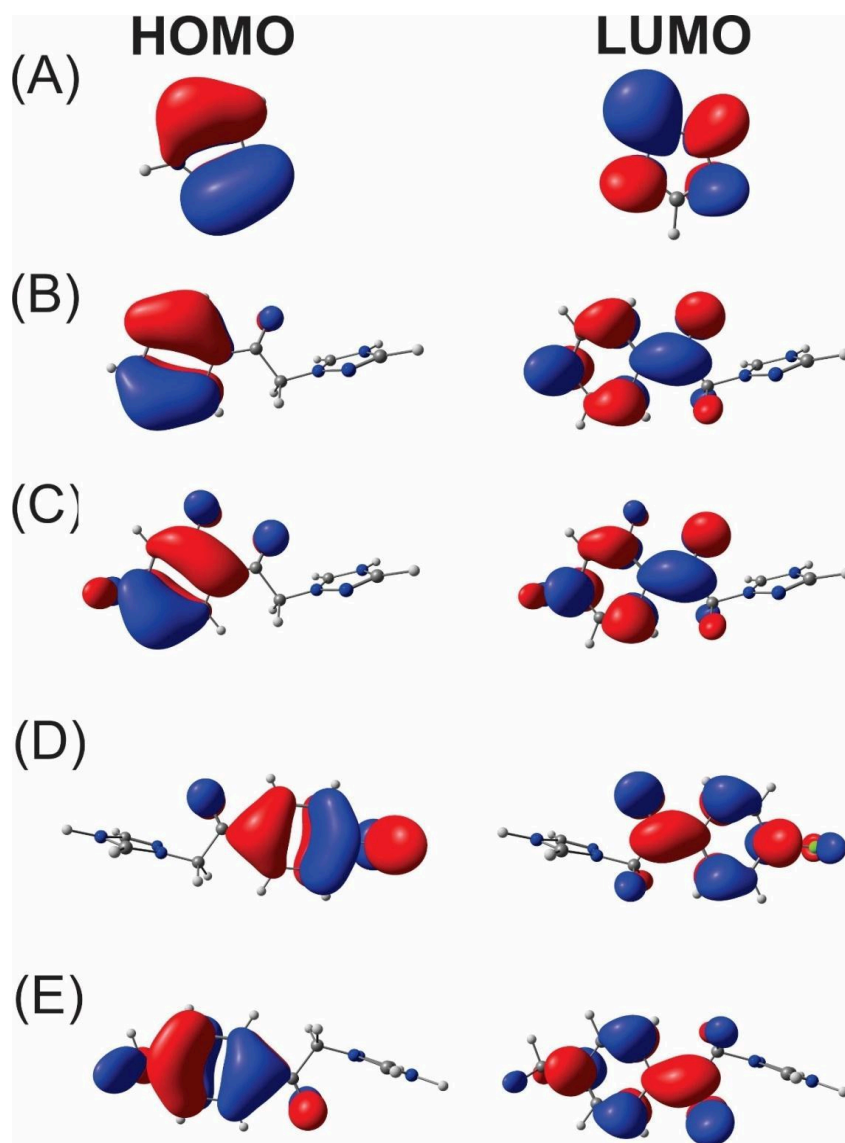
Figure 22 shows the optimized molecular geometries in the ground state (absence of negative frequencies) for the triazole and triazole derivatives at B3LYP/6-311++G(d,p) level of theory in water as an implicit solvent. The triazoles derivatives are not planar: considering the TR-1 molecule, the torsion angle (C12-C9-N4-N3) is about 90.613°; the TR-2 molecule exhibits a torsion angle (C12-C9N4-N3) of 90.278°, the TR-3 molecule shows a torsion angle (C12-C9-N3-N4) of 84.120°, and the TR-4 molecule shows the torsion angle (C2-C1-N10-N12) of 89.233°. Those results show that there is a dependence on how the molecule can approach the metallic surface to make an effective covalent interaction.

Figure 22 - Optimized geometries at 6-311++G(d,p) level of theory for the inhibitors (A) TR (B) TR-1 (C) TR-2 (D) TR-3 and (E) TR-4.



Source: Author

Figure 23 - Calculated Frontier Molecular Orbitals (FMO) at 6-311++G(d,p) level of theory for the inhibitors (A) TR (B) TR-1 (C) TR-2 (D) TR-3 and (E) TR-4.



**Source:** Author

Figure 22 shows the calculated Frontier Molecular Orbitals at 6-311++G(d,p) level of theory for the triazole and the derivatives molecules. The HOMO is mainly spread over the benzyl group in all the molecules, hence the probable interaction between the inhibitor molecule and the copper surface occurs when the benzyl group donates electronic density to the empty orbitals of the metal and this scenario required that the benzyl group would be parallel to the metallic surface.



Table 11 - Calculated global quantum reactivity descriptors at 6-311++G(d,p) level of theory.

| Property   | TR      | TR-1     | TR-2     | TR-3     | TR-4     |
|--|---------|----------|----------|----------|----------|
| HOMO energy ( $E_{HOMO}/\text{eV}$ )                         | -9.4851 | -7.6103  | -7.7276  | -7.5071  | -7.3678  |
| LUMO energy ( $E_{LUMO}/\text{eV}$ )                         | -1.8814 | -2.4703  | -2.5625  | -2.5827  | -2.3807  |
| Energy gap ( $\Delta E_{Gap}/\text{eV}$ )                    | 7.6037  | 5.1400   | 5.1650   | 4.9245   | 4.9871   |
| Ionization Potential (I / eV)                                | 9.4851  | 7.6103   | 7.7276   | 7.5071   | 7.3678   |
| Electron Affinity (A / eV)                                   | 1.8814  | 2.4703   | 2.5625   | 2.5827   | 2.3807   |
| Electronegativity ( $\chi/\text{eV}$ )                       | 5.6833  | 5.0403   | 5.1450   | 5.0449   | 4.8743   |
| Global Hardness ( $\eta/\text{eV}$ )                         | 3.8019  | 2.5700   | 2.5825   | 2.4622   | 2.4935   |
| Global Softness ( $\sigma/\text{eV}^{-1}$ )                  | 0.2630  | 0.3891   | 0.3872   | 0.4061   | 0.4010   |
| Electrophilicity index ( $\varepsilon/\text{eV}$ )           | 4.2479  | 4.9425   | 5.1251   | 5.1683   | 4.7640   |
| Nucleophilicity index ( $\omega/\text{eV}^{-1}$ )            | 0.2354  | 0.2023   | 0.1951   | 0.1935   | 0.2099   |
| Electric total polarizability ( $\alpha_{tot}/\text{a.u.}$ ) | 44.8683 | 176.0153 | 175.0647 | 197.2900 | 197.1660 |
| Fraction of electrons transferred ( $\Delta N$ )             | -0.0925 | -0.9806  | -0.9961  | -1.0245  | -0.9774  |

Source: Author

Table 11 shows the results for the calculated energy values of the HOMO and LUMO. According to those results, the order for the corrosion inhibition power is  $\text{TR} < \text{TR-2} < \text{TR-1} < \text{TR-3} < \text{TR-4}$ , which disagrees with the experimental order predicted by the electrochemical experiments  $\text{TR} < \text{TR-4} < \text{TR-1} < \text{TR-3} < \text{TR-2}$ . The TR-2 molecule has two fluorine atoms bonded to the benzyl group and those atoms can withdraw electronic density by electronegativity and the formyl group that withdraws by resonance effect from the ring, which decreases the interaction between the molecule and the metal. The TR-1 molecule has only the formyl group bonded to the benzyl ring withdraws electronic density of the ring by the resonance effect, hence it is expected that the nucleophilic character for the TR-1 molecule should be higher than the TR-2 molecule. The TR-3 molecule has the chlorine atom bonded in the benzyl ring, the withdrawal effect is lower than the TR-2 molecule which expects a higher corrosion inhibition when compared to the TR-2 molecule, and the nucleophilic character should be lower than the TR-1 molecule. Finally, the TR-4 should exhibit higher nucleophilic character, consequently, the higher reactivity with the copper surface due to the methyl group that can donate electronic density to the

ring. Therefore, for the first quantum reactivity descriptor, the nucleophilic character cannot explain the experimental order to the corrosion inhibition power. However, for the LUMO energy values, the predicted order is  $TR < TR-4 < TR-1 < TR-2 \approx TR-3$ . This order is approximate to the experimental. The corrosion inhibition efficiency for the TR-2 and TR-3 respectively 83.55% and 81.68% which are similar values. For the TR-2 and TR-3 molecules, the ligands are classified as electron withdraw which increases the electrophilic character for the molecule. The back bonding of the electronic density from the metal to the empty molecular orbitals for those molecules is more favourable than the others which have for the TR-1 no ligand and TR-4 an electron donor ligand (the methyl group). Therefore, the electrophilic character seems to explain the corrosion inhibition power for this class of molecules.

Table 11 shows the results for the other quantum reactivity descriptors. The order predicted by the energy gap is  $TR < TR-2 < TR-1 < TR-3 < TR-4$ , which does not agree with the experimental order. The energy gap considers both the HOMO and the LUMO energy values, consequently, the nucleophilic and electrophilic character of the molecule. Therefore, since the nucleophilic character cannot be used to explain the corrosion inhibition efficiency for those molecules, the energy gap will fail to predict the correct order.

As the Ionization Potential and the Electron Affinity are related to the nucleophilic and electrophilic character respectively, the order predicted by those descriptors is the same as HOMO and LUMO. Again, the electron affinity (electrophilic character) has more importance to define the reactivity of those molecules with the copper surface.

The order predicted by the electronegativity is as follow:  $TR-4 < TR-1 < TR-3 < TR-2 < TR$ . This order is also quite similar from the experimental with only the TR overestimated to be the best inhibitor. Since the electronegativity of the inhibitor molecules are higher than the bulk copper, the flow of the electronic density is from the metallic surface to the molecule, hence the major factor for the interaction between those compounds are the electrophilic character of the inhibitor. The TR-2 and TR-3 molecules have the higher electrophilic character than the TR-1 and TR-4 molecules. The fraction of electrons transferred confirms that the flow of electronic density is from the copper surface to the studied molecules due to its negative mathematical sign. The predicted order by this descriptor is  $TR < TR-4 < TR-1 < TR-2 \approx TR-3$ , and this order is like the experimental with both TR-2 and TR-3 showing similar values to its corrosion inhibition power.

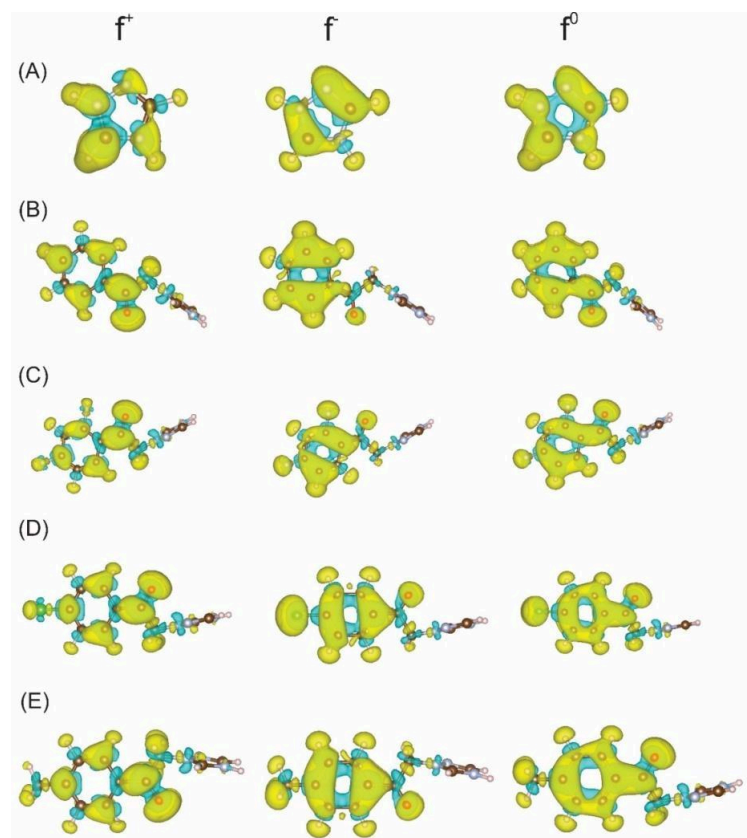
The order predicted by the global hardness and the global softness is the same:  $TR < TR-2 < TR-1 < TR-4 < TR-3$ . The global hardness and the global softness are related to the energy gap; hence those descriptors are considering both nucleophilic and electrophilic character of the molecule. However, it has been seen that only the electrophilic character commands the corrosion inhibition power and for this reason, it overestimate the character of the TR-4 and underestimate the inhibitor character of the TR-2 molecule.

To prove that the electrophilic character contributes mainly to the corrosion inhibition power for those molecules, the electrophilic index was computed, and the predicted order was as follows:  $TR < TR-4 < TR-1 < TR-2 \approx TR-3$ . This order is very similar to the experiment. This result agrees with the LUMO and the fraction of transferred electrons. The nucleophilic index was also computed, and the order predicted is as follows:  $TR-2 \approx TR-3 < TR-1 < TR-4 < TR$ . This order is exactly the inverse from the experimental. Finally, the electric total polarizability was calculated, and the predicted order for the corrosion inhibition power was as follows:  $TR < TR-2 \approx TR-1 < TR-4 \approx TR-3$ . This descriptor predicted that due to the lower size of the fluorine atoms present in the TR-2 molecule, the electronic density available to donate has almost the same size as the TR-1 molecule which does not have any ligand. The chlorine atom is larger than the methyl group which implies a higher electronic density to donate to the metal. However, the electron-donating character is not too relevant to explain the trend of those inhibitors.

The graphical Electronic Fukui functions analysis for the triazole derivatives are shown in Figure 24, the triazole molecule exhibit the atoms N1, C2, N3, and N4 susceptible to a nucleophilic attack, the atoms N1, C2, N3, and C5 susceptible to an electrophilic attack, and the atoms N1, C2, N3, N4, and C5 susceptible to a radical attack. The TR-1 molecule shows the atoms C12, C13, C15, C19, and C23 susceptible to a nucleophilic attack, the atoms C14, C15, C17, C19, C21, and C23 susceptible to an electrophilic attack, and the atoms C12, O13, C14, C15, C17, C19, C21, and C23 susceptible to a radical attack. The TR-2 molecule shows the atoms C12, O13, C15, C18, and C21 susceptible to a nucleophilic attack, the atoms O13, C14, C15, C16, C18, C19, and C21 susceptible to an electrophilic attack, and the atoms C12, O13, C14, C15, C16, C18, C19, and C21 susceptible to a radical attack. The TR-3 molecule shows the atoms C12, O13, C15, C19, C120, C23 susceptible to a nucleophilic attack, the atoms C14, C15, C17, C19, C120, C21, and C23 susceptible to an electrophilic attack, and the atoms C12, O13, C14, C15, C17, C19, C120, C21, and C23 susceptible to a radical attack. The TR-4

molecule shows the atoms C2, O4, C5, C7, and C9 susceptible to a nucleophilic attack, the atoms C3, O4, C5, C6, C7, C8, and C9 susceptible to an electrophilic attack, and the atoms C2, C3, O4, C5, C6, C7, C8, and C9 susceptible to a radical attack. On the triazole molecule, the most susceptible atoms for a nucleophilic attack are N1, C2, and N4; for the electrophilic attack, the most susceptible atoms are N3 and C5. For the TR-1 molecule, the most susceptible atoms to a nucleophilic attack are C2, N3, C5, N7, C9, C12, O13, and C19; for the electrophilic attack, the most susceptible atoms are N4, C14, C15, C17, C21 and C23.

Figure 24 - Isosurface for the Electronic Fukui functions for the nucleophilic attack ( $f^+$ ), electrophilic attack ( $f^-$ ), and radical attack ( $f^0$ ) for the (a) TR (b) TR-1 (c) TR-2 (d) TR-3 and (e) TR-4.

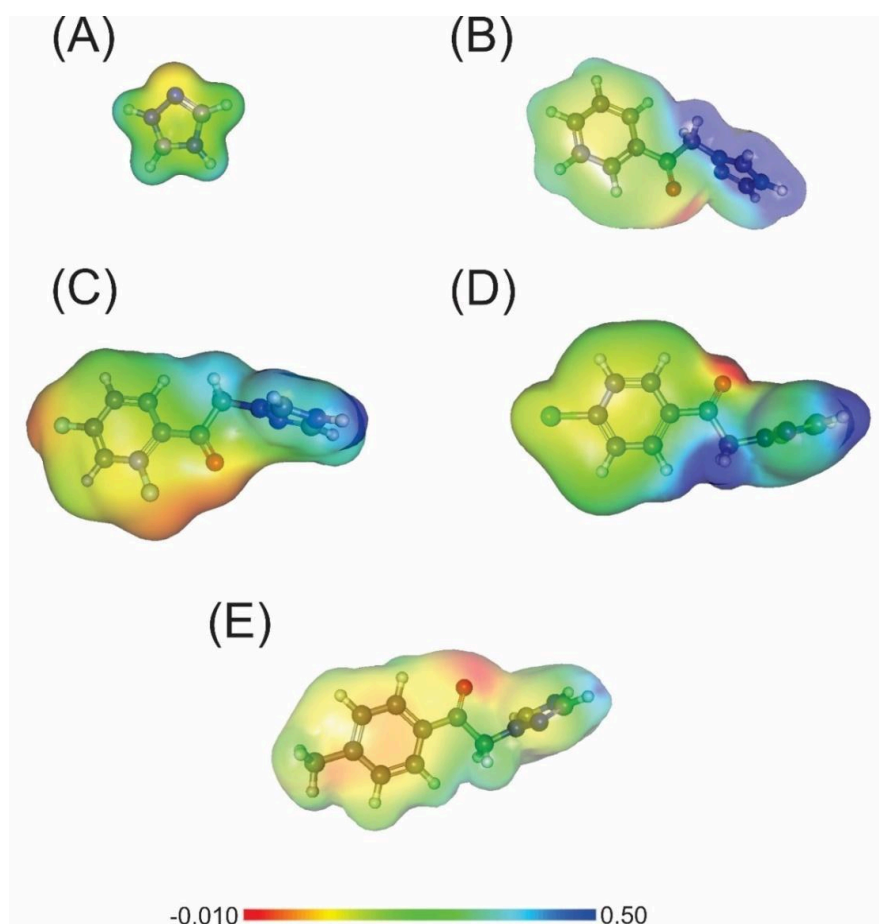


Source: Author

This result confirms that the benzyl ring donates electronic density to the copper surface. For the TR-2 molecule, the most susceptible atoms to a nucleophilic attack are C2, N3, C5, N7, C9, C12, O13, and C21; for the electrophilic attack, the most susceptible atoms are N4, C14, C15, C16, C18, C19, F23, and F24. For the TR-3 molecule, the most

susceptible atoms for a nucleophilic attack are C2, N3, C5, N7, C9, C12, O13, C15, and C23; for the electrophilic attack, the most susceptible atoms are N4, C14, C17, 19, C120, and C21. For the TR-4 molecule, the most susceptible atoms for a nucleophilic attack are C1, C2, O4, C5, C9, C11, N12, and N13; for the electrophilic attack, the most susceptible atoms are C3, C6, C7, C8, N10, C14, and C15.

Figure 25 - Calculated Molecular Electrostatic Potential (MEP) for the (a) TR (b) TR-1 (c) TR-2 (d) TR-3 and (e) TR-4.



Source: Author

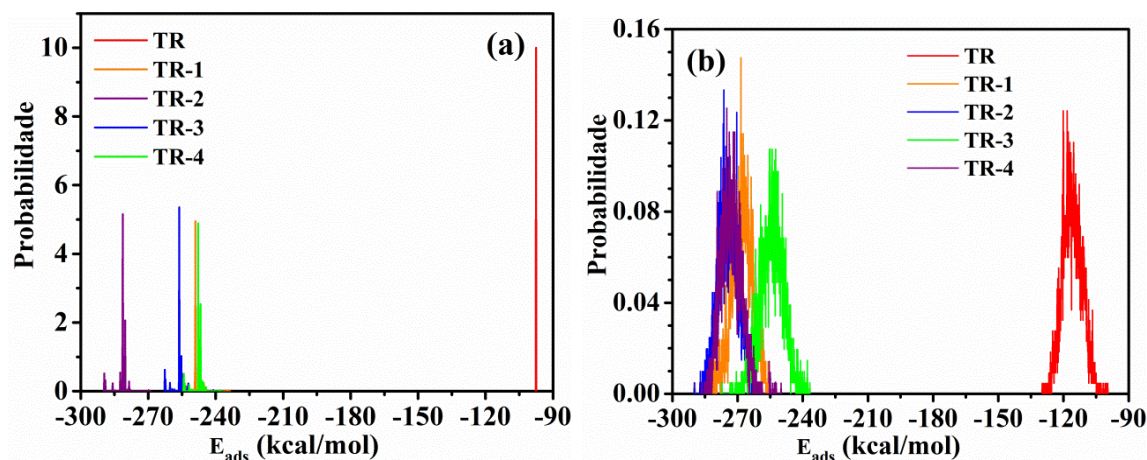
As was seen in the Fukui functions analysis, the atoms present in the benzyl ring are responsible for the electron-donation power of the molecule and the atoms in the triazole ring are responsible for the electron-accepting power. The Molecular Electrostatic Potential of those molecules, shown in Figure 25, show that the benzyl ring has a partially negative charge region that can interact by nucleophilic interaction and the triazole ring has

partially and positively charged regions that are responsible to the electrophilic interactions. The oxygen atom of the carbonyl group can also donate electronic density due to its negatively charged.

Figure 26 shows the distribution of the inhibitors over the modeled copper surface. The interaction energies of those molecules with its surface were obtained using COMPASS force field, in absence and presence of explicit water molecules, which was 380 of them in the box. As it can be seen, Figure 26a the TR-2 molecule showed the lowest interaction energy between the inhibitor molecules, having a higher probability of having a  $-281.86$  kcal/mol energy over the copper surface, which suggests that the active sites of the solid had better interaction with TR-2 molecule as corrosion inhibitor. Other molecules, such as TR-1, TR-3 and TR-4 had similar interaction energy values (between  $-247.78$  kcal/mol and  $-256.42$  kcal/mol) but lower than TR-2. The reference molecule, TR, had a small interaction energy between the studied molecules,  $-97.52$  kcal/mol. When compared with modified triazole molecules, the TR one has no lateral group, which decreases the interaction between them and copper surface.

Considering the adsorption in explicit water, Figure 26b, the triazole compounds had shifted their interaction energies towards more negative values, except from TR-2, which remained the same. This shows the effect of the solvent over the interaction energy during the adsorption process. Also, it can be seen that the most probable molecules which interacts with copper surface do not presented a defined trend as shown in vacuum mode in Figure 26a. This can be explained that the explicit solvent model brings a gaussian-like shape, and the expected probabilities are higher than in vacuum, once the interaction between water-water, water-inhibitor and water-copper surface are prominent. Therefore, the probability plots are different.

Figure 26 - Energy probability distribution of adsorption energy of the inhibitor molecules using a copper surface along COMPASS force field in vacuum (a) and explicit water molecules (b).



Source: Author

Considering the calculated corrosion inhibition efficiency from impedance data and adsorption energies from Monte Carlo simulations, Figure 27 shows the actual correlation between those data. From both vacuum and explicit water models, the observed trend was, from the lowest to the highest: TR < TR-4 < TR-1 < TR-3 < TR-2, the same sequence found in experimental data. Using the COMPASS force field in the Monte Carlo

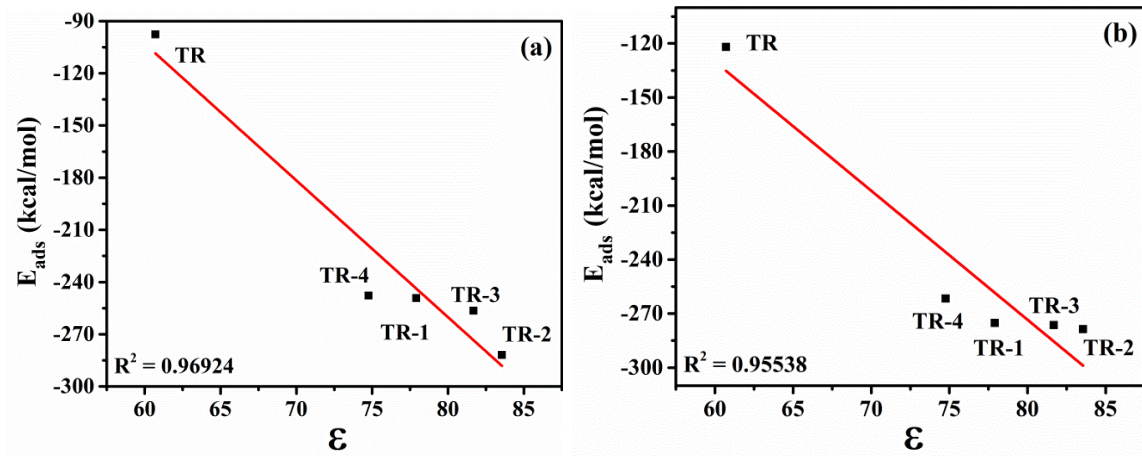
simulation, the correlation shown in Figure 27 brought two linear equations considering vacuum (Eq.39) and explicit water model (Eq.40):

$$E_{ads} = 368.66 - 7.86 \times \varepsilon \quad \text{Eq.39}$$

$$E_{ads} = 299.67 - 7.16 \times \varepsilon \quad \text{Eq.40}$$

In this context, those equations will compute the anticorrosion efficiency for other similar triazole compounds, which can predict the behaviour of those inhibitor in a similar medium.

Figure 27 – Correlation between adsorption energies from maximum probabilities in Figure 26 and inhibition efficiency for vacuum (a) and explicit water (b) media using COMPASS force field.



Source: Author

Since Monte Carlo simulations can show the molecular position of the inhibitor molecule, Figure 28 shows the relative position of those molecules over the simulated copper surface in a box containing explicit water molecules. In general, the most hydrophobic molecules can diffuse towards the metallic surface and creating a adsorbed film in it. Considering the copper electrode, the corrosion inhibitor should block the oxygen gas diffusion towards the electrode surface, reacting with metallic copper and creating copper (II) oxide, one corrosion product. In this context, the molecular solvent energy can show the affinity of the corrosion inhibitor with water molecule, and the Eq.41 shows the way this value was calculated (MENDONÇA et al., 2017):

$$E_{mol-sol} = E_t - [E_{mol} + E_{supsup} + E_{sup-mol} + E_{sup-sol} + E_{sol} + N \times E_{sol}] \quad \text{Eq.41}$$

Where:

$E_{mol-sol} \rightarrow$  is the interaction energy between the water molecule and corrosion inhibitor,

$E_t \rightarrow$  is the total energy of the simulated system,

$E_{mol} \rightarrow$  is the energy of the molecule,

$E_{sup} \rightarrow$  is the surface energy of the electrode

$E_{sup-mol} \rightarrow$  is the interaction energy between water molecule and electrode surface,

$E_{sol} \rightarrow$  is the energy of the water molecule,

$N \rightarrow$  is the number of the water molecules in the simulation.



From Eq.41, Table 12 shows the interaction energy between the inhibitor and water molecules. Since the most hydrophobic, more adherent to the metallic surface the inhibitor is, the observed energy trend is, from lowest to highest: TR < TR-4 < TR-1 < TR-3 < TR-2. Therefore, TR-2, which was shown as the best inhibitor molecule among all others, is the most hydrophobic molecule.

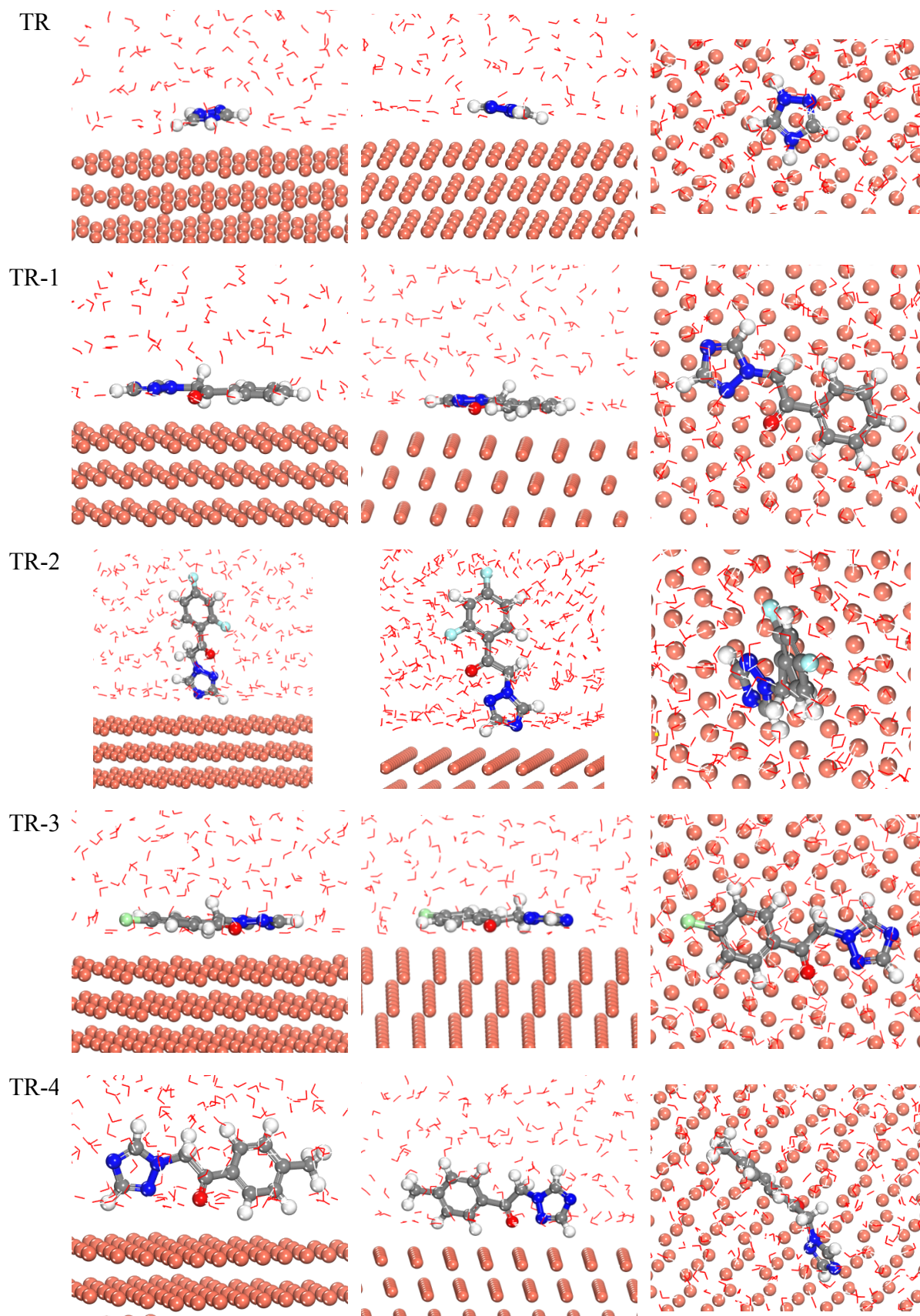
Table 12 – Interaction energies from studied inhibitor molecules

| Inhibitor | $E_t$     | $E_{sup}+E_{mol}+E_{sup\_mol}$ | $E_{sup}+N \times E_{H_2O}+E_{H_2O\_H_2O}+E_{sup\_H_2O}$ | $E_{sup}$ | $E_{mol\_H_2O}$ |
|-----------|-----------|--------------------------------|--|-----------|-----------------|
| TR        | -8,284.68 | -3,965.47                      | -8275.46   | -3,976.40 | -20.15          |
| TR-1      | -8,287.23 | -4,026.44                      | -8202.83   | -3,976.40 | -34.37          |
| TR-2      | -8,279.10 | -4,004.24                      | -8204.95   | -3,976.40 | -46.31          |
| TR-3      | -8,288.25 | -4,032.97                      | -8190.91   | -3,976.40 | -40.77          |
| TR-4      | -8,264.73 | -4,019.04                      | -8188.73   | -3,976.40 | -33.36          |

**Source:** Author

To understand better how the inhibitor molecules behave during the adsorption over the copper electrode, Figure 28 shows the molecular positions of the inhibitors at the maximum probabilities for each one in an explicit solvent modelling.

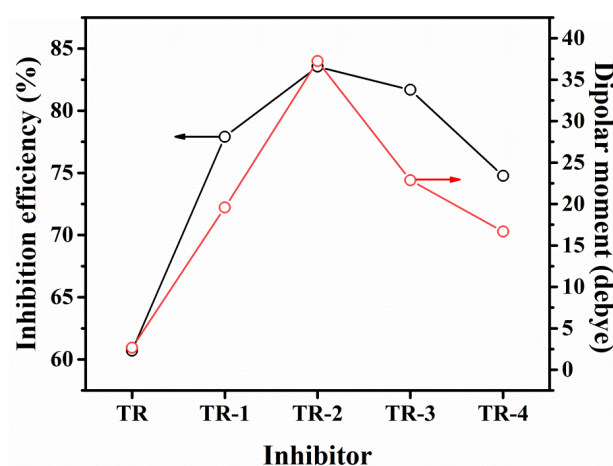
Figure 28 – Preferred molecular orientation of the inhibitor molecules over a copper surface in a simulation with explicit water molecules.



Source: author

In Figure 28, it is worth to describe that the molecules presented different orientations: except for TR-2 and TR-4, all other inhibitor molecules had a flat position in relation to the copper surface. Considering the TR-2 molecule, the triazolic ring is interacting directly over the copper surface, whereas TR-4 molecule has a lateral interaction over the copper surface. TR-2 and TR-4 molecules have in their structure, fluorine, and methyl groups, respectively. In this context, those groups in the benzene ring have a degree of apolarity, and this effect in the electrode surface can repel this part of the inhibitor molecules, and the interacting group can be more polar (or less polar) than the copper surface. Considering this hypothesis, other inhibitor molecules, such as TR, TR-1 and TR-3 have an opposite polarity if compared with the copper surface. Therefore, this difference in polarity can affect the corrosion inhibition; Figure 29 shows the correlation between the calculated dipolar moment with corrosion efficiency from impedance results of all inhibitor molecules.

Figure 29 - Correlation between corrosion efficiency and dipolar moment for all inhibitor molecules.



Source: Author

Figure 29 shows the correlation of corrosion efficiency and dipolar moment for all inhibitor molecules. As it can be seen, the TR-2 is the most polar molecule between the studied inhibitors, and all others are lower than TR-2. Also, the corrosion efficiency also shows the same trend. When we observe the molecular position of the inhibitors towards the copper surface, the hypothesis of the apolarity of the side group (or the overall lower polarity) can be confirmed. Therefore, the polarity trend seen in Figure 29 is, from lowest to the highest: TR < TR-4 < TR-1 < TR-3 < TR-2, which is the same trend observed for inhibition efficiency. Therefore, the best triazole for inhibiting the corrosion of copper electrodes in acidic medium is TR-2.

#### 4.4 Conclusions

It was possible to make modifications over a triazole molecule for having a better corrosion inhibitor for copper electrode in  $\text{H}_2\text{SO}_4$  acidic medium than triazole itself. The electrochemical data, such as OCP, LPP and EIS experiments showed that the TR-2 molecule was superior than other modified triazole molecules on both retarding the oxygen gas from the surface of copper electrode and shifting the corrosion potential of the electrode towards more negative values than blank solution. In this context, the impedance data showed that TR-2 had diminished the diffusion of  $\text{Cu}^+$  ion, which is the starter for a catalytic corrosion reaction in the copper electrode. The isotherm data showed that TR-2 had the lowest Gibbs adsorption energy between all inhibitor molecules, and the computational results showed that. Considering the DFT data, TR-2 and TR-3 data presented the same LUMO energy value due to the ligands that come with those molecules, having TR-2 two fluorine atoms, and TR-3 a chlorine atom, which removes electron density from the molecules but increases their polarities. The Monte Carlo simulations showed that TR-2 molecule had the highest interaction energy, which confirms the Langmuir isotherm discussion, and also those molecule have the highest interaction with water, a result that explains why TR-2 is a good corrosion inhibitor and confirmed all experimental data presented in this paper.

## REFERENCES

- ALLOUCHE, A.-R. Gabedit-A graphical user interface for computational chemistry softwares. **Journal of Computational Chemistry**, v. 32, n. 1, p. 174–182, 15 jan. 2011.
- ATKINS, P. et al. **Inorganic Chemistry**. 5<sup>o</sup> ed. Oxford, 2011.
- BALASUBRAMANIAM, R. On the corrosion resistance of the Delhi iron pillar. **Corrosion Science**, v. 42, n. 12, p. 2103–2129, 2000.
- BELGHITI, M. E. et al. Anticorrosive properties of two 3,5-disubstituted-4-amino-1,2,4-triazole derivatives on copper in hydrochloric acid environment: Ac impedance, thermodynamic and computational investigations. **Surfaces and Interfaces**, v. 21, n. August, p. 100692, 2020.
- BEZERRA, F. D. A. **Síntese Químioenzimática dos Enantiômeros da Propafenona e Síntese de Substâncias Triazólicas**. Fortaleza, 2018.
- BRUG, G. J. et al. The analysis of electrode impedances complicated by the presence of a constant phase element. **Journal of Electroanalytical Chemistry and Interfacial Electrochemistry**, v. 176, n. 1–2, p. 275–295, set. 1984.
- CALDONA, E. B. et al. Corrosion inhibition of mild steel in acidic medium by simpleazole-based aromatic compounds. **Journal of Electroanalytical Chemistry**, v. 880, p. 114858, 2021.
- CANCÈS, E.; MENNUCCI, B.; TOMASI, J. A new integral equation formalism for the polarizable continuum model: Theoretical background and applications to Isotropic and anisotropic dielectrics. **Journal of Chemical Physics**, v. 107, n. 8, p. 3032–3041, 1997.
- CHATTARAJ, P. K.; GIRI, S.; DULEY, S. Update 2 of: Electrophilicity Index. **Chemical Reviews**, v. 111, n. 2, p. PR43–PR75, 9 fev. 2011.
- Chemcraft - graphical software for visualization of quantum chemistry computations**. , 2004. Disponível em: <https://www.chemcraftprog.com>. Acesso em:22/09/2022
- CHEN, Z. et al. New surfactants N - alkyl - N , N - dimethyl - N - ( 3 - thienylmethylene ) ammonium bromides : Preparation and anticorrosion evaluation. **Materials and Corrosion**, n. February, p. 820–837, 2019.
- CHERMETTE, H. Chemical reactivity indexes in density functional theory. **Journal of Computational Chemistry**, v. 20, n. 1, p. 129–154, 15 jan. 1999.
- CHITER, F. et al. Chemical interaction, self-ordering and corrosion inhibition properties of 2-mercaptobenzothiazole monolayers: DFT atomistic modeling on metallic copper. **Corrosion Science**, v. 209, n. September, p. 110658, 2022.
- CORDEIRO, G. G. O.; BARCIA, O. E.; MATTOS, O. R. Copper electrodisolution mechanism in a 1M sulphate medium. **Electrochimica Acta**, v. 38, n. 2–3, p. 319–324, 1993.

- COSTA, S. N. et al. Carbon steel corrosion inhibition in acid medium by imidazole-based molecules: Experimental and molecular modelling approaches. **Journal of Molecular Liquids**, v. 326, p. 115330, mar. 2021.
- DENNINGTON, R.; KEITH, T.; MILLAM, J. **GaussView**. United State: Semichem Inc., 2009.
- DEWAR, M. J. S. et al. AM1: A New General Purpose Quantum Mechanical Molecular Model. **Journal of the American Chemical Society**, v. 107, n. 13, p. 3902–3909, 1985.
- DITCHFIELD, R.; HEHRE, W. J.; POPLE, J. A. Self-Consistent Molecular-Orbital Methods. IX. An Extended Gaussian-Type Basis for Molecular-Orbital Studies of Organic Molecules. **The Journal of Chemical Physics**, v. 54, n. 2, p. 724–728, 15 jan. 1971.
- EL ASRI, A. et al. Computational and experimental studies of the inhibitory effect of imidazole derivatives for the corrosion of copper in an acid medium. **Journal of Molecular Liquids**, v. 345, p. 117813, 2022.
- FERKOUS, H. et al. Corrosion inhibition of mild steel by 2-(2-methoxybenzylidene)hydrazine-1-carbothioamide in hydrochloric acid solution: Experimental measurements and quantum chemical calculations. **Journal of Molecular Liquids**, v. 307, p. 112957, 2020.
- FOUDA, A. S. et al. A comparative study of the corrosion inhibition of carbon steel in HCl solution by 1-[(5-mercapto-1H-1,2,4-triazole-3-yl) diazenyl] naphthalene-2-ol (HL) and its manganese complex. **Chemical Data Collections**, v. 28, p. 100479, 2020.
- HUANG, H.; BU, F. Correlations between the inhibition performances and the inhibitor structures of some azoles on the galvanic corrosion of copper coupled with silver in artificial seawater. **Corrosion Science**, v. 165, n. May 2019, p. 108413, 2020.
- ICZKOWSKI, R. P.; MARGRAVE, J. L. Electronegativity. **Journal of the American Chemical Society**, v. 83, n. 17, p. 3547–3551, 1961.
- ITUEN, E. et al. Inhibition of erosion corrosion of pipework steel in descaling solution using 5-hydroxytryptamine-based additives: Empirical and computational studies. **Journal of Molecular Structure**, v. 1204, p. 127562, 2020.
- JANAK, J. F. Proof that  $\partial E / \partial n_i = \epsilon$  in density-functional theory. **Physical Review B**, v. 18, n. 12, p. 7165–7168, 15 dez. 1978.
- JIANG, L. et al. 1,2,4-Triazole as a corrosion inhibitor in copper chemical mechanical polishing. **Thin Solid Films**, v. 556, p. 395–404, 2014.
- JOG, K. V. et al. Effect of chemical structure on the microbial nitrification inhibition and copper corrosion inhibition properties of azole compounds. **Journal of Cleaner Production**, v. 366, n. June, p. 132871, 2022.
- KOOPMANS, T. Über die Zuordnung von Wellenfunktionen und Eigenwerten zu den Einzelnen Elektronen Eines Atoms. **Physica**, v. 1, n. 1–6, p. 104–113, 1934.

LIU, Z. Y. et al. The inhibition efficiencies of some organic corrosion inhibitors of iron: An insight from density functional theory study. **Computational and Theoretical Chemistry**, v. 1214, n. February, p. 113759, 2022.

LU, T.; CHEN, F. Multiwfn: A multifunctional wavefunction analyzer. **Journal of Computational Chemistry**, v. 33, n. 5, p. 580–592, 15 fev. 2012.

MA, Q. et al. 1,2,3-Triazole derivatives as corrosion inhibitors for mild steel in acidic medium: Experimental and computational chemistry studies. **Corrosion Science**, v. 129, n. September, p. 91–101, 2017.

MA, T. et al. Corrosion control of copper wiring by barrier CMP slurry containing azole inhibitor: Combination of simulation and experiment. **Colloids and Surfaces A: Physicochemical and Engineering Aspects**, v. 599, n. March, 2020.

MENDONÇA, G. L. F. et al. Understanding the corrosion inhibition of carbon steel and copper in sulphuric acid medium by amino acids using electrochemical techniques allied to molecular modelling methods. **Corrosion Science**, v. 115, p. 41–55, 2017.

MENNUCCI, B.; CANCÈS, E.; TOMASI, J. Evaluation of solvent effects in isotropic and anisotropic dielectrics and in ionic solutions with a unified integral equation method: Theoretical bases, computational implementation, and numerical applications. **Journal of Physical Chemistry B**, v. 101, n. 49, p. 10506–10517, 1997.

MICHAELSON, H. B. The work function of the elements and its periodicity. **Journal of Applied Physics**, v. 48, n. 11, p. 4729–4733, nov. 1977.

MOMMA, K.; IZUMI, F. VESTA 3 for three-dimensional visualization of crystal, volumetric and morphology data. **Journal of Applied Crystallography**, v. 44, n. 6, p. 1272–1276, 1 dez. 2011.

OBOT, I. B.; MACDONALD, D. D.; GASEM, Z. M. Density functional theory (DFT) as a powerful tool for designing new organic corrosion inhibitors. Part 1: An overview. **Corrosion Science**, v. 99, p. 1–30, out. 2015.

ORAZEM, M. E.; TRIBOLLET, B. **Electrochemical Impedance Spectroscopy**. Hoboken, NJ, USA: John Wiley & Sons, Inc., 2008.

PARLAK, A. E. et al. Experimental, DFT and Theoretical Corrosion Study for 4-(((4-ethyl-5-(thiophen-2-yl)-4H-1,2,4-triazole-3-yl)thio)methyl)-7,8-dimethyl-2H-chromen-2-one. **Arabian Journal of Chemistry**, v. 15, n. 9, p. 104088, 2022.

PARR, R. G.; SZENTPÁLY, L. V.; LIU, S. Electrophilicity Index. **Journal of the American Chemical Society**, v. 121, n. 9, p. 1922–1924, mar. 1999.

PEARSON, R. G. Hard and Soft Acids and Bases. **Journal of the American Chemical Society**, v. 85, n. 22, p. 3533–3539, 1963.

PEARSON, R. G. Recent advances in the concept of hard and soft acids and bases. **Journal of Chemical Education**, v. 64, n. 7, p. 561–567, 1987.

POLLOCK, L. J. TOXICITY OF PYRIDINE IN MAN. **Archives of Internal Medicine**, v. 71, n. 1, p. 95, 1 jan. 1943.

QIU, Y. et al. Insight into synergistic corrosion inhibition of 3-amino-1,2,4-triazole-5-thiol (ATT) and NaF on magnesium alloy: Experimental and theoretical approaches. **Corrosion Science**, v. 208, n. August, p. 110618, 2022.

RAJESH KUMAR SINGH VIKAS KUMAR, R. K. Study the Corrosive Effect of Greenhouse Gases on Metallic and Non-metallic Materials. **International Journal of Metallurgy and Alloys**, v. 7, n. 2, p. 17–28, 2021.

ROBERGE, P. R. Impact of climate change on corrosion risks. **Corrosion Engineering, Science and Technology**, v. 45, n. 1, p. 27–33, 27 fev. 2010.

SHINGAYA, Y.; ITO, M. Comparison of a bisulfate anion adsorbed on M(111) (M = Pt, Rh, Au, Ag and Cu). **Journal of Electroanalytical Chemistry**, v. 467, n. 1, p. 299–306, 1999.

SUN, X.; YU, L. Investigation of polyacrylamide containing capsaicin monomer as a novel corrosion inhibitor for mild steel in hydrochloric acid. **Materials and Corrosion**, v. 69, n. 8, p. 1095–1103, 2018.

SILVA, E. F. et al. Electrochemical and surface enhanced Raman spectroscopy study of Guanine as corrosion inhibitor for copper. **Corrosion Science**, v. 191, n. July, p. 109714, 2021.

SWATHI, N. P. et al. A new 1,2,4-triazole derivative as an excellent corrosion inhibitor: Electrochemical experiments with theoretical validation. **Materials Chemistry and Physics**, v. 291, n. August, p. 126677, 2022.

TANTAWY, A. H.; SOLIMAN, K. A.; ABD EL-LATEEF, H. M. Novel synthesized cationic surfactants based on natural piper nigrum as sustainable-green inhibitors for steel pipeline corrosion in CO<sub>2</sub>-3.5%NaCl: DFT, Monte Carlo simulations and experimental approaches. **Journal of Cleaner Production**, v. 250, p. 119510, 2020.

TCHOUMENE, R.; KENNE DEDZO, G.; NGAMENI, E. Intercalation of 1,2,4-triazole in methanol modified-kaolinite: Application for copper corrosion inhibition in concentrated sodium chloride aqueous solution. **Journal of Solid State Chemistry**, v. 311, n. February, p. 123103, 2022.

THIRUMOOLAN, D. et al. Corrosion resistant performance of hydrophobic poly(N-vinyl imidazole-co-ethyl methacrylate) coating on mild steel. **Progress in Organic Coatings**, v. 89, p. 181–191, 2015.

VARVARA, S. et al. Experimental characterization, machine learning analysis and computational modelling of the high effective inhibition of copper corrosion by 5-(4-pyridyl)-1,3,4-oxadiazole-2-thiol in saline environment. **Electrochimica Acta**, v. 398, p. 139282, 2021.

VERMA, C.; QURAISHI, M. A.; SINGH, A. 2-Amino-5-nitro-4,6-diarylcyclohex-1-ene-1,3,3-tricarbonitriles as new and effective corrosion inhibitors for mild steel in 1 M HCl:



Experimental and theoretical studies. **Journal of Molecular Liquids**, v. 212, p. 804–812, 2015.

VERNON, L. S. Corrosion Inhibitors in Coatings - Toxicity, Regulations and Liability **CORROSION** **96**, 24 mar. 1996.

VON SZENTPÁLY, L. Studies on electronegativity equalization. **Journal of Molecular Structure: THEOCHEM**, v. 233, p. 71–81, set. 1991.

WAZZAN, N.; OBOT, I. B.; FAGIEH, T. M. The role of some triazoles on the corrosion inhibition of C1020 steel and copper in a desalination descaling solution. **Desalination**, v. 527, n. January, p. 115551, 2022.

YADAV, M. et al. Experimental and Quantum Studies on Adsorption and Corrosion Inhibition Effect of Imidazole Derivatives on N80 Steel in Hydrochloric Acid. **Surface Review and Letters**, v. 20, n. 06, p. 1350057, 2013.

YANG, W.; PARR, R. G. Hardness, softness, and the fukui function in the electronic theory of metals and catalysis. **Proceedings of the National Academy of Sciences of the United States of America**, v. 82, n. 20, p. 6723–6726, 1985.

ZHANG, Z. et al. A study of the inhibition of iron corrosion by imidazole and its derivatives self-assembled films. **Corrosion Science**, v. 51, n. 2, p. 291–300, 2009.

ZHAO, Y.; TRUHLAR, D. G. The M06 suite of density functionals for main group thermochemistry, thermochemical kinetics, noncovalent interactions, excited states, and transition elements: two new functionals and systematic testing of four M06-class functionals and 12 other function. **Theoretical Chemistry Accounts**, v. 120, n. 1–3, p. 215–241, 2008.